



This is to certify that the

dissertation entitled

**BIFURCATION DYNAMICS AS A CAUSE OF THE
RECENT VOLTAGE COLLAPSE PROBLEMS ON THE
WSCC SYSTEM**

presented by

Shuzhen Liu

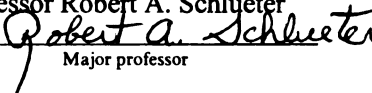
has been accepted towards fulfillment

of the requirements for

Ph. D. Electrical Engineering

_____ degree in _____

Professor Robert A. Schlueter


Major professor

Date May 12, 1999



PLACE IN RETURN BOX to remove this checkout from your record.
TO AVOID FINES return on or before date due.
MAY BE RECALLED with earlier due date if requested.

DATE DUE	DATE DUE	DATE DUE
<hr/>	<hr/>	<hr/>
<hr/>	<hr/>	<hr/>
<hr/>	<hr/>	<hr/>
<hr/>	<hr/>	<hr/>
<hr/>	<hr/>	<hr/>

**BIFURCATION DYNAMICS AS A CAUSE OF THE RECENT VOLTAGE
COLLAPSE PROBLEMS ON THE WSCC SYSTEM**

By

Shuzhen Liu

A DISSERTATION

Submitted to
Michigan State University
in partial fulfillment of the requirements
for the degree of

DOCTOR OF PHILOSOPHY

Department of Electrical and Computer Engineering

1999

ABSTRACT

BIFURCATION DYNAMICS AS A CAUSE OF THE RECENT VOLTAGE COLLAPSE PROBLEMS ON THE WSCC SYSTEM

By

Shuzhen Liu

The voltage collapse problem is considered as the principal threat to power system stability, security and reliability in many utilities around the world. Recently, three severe blackouts occurred on the WSCC power system, which have caused loss of power for millions of customers. Although reasonably accurate models of that complex system have been assembled and can reasonably accurately capture the sequence of events that occurred, there is no clear diagnostic theoretical explanation of what occurred and why. This dissertation is the first attempt to understand the dynamics through sensitivity analysis.

This work consists of three parts of theoretical explanations of the cause of the recent blackouts on the WSCC system.

First, a theoretical analysis and simulation study of the excitation control system, especially the maximum excitation limiter, is presented. This part explains why maximum excitation limiters fail to reduce field current limit violations when large inter-area oscillations are present, and why this can lead to switching from an AC regulator to a DC regulator excitation control, and finally to tripping of the generator off the system.

Secondly, voltage PV controllability, load PV controllability, voltage PQ controllability and load PQ controllability are defined. The conditions on sensitivity matrices S_{QGE} , S_{QGQ_L} , S_{Q_LV} and S_{VE} that indicate when each type of controllability is

retained and when it is lost, are derived. Furthermore, it is proven and confirmed through simulation that the occurrence of loss of different controllabilities has certain patterns and that loss of controllability is affected by the load characteristics.

Finally, a theoretical justification and simulation study for the dynamic response to bifurcation sequences associated with voltage collapse are presented. This part establishes that a saddle node bifurcation followed by an inevitable singularity induced bifurcation produces the characteristic negative voltage spike observed on the WSCC system blackouts.

In summary, the purpose of the sensitivity analysis is to identify the subsystem which initially experiences instability, to identify why this instability occurs and how this instability could cascade to other subsystems, and to identify what can be done to cure the instability problems and when and where the cure should be applied. This dissertation provides both diagnostic theoretical justifications and comprehensive simulation results on the dynamic phenomena similar to those observed during the recent WSCC system blackouts.

To my mother, father and daughter

ACKNOWLEDGMENTS

I would like to express my sincere gratitude to my advisor, Professor Robert A. Schlueter, for his valuable academic guidance, continuous spiritual encouragement and financial support throughout the time taken to complete this work. Without his great help, I would not have reached this point today.

Special thanks also go to Professor Hassan Khalil, Professor Steven Shaw and Professor Chichia Chiu for their intellectual contributions to this dissertation.

I am indebted to my husband Zhibo for his continuous assistance.

I also wish to thank Dr. Khadija Ben Kilani for her helping hand and friendship.

TABLE OF CONTENTS

DEDICATION	iv
ACKNOWLEDGMENTS	v
LIST OF TABLES	ix
LIST OF FIGURES.....	x
 CHAPTER 1 INTRODUCTION	 1
1.1 Voltage Stability	1
1.2 WSCC System Blackouts	2
1.3 Excitation Control System	7
1.4 Bifurcations in Power System.....	11
1.5 Hypotheses.....	18
1.6 Relevant Literatures	22
 CHAPTER 2 POWER SYSTEM MODELING	 23
2.1 A General Power System Model.....	23
2.2 Excitation Control System Model	25
2.3 Maximum Excitation Limiter Model	26
2.4 Power System Load Model.....	27
 CHAPTER 3 PROBLEM ANALYSIS	 31
3.1 Disablement of Current MXL due to Oscillation.....	32
3.1.1 Theoretical Analysis	32
3.1.2 Analysis of Boundary Δ^* Where MXL Operates Correctly and Malfunctions.....	36
3.1.3 Simulation Results	39

3.2	Excitation Control System Tripping and Unit Tripping.....	45
3.3	Uncontrollable Spreading Voltage Collapse.....	46
CHAPTER 4 VOLTAGE AND LOAD CONTROLLABILITY.....		47
4.1	Introduction.....	47
4.2	Sensitivity Matrices.....	48
4.3	Voltage and Load PV Controllability.....	52
4.3.1	Voltage PV Controllability.....	52
4.3.2	Load PV Controllability.....	53
4.4	Voltage and Load PQ Controllability.....	53
4.4.1	Voltage PQ Controllability.....	53
4.4.2	Load PQ Controllability.....	54
4.5	Effects of Loss of Load PQ Controllability	55
4.6	Effects of Load Characteristics	60
4.7	Validation of Theory	63
CHAPTER 5 THEORETICAL AND SIMULATION JUSTIFICATION FOR THE DYNAMIC RESPONSE TO BIFURCATION SEQUENCE ASSOCIATED WITH VOLTAGE COLLAPSE		76
5.1	Introduction.....	77
5.2	Test Matrices for Static Bifurcation in Flux Decay Dynamics.....	79
5.3	Effects of Loss of Voltage PQ Controllability on Stability of Generators with Exciters	82
5.4	Effects of Loss of Voltage PV Controllability and Disablement of the Excitation Control System on Stability of Generator Dynamics	83
5.5	Justification of the Bifurcation Sequence that Occurs due to Loss of Voltage PV Controllability and Disablement of the Excitation Control System on a Specific Generator	84
5.6	Justification of the Large Negative Voltage Spike that Develops due to Loss of Voltage PQ Controllability on Generator Response	

with or without Excitation Control.....	86
5.7 Simulation Study	89
CHAPTER 6 CONCLUSIONS AND FUTURE WORK.....	95
APPENDIX A:THEOREM PROOFS.....	99
APPENDIX B:PUBLICATIONS	107
REFERENCES	108

LIST OF TABLES

Table 4.1	Bus data 66
Table 4.2	Line data 66
Table 4.3	Generator data 67
Table 4.4	Exciter data 67

LIST OF FIGURES

Figure 1.1	July 2, 1996 WSCC system blackout recordings: (a) Voltage recording (b) Power recording	5
Figure 1.2	August 10, 1996 WSCC system blackout recordings (a) Voltage recording (b) Power recording.....	6
Figure 1.3	December 14, 1994 WSCC blackout voltage recording	6
Figure.1.4	Block diagram of excitation control system.....	8
Figure 1.5	A typical bifurcation sequence (a): P-V Curve; (b): Critical modes movement	14
Figure 2.1	Excitation control system model.....	25
Figure 2.2	Model of maximum excitation limiter	26
Figure 3.1	I_{fd} with oscillation component.....	33
Figure 3.2	Plot for determining Δ^*	37
Figure 3.3	Relationship between I_0 and I_1	38
Figure 3.4	The MXL action when $I_0 < R$	40
Figure 3.5	The MXL action when $I_0 = R$	41
Figure 3.6	The MXL action when $I_0 > R$ but $A_1 < A_2$	42
Figure 3.7	The MXL action when $I_0 > R$ but $A_1 > A_2$ (The effect of increasing I_0 for certain I_1)	43

Figure 3.8	The effect of increasing I_1 for certain I_0	44
Figure 4.1	A three-machine 9-bus test system	68
Figure 4.2	E'_q , $S_{Q_L V}^{-1}$, $S_{Q_G E}$, S_{VE} and $S_{Q_G Q_L}$ for case 1	69
Figure 4.2	E'_q , $S_{Q_L V}^{-1}$, $S_{Q_G E}$, S_{VE} and $S_{Q_G Q_L}$ for case 2	70
Figure 4.4	$S_{Q_L V}^{-1}$ for case 1	71
Figure 4.5	$S_{Q_L V}^{-1}$ for case 2	72
Figure 4.6	$S_{Q_L V}^{-1}$, $S_{Q_G E}$, S_{VE} and $S_{Q_G Q_L}$ for case 1	73
Figure 4.7	$S_{Q_L V}^{-1}$, $S_{Q_G E}$, S_{VE} and $S_{Q_G Q_L}$ for case 2	74
Figure 4.8	Effects of load characteristics	75
Figure 5.1	Simulation result for theorems 5.1 and 5.8	92
Figure 5.2	Simulation result for theorems 5.2 and 5.3	93
Figure 5.3	Simulation result for theorems 5.4, 5.5, 5.6, 5.7 and 5.9	94

CHAPTER 1

INTRODUCTION

1.1 Voltage Stability

Voltage stability problem is a subset of overall power system stability problem. Voltage instability results in progressive voltage increase or decrease that can spread uncontrollably throughout a power system. A power system at a given operating state and subject to a given disturbance undergoes voltage collapse if post-disturbance equilibrium point is unstable or does not exist. Voltage collapse may be total (blackout) or partial [2]. Voltage collapse problems are considered the principal threat to power system stability, security and reliability in many utilities around the world.

The classic voltage collapse problem in a load flow model is always considered a reactive supply demand problem. Two types of voltage collapse problems have been identified to exist on a load flow model: loss of control voltage collapse and clogging voltage collapse. A loss of control voltage collapse is caused by exhaustion of reactive reserve with resultant loss of voltage control on a particular set of generators, synchronous condensers, or SVC's. The loss of control voltage collapse not only cuts off the reactive supply to a subregion requiring reactive power, but also increases reactive network losses that prevent sufficient reactive supply from reaching that region. A clogging voltage collapse occurs due to I^2X series reactive losses, tap changers reaching tap limits, switchable shunt capacitors reaching susceptance limits, and shunt capacitive reactive

supply withdrawal due to decreasing voltage. These network reactive losses can completely choke off the reactive flow to a subregion needing reactive supply without any exhaustion of reactive reserves and loss of voltage control on generators, synchronous condensers or SVC's [11].

The loss of control voltage collapse should have occurred in the algebraic model of a differential algebraic power system model since the load flow model is a bifurcation subsystem model if excitation systems are sufficiently high gain, the maximum excitation limiters act correctly, and the excitation control systems are not disabled [32]. Although there is yet much to discover how the loss of control voltage stability problem in a load flow model is evidenced in a differential algebraic power system model, this thesis is on a totally different voltage stability problem. This voltage stability problem was observed in the Western System Coordination Council (WSCC) system on December 14, 1994 [20], July 2, 1996 [18] and August 10, 1996 [21] and was neither a clogging nor a loss of control voltage instability problem because it was initiated in the differential submodel rather than in the algebraic submodel of the differential algebraic power system model.

1.2 WSCC System Blackouts

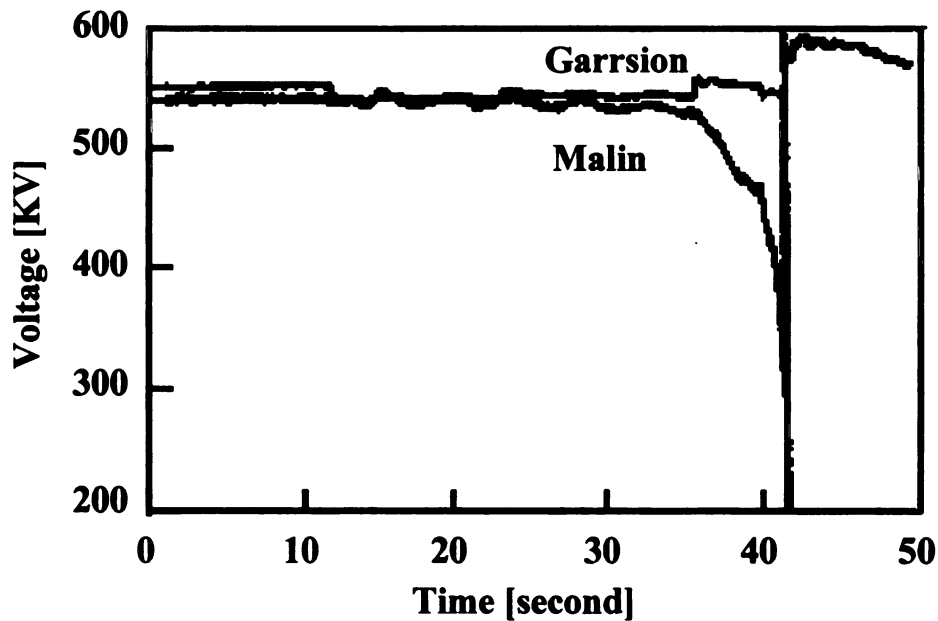
WSCC system is the entire power system network west of Denver including Canada. In each of the December 14, 1994, July 2, 1996 and August 10, 1996 blackouts [18, 20, 21], there were large interarea oscillations observed before the blackouts, and the blackouts occurred after some fault or contingency. Based on the existing operating and design criteria, the contingency should not have resulted in blackouts and certainly not have produced such severe blackouts that each caused loss of power for millions of customers. Although reasonably accurate models of that complex system have been assembled and can reasonably accurately capture the sequence of events that occurred, there is no clear

diagnostic theoretical explanation of what occurred and why. On the August 10, 1996 blackout, it was clear that the excitation control system failed on the McNary station generators that led to the tripping of generators at that station [21]. Since (1) these blackouts have led to significant reduction in power transfer limits in the WSCC system, (2) there were significant deregulated power flows from one subregion to another on August 10, 1996 that raise the possibility that this type of problem could affect other regions of the US and other countries experiencing deregulation of their utilities, and (3) the causes and cures for these stability problems are so poorly understood, this particular voltage stability problem was singled out for study in this thesis. Moreover, the study will be the first attempt to understand the dynamics after each bifurcation in the sequence of bifurcations that possibly produced these blackouts.

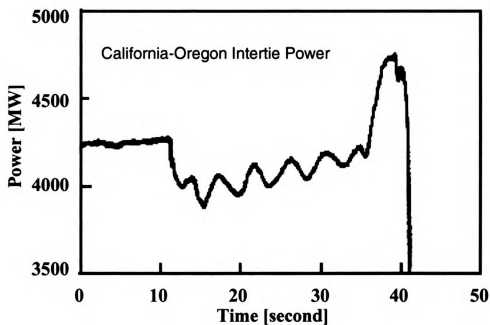
From the records of the July 2, 1996 [18] and August 10, 1996 [21] power blackouts in the Western United States, it is observed that although the cascading tripping of units and lines has been described as voltage collapse, neither blackout was due to the classical or any known kind of voltage instability problem.

These three loss of voltage stability incidents couldn't be loss of control voltage instability because the time frame was too short for tap changers and capacitors to act that are associated with the recovery of voltage and load in the distribution system [11, 33]. Recovery of voltage and load causes the generators to exhaust reactive reserves and causes the Maximum Excitation Limiter (MXL) control to act that allows generator excitation system voltage setpoints to decline as reactive load or reactive network losses increase. This decline of generator exciter setpoints due to increased network reactive load and losses begets more reactive load and losses and more voltage decline that causes the cascading voltage collapse associated with loss of control voltage instability. The recent two blackouts couldn't be clogging voltage instability because the system was not heavily loaded when the outages occurred [11].

Furthermore, the stability controls were effective and responded correctly to the early contingencies. The response of these stabilizing controls should have ensured stability and prevented further outages if these stability problems were loss of control or clogging voltage stability problems. In each of the July 2, 1996 and August 10, 1996 blackouts, sharp spike reductions in both voltage and power were observed as shown in Figure 1.1 and Figure 1.2. A sharp spike reduction in voltage was also observed in December 14, 1994 blackout as shown in Figure 1.3.

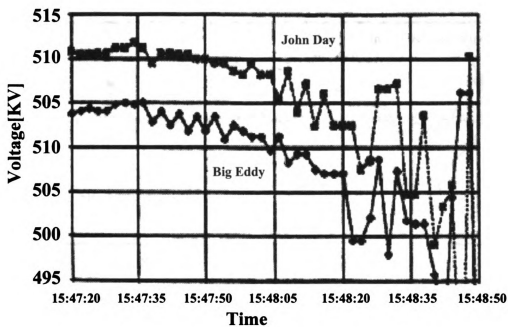


(a) Voltage recording

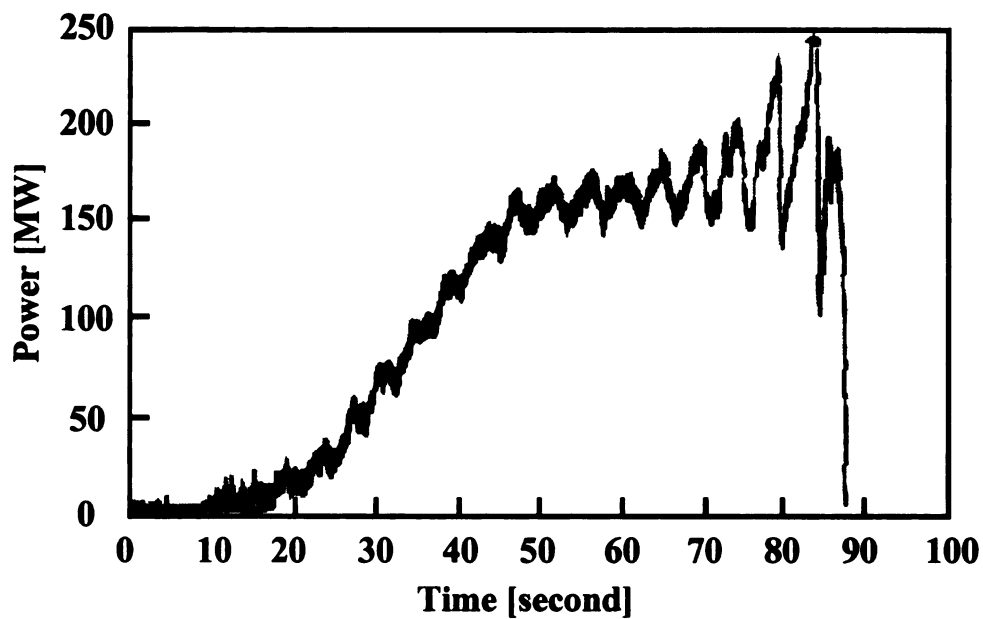


(b) Power recording

Figure 1.1 July 2, 1996 WSCC system blackout recordings



(a) Voltage recording



(b) Power recording

Figure 1.2 August 10, 1996 WSCC system blackout recordings

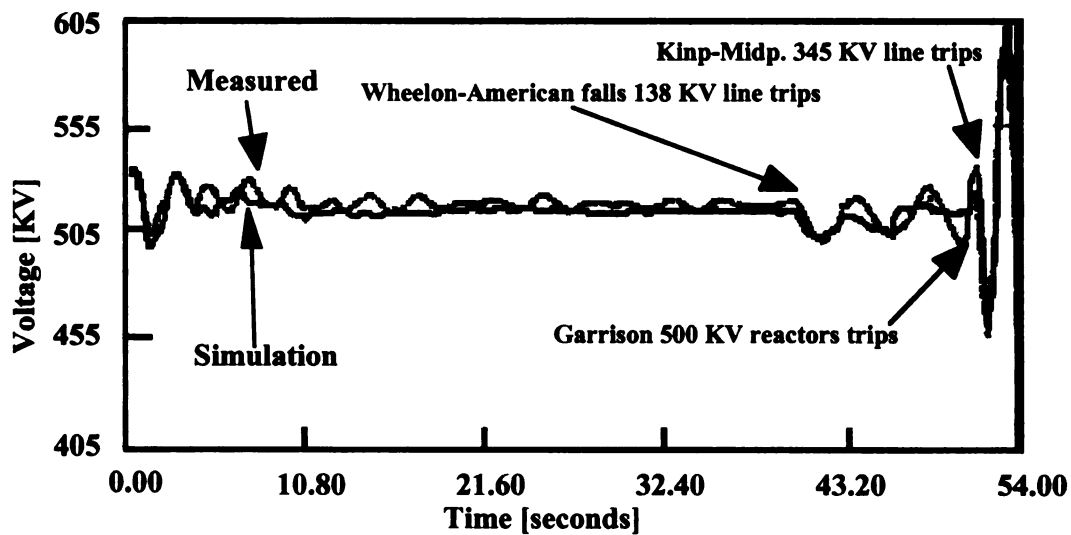


Figure 1.3 December 14, 1994 WSCC blackout voltage recording

Since malfunction of the excitation control system is hypothesized to be at the center of these blackouts, the description on how it has been modified and improved over time to handle voltage instability problems is discussed in the next section.

1.3 Excitation Control System

The functional block diagram of a synchronous generator excitation control system [1] is shown in Fig.1.4.

Voltage stability is affected greatly by the excitation control system. The basic function of an excitation control system is to provide direct current to the synchronous machine field winding and thus to control the internal induced voltage of the generator. In addition, the excitation control system performs corrective and protective functions essential to the satisfactory performance of the power system by controlling the field winding voltage and thereby the field current.

The corrective functions include:

(a) Prevention of transient instability for faults, line outage, or generator outage contingencies using a high ceiling voltage, short rise time exciter, and sufficient damping to prevent multiple swing instability;

(b) Effective control of generator or network voltage through use of a line drop compensator. Effective voltage control requires selecting a control bus or point in the network where voltage is to be controlled and using a high gain exciter to maintain control bus voltage at the desired setpoint; [1, 3]

(c) Effective coordination of generator exciter setpoints to assure effective primary control of voltage at every network bus within limits of $0.95 \leq |V| \leq 1.05$ pu [33]. This

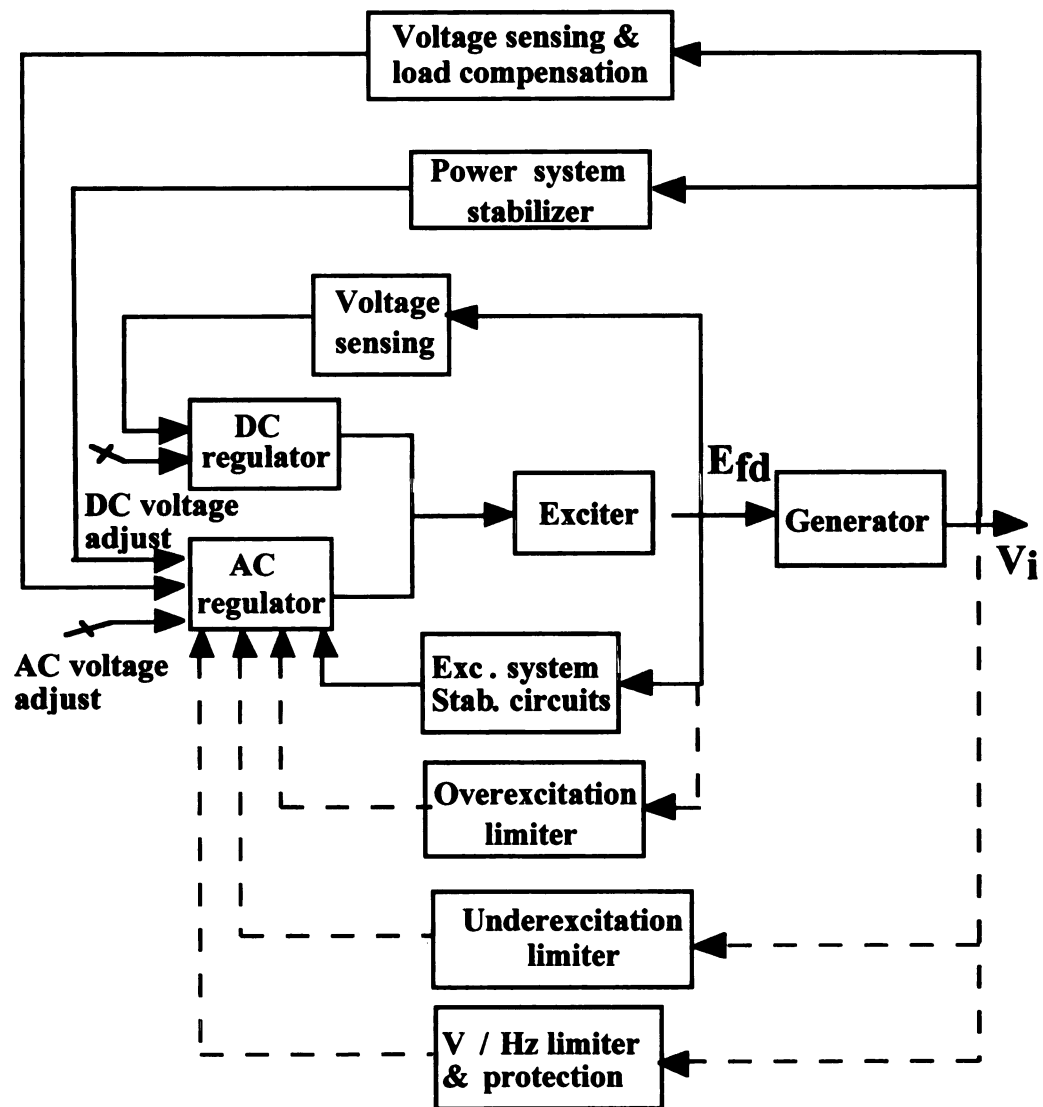


Fig.1.4 Block diagram of excitation control system

function is supplemented by under load tap changers and switchable shunt capacitors especially at subtransmission and distribution system buses that are electrically distant from generators. This coordination of generator exciter setpoints is also required to prevent a generator from exceeding its field current limit and thus from exceeding generator reactive capability in the process of holding control bus voltage to setpoint values.

The protective functions [1, 2] associated with an excitation control system are:

(a) A dc regulator is a backup system for the ac regulator in case that the field current is not reduced below the continuous rating limit after a suitable duration. This dc regulator was first installed in the mid 70's as a means of preventing the kind of voltage instability that caused the blackout on the Electricite de France in 1978. It replaces a manual system which requires the operator to adjust field voltage and current on this backup manual controller in response to stress on the system that reduces generator internal voltage via armature reaction. The dc regulator provides a backup control that automatically adjusts field current and voltage to continuously track the changes produced by the ac regulator without exceeding field current limitation. If the ac regulator is disabled by an overexcitation limiter relay, the dc regulator ensures that reactive supply and generator voltage are maintained at what the ac regulator would require. In manual control, operators might not continually adjust field voltage to values being produced by the ac regulator due to inattention or other pressing matters. Reduction of reactive supply due to ineffectiveness of manual control when the ac regulator is tripped by a field current limiter relay, can cause a cascading trip of excitation control systems and reduction of voltage setpoints and thus reactive outputs on other nearby generators that produce voltage collapse. Thus, the dc regulator is a significant advance by preventing the reduction of generator reactive supply on one or more generators when the excitation control systems are tripped by overexcitation limiter relays.

(b) A Maximum Excitation Limiter (MXL) reduces field current on a generator below continuous rating limits by (i) overriding but not disabling the ac regulator (ii) effectively reducing the exciter's voltage setpoint through the summer as is shown in the excitation control system block diagram (Figure 1.4). This MXL action prevents disabling the stabilization of an excitation control system. The MXL allows the excitation control system to retain the stabilizing effects of the power system stabilizer on oscillations and the effects of the excitation control system on steady state stability. Without MXL, which was first introduced more recently than the dc regulator, the ac regulator was disabled by a field current overexcitation limiter relay whenever continuous field current limit violations occurred for a sufficiently long duration or whenever the ac regulator was not acting properly. Loss of the excitation systems' stabilization control could trigger voltage instability. The MXL accomplishes reduction of field current without losing the stabilization effects of the excitation system or by providing the stabilizing signals if the excitation control is overridden.

There are two relay based protective functions of the excitation control system [1, 2]:

(1) The field current limiter relay that disables the ac regulator with or without MXL when the field current remains above continuous limit or when the excitation system/MXL controller is faulty. The field current limiter relay should operate infrequently when a MXL is present compared to when a MXL is not present. The field current limiter can be a two step device that reduces field current to continuous rating in 10 seconds if field current exceeds 208% of rating or in 30 seconds if field current exceeds 145% rating. An inverse time overcurrent relay can also be used that keeps the field current below the specified level [1].

A second inverse time field current relay can trip the generator if the dc regulator does not maintain field current below the actual field current limit curve that would produce

equipment damage if exceeded. This curve allows larger field current or duration than the inverse time curve that trips the ac regulator with or without MXL [1].

(2) An armature current limiter relay that acts on armature currents in a similar manner to field current relay. Both relays act to prevent overheating and equipment damage on the generator. The armature current capability of the machine [1] is shown below:

Time(seconds)	10	30	60	120
Armature current (percent)	226	154	130	116

1.4 Bifurcations in Power System

The bifurcation phenomena in the nonlinear power system refers to characterizing the qualitative change in the response of the system for a smooth continuous change in parameter μ over a specified range. For the following model:

$$\begin{aligned}\dot{x} &= f(x, \theta, V_t, \mu) \\ 0 &= G_p(x, \theta, V_t, \mu) \\ 0 &= G_Q(x, \theta, V_t, \mu)\end{aligned}$$

where x is the generator dynamic state variables, θ and V_t are the angle and voltage at generator terminal, high side transformer and load buses, μ is the parameter of interest. The function f represents the generator and excitation control systems on all generators in the system, G_p is the active power balance equation that describes the network power distribution from generators to loads. G_Q is the reactive power balance equation that describes how reactive power is supplied and how voltage is controlled in the network.

The full Jacobian matrix of the above model is:

$$J(\mu) = \begin{bmatrix} A_1 & B_1 & C_1 \\ A_2 & B_2 & C_2 \\ A_3 & B_3 & C_3 \end{bmatrix}$$

It has been proven [32] that if matrix $J_c(\mu) = \begin{bmatrix} B_2 & C_2 \\ B_3 & C_3 \end{bmatrix}$ is nonsingular, then an equivalent differential equation model $\dot{x} = f(x, \theta(x(\mu)), V_r(x(\mu)))$ can be uniquely obtained with equivalent differential Jacobian matrix

$$J_x(\mu) = A_1 - [B_1 \quad C_1] \begin{bmatrix} B_2 & C_2 \\ B_3 & C_3 \end{bmatrix}^{-1} \begin{bmatrix} A_2 \\ A_3 \end{bmatrix}$$

Similarly, if matrix $A_1(\mu)$ is nonsingular, then an equivalent algebraic equation model $0 = g(x(\theta(\mu), V_r(\mu)), \theta(\mu), V_r(\mu))$ can be uniquely obtained with equivalent algebraic Jacobian matrix

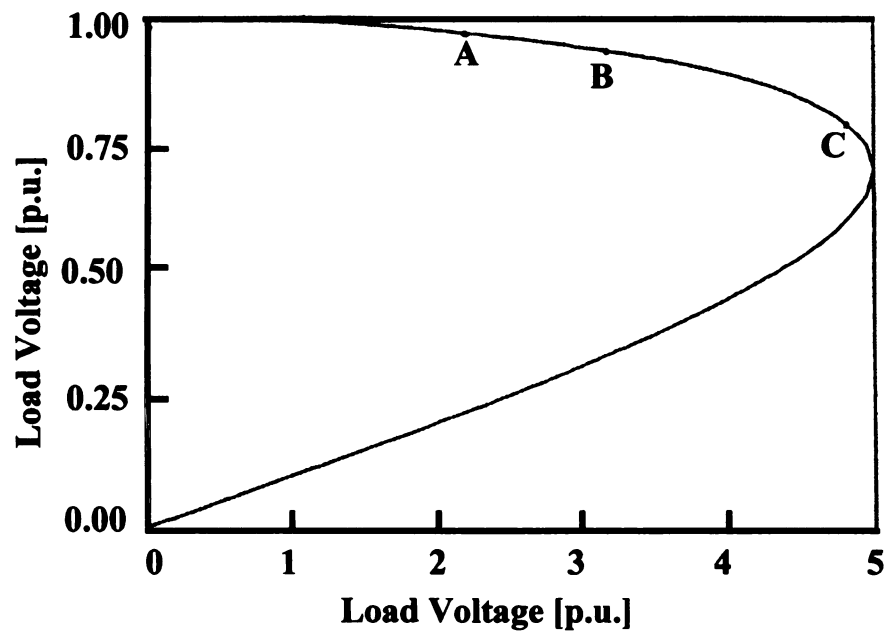
$$J_y(\mu) = \begin{bmatrix} B_2 & C_2 \\ B_3 & C_3 \end{bmatrix} - \begin{bmatrix} A_2 \\ A_3 \end{bmatrix} [A_1]^{-1} [B_1 \quad C_1]$$

Saddle node bifurcation occurs at $\mu = \mu^*$ when (i) $J_c(\mu^*)$ is nonsingular, (ii) $J_x(\mu^*)$ has one real eigenvalue that crosses the imaginary axis of the complex plane, and (iii) certain transversality conditions hold.

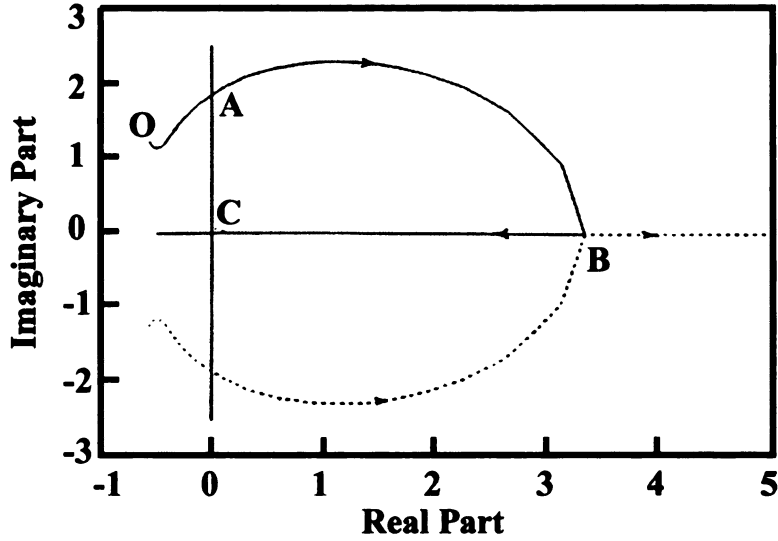
Hopf bifurcation occurs at $\mu = \mu^*$ when (i) $J_c(\mu^*)$ is nonsingular, (ii) $J_x(\mu^*)$ has one pair of imaginary eigenvalues with zero real parts, and (iii) certain transversality conditions hold. There are two different Hopf bifurcations: (a) supercritical Hopf bifurcation which occurs when a stable limit cycle exists around an unstable equilibrium point and the stable limit cycle grows as μ moves away from μ^* ; (b) subcritical Hopf bifurcation occurs when an unstable limit cycle exists around a stable equilibrium point and the orbit size shrinks to zero as μ approaches μ^* .

Singularity induced bifurcation occurs when the equivalent differential Jacobian matrix $J_x(\mu)$ is nonsingular with eigenvalues crossing from the right half plane to the left half plane or vice versa by going through infinity, rather than across the imaginary axis. At this point, one real eigenvalue of the system is at infinity and the rest of them are bounded [45, 4].

A sequence of bifurcations generally causes voltage collapse. A commonly observed sequence of bifurcations [35] is shown in Figure 1.5.



(a) P-V Curve



(b) Critical Modes Movement

Figure 1.5 A Typical bifurcation sequence

Hopf bifurcation is followed by node focus bifurcation, singularity induced bifurcation and saddle node bifurcation. Such a bifurcation sequence has been observed in several example systems [9, 35]. The exact point where blackout is inevitable has not been established and may be at the point of node focus bifurcation, and may be at the point of singularity induced bifurcation. The point of singularity induced bifurcation is certain to result in a blackout. Since [6] has shown that

(1) the algebraic model can be broken into coherent bus groups called voltage control areas where each has a unique voltage collapse problem.

(2) There is a unique eigenvalue λ_k of the Jacobian J associated with each coherent bus group.

(3) The voltage collapse for any coherent bus group occurs where certain subsets of the generator excitation controller are overridden by maximum excitation limiters, and thus

lose control of voltage, and unable to provide additional reactive supply. The subset of generators associated with the voltage collapse in a voltage control area is called the associated reactive reserve basin.

(4). The reactive reserve basins are nested subsets of generators. It has been proven [11] that exhaustion of reactive reserve via MXL action on each of the generators in the reactive reserve basin causes the eigenvalue associated with the voltage control area to approach zero.

(5). It has been shown via simulation [11] that exhaustion of some small reactive reserve basin in a nested set causes a cascading exhaustion of reserve and MXL action that loses voltage control on all of the generators in larger and larger reactive reserve basins. This causes several eigenvalues of voltage control areas associated with larger and larger reactive reserve basins to approach zero. This implies a sequence of singularity induced bifurcation can occur.

The classical voltage instability problem, that caused first known voltage collapse in Electricite de France in 1978, occurred long before the development of MXL and DC regulators. This classical voltage instability problem occurred when overexcitation relays disabled that excitation control system because there was no MXL to override the excitation control system without disabling its stabilizing effects that include (i) damping oscillations (ii) overcoming armature reaction effects and (iii) manual control effects that can reduce that reactive power output of the generator after overexcitation limiter relay disable the excitation control system. The bifurcation subsystem in a generator without an excitation control system is for the saddle node bifurcation that produces instability has been shown to be the flux decay state $\Delta E'_q$ in [32]. The instability in $\Delta E'_q$ is assumed to describe the voltage collapse produced in Electricite de France. It will be shown that instability in $\Delta E'_q$ describes a voltage instability that in itself is not voltage collapse but inevitably produces the singularity induced bifurcation that does produce voltage collapse. The response of the $\Delta E'_q$

state as this voltage collapse occurs due to the bifurcation sequence of saddle node bifurcation followed by singularity induced bifurcation will be described in this thesis. The analysis of how the algebraic equations can experience voltage instability is needed in Chapter 4 before the resultant dynamic response can be described in Chapter 5.

The development of the dc regulator and the maximum excitation limiter was felt to eliminate the possibility that this classical voltage instability could occur. The analysis and simulation results in Chapter 3 shows that sufficiently large interarea oscillation produced by Hopf bifurcation will disable the MXL and cause the excitation control system to be disabled. The classical voltage collapse produced by saddle node bifurcation inevitably followed by singularity induced bifurcation thus not only describe the Electricite de France voltage collapse but also the three voltage collapse problems on the WSCC system where large interarea oscillations existed before the equipment outage that produced the three cascading voltage collapse problems on this system.

The results in [5] suggest that the loss of control and clogging voltage instability have a counterpart in the differential or differential algebraic model. Clogging voltage instability or algebraic bifurcation which occurs in the distribution system and remote to the location of any generator has little or no impact on generator reactive generation as would singularity induced bifurcation. Clogging voltage instability or algebraic bifurcation is understood solely from load flow based results in [5] and is not studied in this thesis. Singularity induced and saddle node bifurcation are two distinctly different differential algebraic model manifestation of loss of control voltage instability in a load flow model. Singularity induced and saddle node bifurcation have very different dynamic behavior when they can occur [45]. The differences in dynamic behaviors of saddle node bifurcation and how saddle node bifurcation may inevitably cause singularity induced bifurcation are investigated in this thesis. This sequence of bifurcation may provide a recognizable signature, a negative spike in bus voltage and real power transfer, that has been observed

on the WSCC system for each of the three major blackouts on December 14, 1994, July 2, 1996 and August 10, 1996.

A recent paper [11] established that the saddle node bifurcation which occurs in the flux decay dynamics is the description of the classic voltage collapse problem. It concluded that: when the excitation control system is completely disabled via an field current limiter relay without loss of PQ or PV controllability, a reduction in generator internal voltage is proven to occur due to increase of reactive load where an increase in internal voltage would occur if the excitation control system (ac regulator) were present. If loss of PV controllability occurs when the field current limiter relay disables the ac regulator, the internal voltage $E'_q(t)$ dynamics are proven to be unstable. A slow decline in $E'_q(t)$ is evident in a simulation [11]. This voltage decline may be due to saddle node bifurcation. Conditions for loss of PV controllability are not well understood and will be investigated further in this thesis. Conditions for the excitation control system to be disabled by an exciter limiter relay is also not well understood and will be investigated in this thesis.

The loss of PV controllability may cause the slow decline in $E'_q(t)$ dynamics; undoing the effects of the dc regulator to maintain voltage and reactive output. Although results in [8] suggest such behavior, there are no theory or simulation results to confirm such behavior. This thesis will attempt to prove that $E'_q(t)$ is reduced if PV controllability is lost and the ac regulator is disabled by the field current limiter relay.

It has not been proven that voltage collapse will necessarily occur when a single generator exciter is disabled by field current limiter relay and a loss of PV controllability occurs. The instability in $E'_q(t)$ reduces voltage dynamically and may reduce $Q_g(t)$ out of the generator that can ultimately cause loss of PQ controllability. Loss of PQ controllability is proven to cause instability in generator flux decay dynamics and cause a dynamic increase in $E'_q(t)$ [11]. A simulation result in [8], however, appears to suggest a very rapid drop in $E'_q(t)$ before PQ controllability is lost followed by a rapid rise in both after PQ

controllability is lost. This behavior and the reason for it will be investigated theoretically and experimentally. This rapid change in voltage appears as a spike and could trigger armature current limiter relays or undervoltage relays that trip generators off line.

1.5 Hypotheses

According to the literature study concerning the WSCC system blackouts above, we have the following hypotheses:

(1) There may exist a new kind of voltage collapse problem which is totally different from the voltage stability problems which are currently understood and for which the dc regulator and Maximum Excitation Limiter have been designed to overcome;

(2) The current MXL is unable to limit the field current level due to the existence of interarea oscillations, as will be proven theoretically and confirmed through simulation in Chapter 3;

(3) The overexcitation protection relays trip off the MXL and ac regulator to use the dc regulator or manual control due to the malfunction of MXL in reducing field current. These relays prevent the generators from damage due to rotor overheating;

(4) When the excitation control system is disabled without loss of PQ controllability or PV controllability, a reduction in voltage in the transmission network can be initiated due to increase in reactive load. Since the dynamics are stable, the dc regulator can increase V_F , I_{fd} and Q_G if needed;

(5) If a slow loss of PV controllability [15] occurs when the excitation control system is disabled, it will cause immediate saddle node bifurcation in flux decay dynamics and thus loss of stability. The instability drives the internal voltage $E'_q(t)$ toward zero. It is

anticipated that generator armature current relays may but not necessarily trip the unit off line. It is believed that the generator armature current relays may be one explanation on what tripped the McNary station generators off the system in the August 10, 1996 blackout;

(6) If PQ controllability [15] is slowly lost as $E'_q(t)$ decline, $E'_q(t)$ will decline more rapidly as loss of PQ controllability approaches;

(7) If a loss of PQ controllability occurs, singularity induced bifurcation can occur. The internal voltage response $E'_q(t)$ becomes stable and rapidly increasing for generators with active excitation control systems as well as for those generators where excitation control systems are disabled. The negative side of the voltage spike in voltage $E'_q(t)$ thus occurs as loss of PQ controllability approaches and finally occurs, the positive side of the spike occurs after loss of PQ controllability occurs. This spike is very likely the spike observed on the WSCC system during the July 2, 1996 and August 10, 1996 blackouts;

(8) After the unstable generators are tripped off line, additional generators will try to pick up the reactive power from the unstable generators as well as the decreased shunt capacitive supply and increased network losses, the field current of these generators will reach their limits and these additional generators will experience the same sequence of bifurcations on those generators that initially get tripped. As a result, a spreading uncontrollable voltage collapse will occur.

These hypotheses are developed based on (a) observations of the time responses of the three recent blackouts on the WSCC system, (b) partially on the theory developed in [11] that describes (i) what causes instability in the generator flux decay dynamic when excitation control systems are disabled and the effects on $\Delta E'_q(t)$, (ii) what causes instability in generator flux decay dynamics when the excitation control systems are active, and (c) partially on the extensions of that theory given in this thesis that more clearly

describes what appears to have caused these three blackouts. The extensions fall into three separate contributions.

(A) Theoretical analysis and simulation results, that show the maximum excitation limiters are disabled by sufficiently large oscillations, are given in Chapter 3 of this proposal. The theory establishes why and when (the size of the oscillation compared to the size of the violation of the continuous rating field current limit) the disablement occurs. Large interarea oscillations existed on the WSCC system before the December 1994, July 1996 and August 1996 blackouts as shown in subsection 1.4 suggests that the maximum excitation limiters may have been disabled and the overexcitation limiter relays may have acted to disable certain excitation control systems and ultimately caused the tripping of generators. The tripping of the McNary station generator unit prior to the voltage spike are very likely to have occurred due to the phenomenon discussed in chapter 3.

(B) Extension of results in [15] that separate PV controllability of ΔQ_G into voltage PV controllability and load PV controllability based on control of ΔQ_G using $\Delta E'_q$ and ΔQ_L respectively. Similarly, PQ controllability of load bus voltages ΔV is broken into voltage PQ controllability and load PQ controllability based on control of ΔV using $\Delta E'_q$ and ΔQ_L respectively. It is proven that if load PQ controllability is lost and other conditions are satisfied, then voltage PQ controllability, voltage PV controllability and load PV controllability are lost. It is also proven that loss of load PQ controllability can occur if shunt capacitive susceptance is added to every bus in a voltage control area, and that the margin to the point of loss of load PQ controllability increases for the addition of shunt inductive susceptance. It is shown that loss of voltage PV controllability can occur before loss of load PQ controllability occurs. Finally, the test matrix elements for $S_{Q_L V}^{-1}$, S_{VE} and $S_{Q_G Q_L}$ associated with a voltage control area, that slowly progresses toward loss of load PQ controllability, can approach infinity, discontinuously change to negative infinity, and then increase toward zero. These properties of the algebraic submodel are all needed to

prove the reasons why stability is lost and why a sharp narrow spike in voltage occurs that was observed in the recorded and simulated responses of the WSCC system for the three recent blackouts. These results are given in Chapter 4 of this thesis.

(C) Prove where and why stability in $\Delta E'_q$ dynamics is lost when the MXL is disabled by oscillations and the overexcitation limiter relay disables the excitation control system. Loss of voltage PV controllability in a voltage control area, that can happen long before loss of load PQ controllability occurs in that voltage control area, causes instability in $\Delta E'_q$ dynamics. The system is shown to be stable if voltage PV controllability holds in the voltage control area of the generator internal bus where the excitation control system is disabled. The unstable response is proven to cause voltage $\Delta E'_q$ on the generator to approach zero.

(D) Prove that this instability in $E'_q(t)$ is like computing a Q-V curve at the generator internal bus if $\{S_{QGE}\}_{ii} < 0$ and $\sum_{j=1}^M [S_{QGE}]_{ij} < 0$ and load PV controllability still holds.

This dynamically administered Q-V curve stress test is proven to lead inevitably to (i) loss of load PQ controllability and bifurcation of the algebraic submodel, and (ii) singularity induced bifurcation of the differential algebraic model.

(E) Prove that loss of load and voltage PQ controllability in a voltage control area causes instability in generators with active excitation control systems in that voltage control area and a rising voltage $\Delta E'_q$.

(F) Prove that slow continuous loss of load PQ controllability in a voltage control area causes a sharp negative spike in $\Delta E'_q$ on a generator with its excitation control system disabled. The slow development of the loss of load PQ controllability causes voltage $\Delta E'_q$ to drop sharply, and a sharp rise in $\Delta E'_q$ occurs after load PQ controllability is lost.

(G) Show that a saddle node bifurcation followed inevitably by a singularity induced bifurcation occurs when the excitation control system is disabled and a loss of voltage PV controllability occurs.

The results in (C-G) are contained in Chapter 5 of this thesis and are proven theoretically and confirmed via simulation results.

1.6 Relevant Literatures

Sensitivity analysis has been used to assess proximity to bifurcation at an equilibrium point. Sensitivity becomes large at the point of bifurcation [56, 57]. Trajectory sensitivity has been used to assess proximity to the boundary of region of attraction [56, 57].

Costi [15] used specific sensitivity matrices to assess proximity to bifurcation in the algebraic model of a power system.

Hu [8] related the network sensitivity matrices to assessing stability of the trajectory on a linearized transient stability model. The network sensitivity matrices were related to controllability of the voltage at load buses and the generation at generator buses. The criteria for controllabilities were based on experience of the requirements for stable behavior in the network.

The sensitivity matrices for controllability are further investigated in chapter 4 of this thesis in order to describe their behavior which affects the stability of the linearized transient stability model. The effects of the behavior of the controllability matrices are investigated in chapter 5.

CHAPTER 2

POWER SYSTEM MODELING

2.1 A General Power System Model

A general power system model, which includes mechanical dynamics, flux decay dynamics, excitation control system dynamics, and real and reactive power balance equations, can be used to test for power system voltage instability. This general power system model consists of two different kinds of nonlinear equations: one is a set of nonlinear differential equations which represents the dynamics of the generator, the other is a set of nonlinear algebraic equations which represents the real and reactive power balance equations for each bus in the network. This model has the following form:

$$M_0 \ddot{\delta} + D_0 \dot{\delta} + F_G(\delta, \theta, E'_q, V_L, y_2) - P_G = 0 \quad (2.1)$$

$$F_L(\delta, \theta, E'_q, V_L, y_2) - P_L = 0 \quad (2.2)$$

$$\dot{E}'_q + G_G(\delta, \theta, E'_q, V_L, y_2) = 0 \quad (2.3a)$$

$$G_L(\delta, \theta, E'_q, V_L, y_2) - Q_L = 0 \quad (2.3b)$$

$$\dot{y}_2 + H(\delta, \theta, E'_q, V_L, y_2) = 0 \quad (2.4)$$

An output equation indicates the reactive generation at the generator internal buses satisfies:

$$G_Q(\delta, \theta, E'_q, V_L, y_2) - Q_G = 0 \quad (2.3c)$$

where δ is the generator angle referenced to a synchronous rotating reference frame and E'_q is a voltage proportional to generator flux linkage; θ and V_L are the angle and voltage at generator terminal, generator transformer high side, and load buses; y_2 is the state of the excitation control system and power system stabilizer dynamics. Equation (2.1) represents generator internal dynamics, equation (2.2) represents real power balance at all other buses in the system, equation (2.3a) is the flux decay differential equations, equation (2.3b) is reactive power balance at all other buses in the system, and equation (2.4) is the generator excitation control system and power system stabilizer dynamics.

The real and reactive power balance equation (2.2) and (2.3b) are:

$$P_k = V_k \sum_{m=1}^n (G_{km} V_m \cos \theta_{km} + B_{km} V_m \sin \theta_{km})$$

$$Q_k = V_k \sum_{m=1}^n (G_{km} V_m \sin \theta_{km} - B_{km} V_m \cos \theta_{km})$$

At any parameter pattern and level $\mu = \mu_e$, the solution (X_e) is a solution to:

$$F(X_e, \mu_e) = 0$$

where:

$$X = \begin{bmatrix} \delta \\ \theta \\ E'_q \\ V_L \\ y_2 \end{bmatrix} \quad \text{and} \quad F(\delta, \theta, E'_q, V_L, y_2) = \begin{bmatrix} P_G \\ P_L \\ G_G \\ G_L \\ H \end{bmatrix} \quad (2.5)$$

The Jacobian of (2.5) is:

$$J = \frac{\partial F}{\partial X}(\delta, \theta, E'_q, V_L, y_2)$$

$$= \begin{bmatrix} A_1 & B_1 & C_1 & D_1 & E_1 \\ A_2 & B_2 & C_2 & D_2 & E_2 \\ A_3 & B_3 & C_3 & D_3 & E_3 \\ A_4 & B_4 & C_4 & D_4 & E_4 \\ A_5 & B_5 & C_5 & D_5 & E_5 \end{bmatrix} \quad (2.6)$$

2.2 Excitation Control System Model

The block diagram of a excitation control system model is shown in Figure 2.1. $G_a(s)$ is represents the transfer function of the AVR (Automatic Voltage Regulator) and any type of exciter, $\frac{K_3}{1+sT_3}$ is the transfer function of the field circuit, $\frac{1}{1+sT_R}$ is the transfer function of the voltage transducer, and $G_{ps}(s)$ is the transfer function of the power system stabilizer.

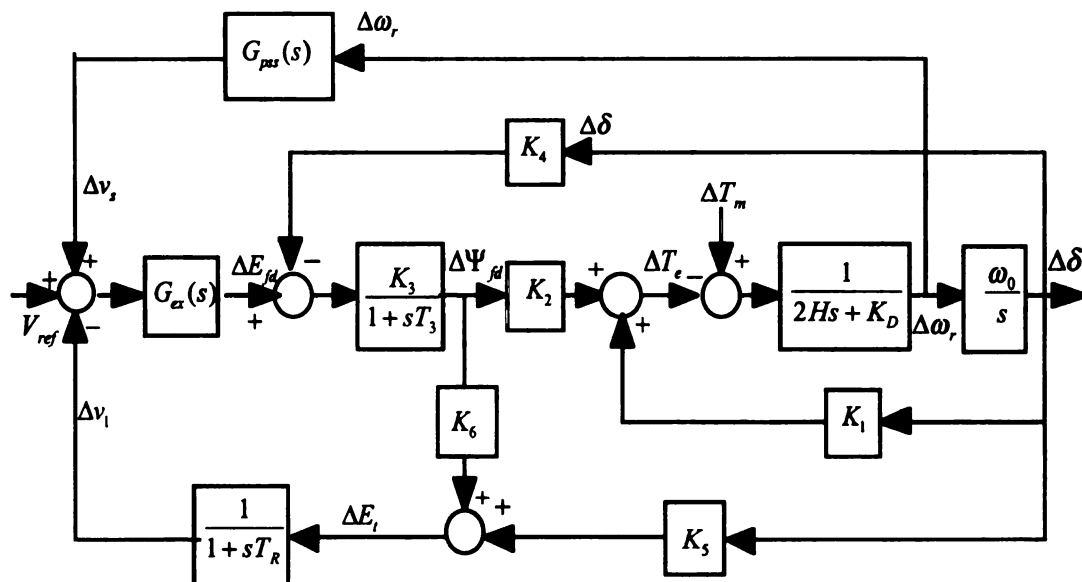


Figure 2.1 Excitation control system model

It is similar to Figure 1.1 except that the dc regulator and the overexcitation limiter, underexcitation limiter, and volt/hertz relays are omitted. The model of the generator inertial dynamics (2.1), flux decay dynamics (2.3a) and generator excitation control system, power system stabilizer and voltage sensor dynamics (2.4) are shown in Figure 2.1.

The maximum excitation limiter is now described that works through the summer of the excitation control system as shown in Figure 2.2. The role of the maximum excitation limiter is described in section 2.4.

2.3 Maximum Excitation Limiter Model

A typical maximum excitation limiter model is shown below

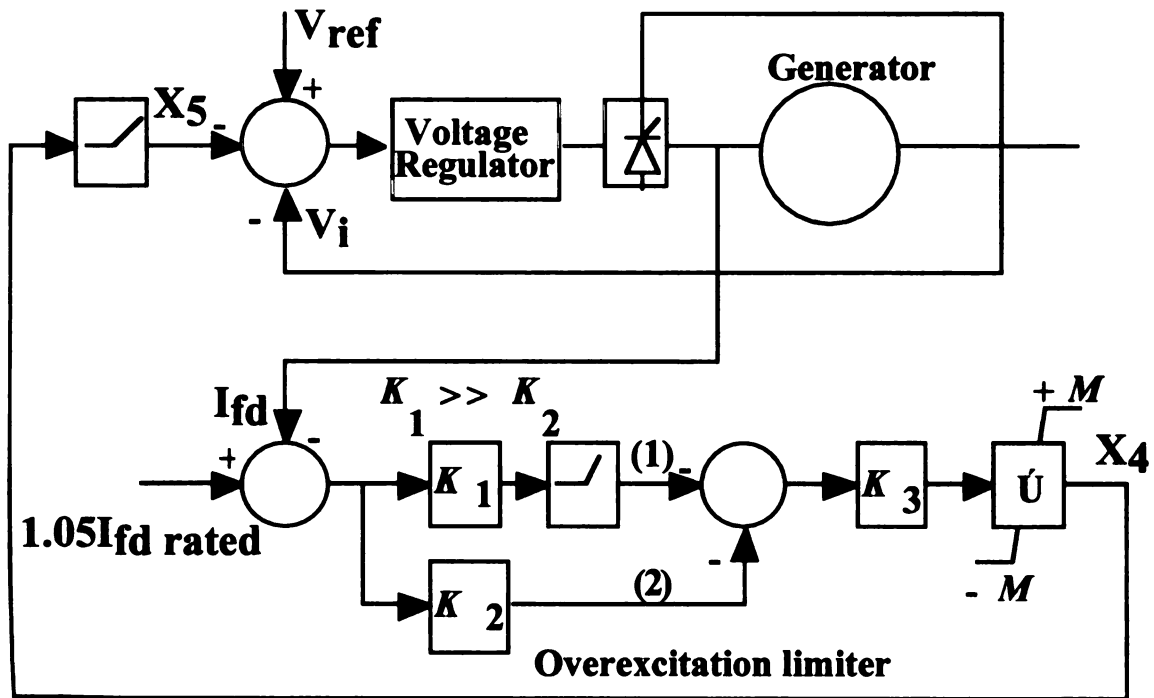


Figure 2.2 Model of maximum excitation limiter

During normal conditions with field current less than the setpoint (typically 105% of rated field current), path 1 and 2 both force the integrator to its lower limit(-M). The input to the voltage regulator summing junction (X_5) is zero. If field current is above the setpoint, path 2 drives the integrator towards a positive value. Once the integrator output becomes positive, the voltage regulator will start to reduce field current. For a step increase in field current above the setpoint, the time to the start of current limiting will be:

$$t = \frac{M}{K_2 \bullet K_3 \bullet (I_{fd} - 1.05I_{fd \text{ rated}})}$$

The parameters can be adjusted so that this time approximates the desired time to obtain field current limiting. Once field current is reduced to the setpoint, path 1 rapidly resets the integrator output X_4 to -M.

2.4 Power System Load Model

Load dynamic response is an important mechanism of power system voltage stability, load modeling is a difficult problem because power system loads are aggregates of many different devices such as fluorescent and incandescent lamps, refrigerators, heaters, compressors, motors, furnaces, and so on. The exact composition of load is not only difficult to estimate, but also changes depending on many factors including time, weather conditions and state of the economy.

The load models are traditionally classified into two broad categories: static load models and dynamic load models.

The static characteristics of load are usually classified into three categories: constant power, constant current and constant impedance load. A widely used load characteristic is the well-known exponential load, which has the general form:

$$P = zP_0 \left(\frac{V}{V_0} \right)^\alpha$$

$$Q = zQ_0 \left(\frac{V}{V_0} \right)^\beta$$

where z is a dimensionless demand variable, V_0 is the reference voltage, and the exponents α and β depend on the type of load (motor, heating, lighting, etc.). Note that zP_0 and zQ_0 are the active and reactive powers consumed under a voltage V equal to the reference V_0 and relate to the amount of connected equipment. These have been called nominal load powers, in contrast to the consumed powers P and Q .

When $\alpha = \beta = 2$,

$$P = zP_0 \left(\frac{V}{V_0} \right)^2$$

$$Q = zQ_0 \left(\frac{V}{V_0} \right)^2$$

it is called constant impedance load.

When $\alpha = \beta = 1$,

$$P = zP_0 \left(\frac{V}{V_0} \right)$$

$$Q = zQ_0 \left(\frac{V}{V_0} \right)$$

it is called constant current load.

When $\alpha = \beta = 0$,

$$P = zP_0$$

$$Q = zQ_0$$

it is called constant power load.

An alternative load representation is based on summing up load components which have the same exponents. A special case is made up of three components: constant impedance, constant current and constant power, it is given by the following quadratic expressions:

$$P = zP_0 \left[a_P \left(\frac{V}{V_0} \right)^2 + b_P \left(\frac{V}{V_0} \right) + c_P \right]$$

$$Q = zQ_0 \left[a_Q \left(\frac{V}{V_0} \right)^2 + b_Q \left(\frac{V}{V_0} \right) + c_Q \right]$$

where $a_P + b_P + c_P = a_Q + b_Q + c_Q = 1$, while zP_0 and zQ_0 are the load real and reactive powers consumed at the reference voltage V_0 .

Even though the use of static load models is often satisfactory, there are, however, many cases where it is necessary to account for the dynamics of load components. For example, study of systems with large concentrations of motors requires representation of load dynamics. Researchers developed various kinds of dynamic load models [30, 38, 39, 40, 41] to represent the dynamic characteristics of the system loads. Since this subject is beyond the scope of this thesis, it is not going to be discussed in detail here.

It is worth noting that load can transition between dynamic load model and static load model. For example, the static models mentioned above can be accomplished using the generic non-linear dynamic model which satisfies:

$$T_P \dot{Z}_P = \left(\frac{V}{V_0} \right)^{\alpha_s} - Z_P \left(\frac{V}{V_0} \right)^{\alpha_t}$$

$$T_Q \dot{Z}_Q = \left(\frac{V}{V_0} \right)^{\beta_s} - Z_Q \left(\frac{V}{V_0} \right)^{\beta_t}$$

This change in load models is needed later to discuss why specific kinds of bifurcations occur and do not occur.

CHAPTER 3

PROBLEM ANALYSIS

A large negative voltage spike was observed on the WSCC system shortly after the McNary station generators were tripped. This large negative voltage spike could have been resulted when the AC regulator portion of the automatic voltage regulator is disabled and the network violates rather weak controllability conditions at generator buses [11, 57, 58, 59]. The theory in [11] indicates the unstable flux decay dynamics on the McNary substation generators, that resulted from disablement of the AC regulator and loss of network controllability on these generators, caused a self destructive stress test to be administered. This stress produces the negative voltage spike and ultimately causes the cascading instability of additional subsystems that may have produced the August 10, 1996 blackout on the WSCC system. The network controllability conditions are often violated in many power systems but have no negative consequences because the AC regulator overcomes this loss of controllability. Failure of the MXL to reduce field current followed by disablement of the AC regulator via an Overexcitation Protection Relay leaves the system vulnerable to a cascading instability of bifurcation subsystems that lead to blackout. The understanding of how the MXL fails to reduce field current is studied in this chapter to understand how and why this sequence occurs. This chapter also provides suggestions on what may be done to avoid such failures in the Maximum Excitation Limiter that lead to OXP relay tripping of the AC regulator, instability in the generator dynamics that administer a self destructive stress test and finally cascading instability of bifurcation subsystems and associated network and generator protective relaying actions.

3.1 Disablement of Current MXL due to Oscillation

The traditional overexcitation limiting and protection mechanism is as follows: The MXL detects the high field current condition and acts through the ac voltage regulator to return the level of excitation to a preset value after a time delay during which overexcitation is permitted. The MXL is supplemented by the Overexcitation Protection (OXP) device. If the MXL function is unsuccessful, the OXP trips the ac regulator after a preset time interval, and then transfers control to a dc regulator and repositions the setpoint to a value corresponding to the rated value. If the tripping of the ac regulator and the repositioning the setpoint has not reduced the field current below $I_{fd\ rated}$, the OXP will also initiate a unit trip after an additional time delay. When oscillation components exist in field current, sometimes the MXL cannot work correctly. This results in the trip of the excitation control system, sometimes, followed by the generator unit trip, and even voltage collapse of the system if the conditions exist as derived in Chapter 5.

3.1.1 Theoretical Analysis

The analysis here is based on the maximum excitation limiter system which is shown in Chapter 2 (Figure 2.2).

Suppose that the field current I_{fd} is composed of a constant component I_0 and an oscillating component $I_1 \cos 2\pi ft$, that is,

$$\begin{aligned} I_{fd}(t) &= I_0 + I_1 \cos 2\pi ft \\ &= I_0 + I_1 \cos \delta(t) \end{aligned} \tag{3.1}$$

where

$$\delta(t) = 2\pi ft$$

and f is the frequency of the oscillation observed in voltage, angle and field current.

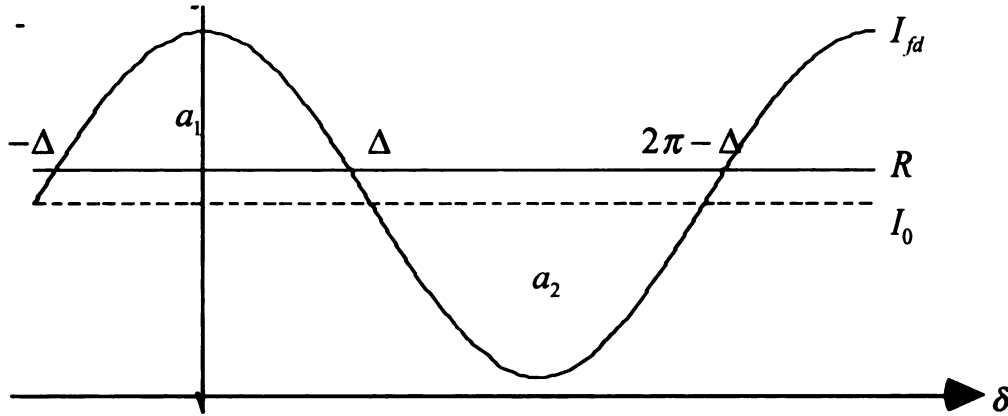


Figure 3.1 I_{fd} with oscillation component

As is shown in Figure 3.1, Δ is determined by

$$I_0 + I_1 \cos \Delta = R \quad (3.2)$$

where R is the continuous field current rating where field current limiting from the MXL occurs. Usually $R = 1.05 I_{fd \text{ rated}}$.

The expressions for the area a_1 (above R) and area a_2 (below R) are now derived, these expressions are then used to analyze the effects on X_4 and X_5 in Figure 2.2. Note that the positive change in X_4 in Figure 2.2 for $I_{fd} > R$ over $(-\Delta, \Delta)$ is $A_1 = K_1 a_1$ and the negative change in X_4 for $I_{fd} < R$ over $(\Delta, 2\pi - \Delta)$ is $A_2 = (K_1 + K_2) a_2$. If $A_1 > A_2$ for each cycle, then X_4 increases, and X_5 will eventually become positive and reduce the excitation setpoint. If $A_1 < A_2$ for each cycle, then X_4 decreases toward the lower limit $-M$, and X_5 will stay at or decrease to zero.

Area a_1 satisfies

$$\begin{aligned} a_1 &= \int_{-\Delta}^{\Delta} (I_0 + I_1 \cos \delta - R) d\delta \\ &= 2(I_0 \Delta - R\Delta + I_1 \sin \Delta) \end{aligned} \quad (3.3)$$

Noting that $R = I_0 + I_1 \cos \Delta$, a_1 becomes

$$\begin{aligned} a_1 &= 2(I_1 \sin \Delta - \Delta I_1 \cos \Delta) \\ &= 2I_1(\sin \Delta - \Delta \cos \Delta) \end{aligned} \quad (3.4)$$

The change in X_4 over interval $(-\Delta, \Delta)$ is

$$\begin{aligned} A_1 &= K_2 a_1 \\ &= 2I_1 K_2 (\sin \Delta - \Delta \cos \Delta) \\ &= 2I_1 B_1 \end{aligned} \quad (3.5)$$

where

$$B_1 = K_2 (\sin \Delta - \Delta \cos \Delta) \quad (3.6)$$

Area a_2 satisfies

$$\begin{aligned} a_2 &= \int_{\Delta}^{2\pi-\Delta} (R - I_0 - I_1 \cos \delta) d\delta \\ &= (R - I_0)(2\pi - 2\Delta) + 2I_1 \sin \Delta \end{aligned} \quad (3.7)$$

Again noting that $R = I_0 + I_1 \cos \Delta$, a_2 becomes

$$\begin{aligned} a_2 &= 2(\pi I_1 \cos \Delta - \Delta I_1 \cos \Delta + I_1 \sin \Delta) \\ &= 2I_1(\sin \Delta - \Delta \cos \Delta + \pi \cos \Delta) \end{aligned} \quad (3.8)$$

The change in X_4 over interval $(\Delta, 2\pi - \Delta)$ is

$$\begin{aligned} A_2 &= (K_1 + K_2) a_2 \\ &= 2I_1 (K_1 + K_2) (\sin \Delta - \Delta \cos \Delta + \pi \cos \Delta) \\ &= 2I_1 B_2 \end{aligned} \quad (3.9)$$

where

$$B_2 = (K_1 + K_2) (\sin \Delta - \Delta \cos \Delta + \pi \cos \Delta) \quad (3.10)$$

According to the value of the constant component I_0 and the preset value R (usually $R = 1.05I_{fd \text{ rated}}$), it can be classified into three cases:

Case 1: $I_0 < R$

When $I_0 < R$, Δ must be less than $\frac{\pi}{2}$. Since $A_1 < A_2$ always holds, the oscillation component does not affect X_5 in Figure 2.2 and it remains zero. The voltage regulator set point is not affected and the excitation system works fine. (It may make X_4 go to the lower limit value faster).

Case 2: $I_0 > R$

When $I_0 > R$, Δ must be greater than $\frac{\pi}{2}$. For this case, we have $A_1 > A_2$, $A_1 = A_2$ and $A_1 < A_2$ three subcases.

(i) If $A_1 > A_2$, the MXL is able to detect the high field current condition and reduces the voltage setpoint on the AC regulator as expected(it may speed up the upper limiting);

(ii) If $A_1 < A_2$, the MXL will mistaken the high field current ($I_0 > R$) as low field current and not reduce the voltage setpoint on the AC regulator, so it fails. This is where the oscillation component will disable and confuse the MXL, and cause the overexcitation protection relay to trip the excitation control system and the maximum excitation limiter;

(iii) If $A_1 = A_2$, the oscillation effects are cancelled out, the MXL does not increase or decrease X_4 thus X_5 even though $I_0 > R$. If $X_5 = 0$, then the field current limit is going to be violated, and the MXL does not reduce I_{fd} . As a result, the excitation control system will be tripped by the overexcitation protection relay. If $X_5 > 0$ and this value is sufficiently large, then X_5 will reduce I_{fd} to below R . to prevent unit tripping If $X_5 > 0$ and this value is not sufficiently large, then the excitation control system must be tripped by the

overexcitation protection relay to prevent thermal damage to the generator field winding or the rotor.

Case 3: $I_0 = R$

When $I_0 = R$, Δ must be less than $\frac{\pi}{2}$. Since $A_1 < A_2$ always holds, the MXL always goes to lower limiting as it should. In this case, X_4 can be affected, but X_5 is not affected.

3.1.2. Analysis of Boundary Δ^* where MXL Operates Correctly and Malfunctions

Suppose that Δ^* is the boundary point where $A_1 = A_2$, or equivalently, $B_1 = B_2$. The value of Δ^* can be determined by the following equations:

$$\begin{cases} I_0 + I_1 \cos \Delta^* = R \\ B_1 = B_2 \end{cases} \quad (3.11)$$

These equations are equivalent to

$$\begin{cases} I_0 + I_1 \cos \Delta^* = R \\ K_2 (\sin \Delta^* - \Delta^* \cos \Delta^*) = (K_1 + K_2) (\sin \Delta^* - \Delta^* \cos \Delta^* + \pi \cos \Delta^*) \end{cases} \quad (3.12)$$

Δ^* depends on K_1 and K_2 based on (3.12). For example, if we set $K_1 = 100$ and $K_2 = 1$, we obtain

$$\begin{aligned} B_1 &= \sin \Delta^* - \Delta^* \cos \Delta^* \\ B_2 &= 101 (\sin \Delta^* - \Delta^* \cos \Delta^* + \pi \cos \Delta^*) \end{aligned}$$

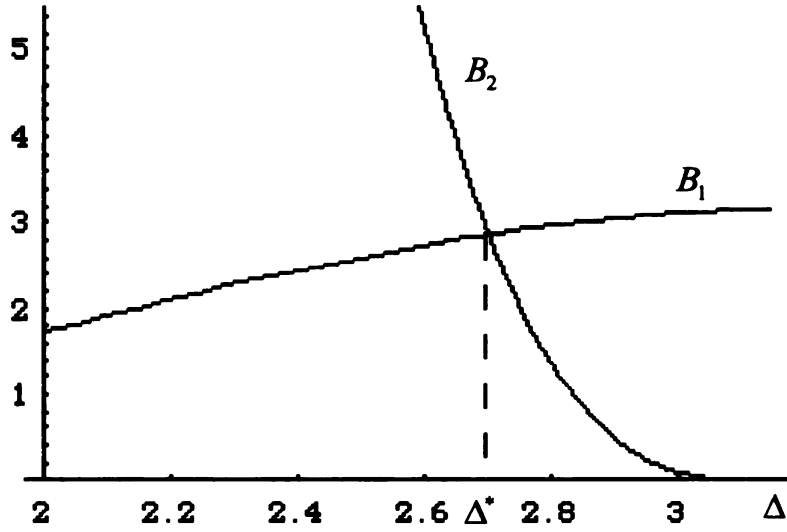


Figure 3.2 Plot for determining Δ^*

The plots of B_1 and B_2 are shown in Figure 3.2. From the plot, we get $\Delta^* = 2.698$. If we set $I_{fd rated} = 1.0$, $R = 1.05$, then, from equation (3.12), we obtain the relationship between I_0 and I_1 when $\Delta^* = 2.698$

$$I_0 = 1.05 - \cos(2.698)I_1 \quad (3.13)$$

Equation (3.13) that provides a boundary in I_0, I_1 space for when MXL operates correctly and when it malfunctions is shown graphically in Figure 3.3.

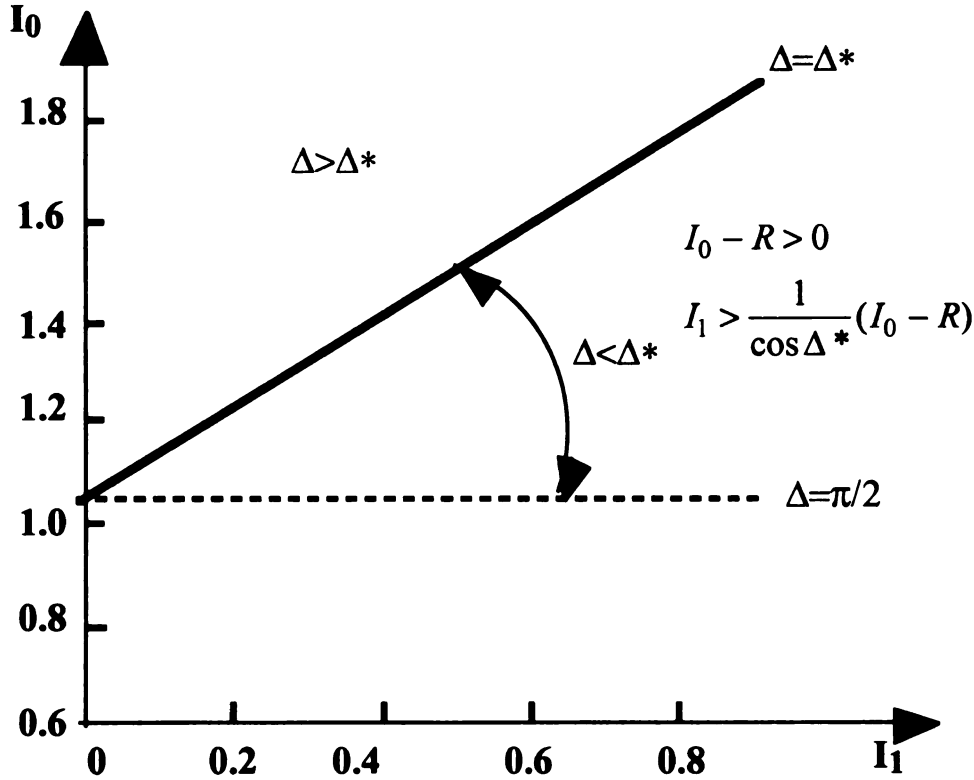


Figure 3.3 Relationship between I_0 and I_1

Since the Maximum Excitation Limiter works incorrectly over $\pi/2 < \Delta < \Delta^*$, and the relationship between I_0 and I_1 is given in Figure 3.3, we can conclude that the area indicated by the arrows in Figure 3.3 is where the MXL works incorrectly. When $I_0 > R$, a complete description of when the MXL works correctly and incorrectly is given below in terms of Δ^* :

(a) With oscillation component, MXL works correctly when $\Delta \leq \pi/2$ (or equivalently $A_1 < A_2$ with $I_0 \leq R$) and when $\Delta \geq \Delta^*$ (or equivalently $I_0 > R$ with $A_1 \geq A_2$). The second case $\Delta \geq \Delta^*$ suggests that the MXL will act to alleviate the field current violation;

(b) MXL does not work correctly when $\pi/2 < \Delta < \Delta^*$. (or equivalently $I_0 > R$ with $A_1 < A_2$);

(c) When $\Delta \geq \Delta^*$, so that the MXL is acting correctly, increase in size of oscillation I_1 given a specific value of I_0 will cause $\Delta < \Delta^*$ and thus the MXL to malfunction as shown in Figure 3.3;

(d) When $\pi/2 < \Delta < \Delta^*$, so that the MXL is working incorrectly, increase in average field current value I_0 given a specific value of I_1 will cause $\Delta \geq \Delta^*$ and thus the MXL to operate properly.

3.1.3 Simulation Results

The problem of MXL disablement can be shown clearly by the following simulations.

Case 1: ($I_0 < R, \Delta < \frac{\pi}{2}$)

For this case, the simulation parameters of the MXL shown in Figure 2.2 and the field current expression 3.1 are: $M=1.5, K_1=100, K_2=1, K_3=1, R=1.05, I_0=1.0, I_1=0.2$. Here, $I_0 < R, \Delta < \frac{\pi}{2}$, the MXL should not act, that is, X_5 should remain zero. Figure 3.4 shows that X_4 reaches its lower limit after a time delay because of the integration, and X_5 remains zero for all the time regardless of the existence of the oscillation component. The MXL works correctly.

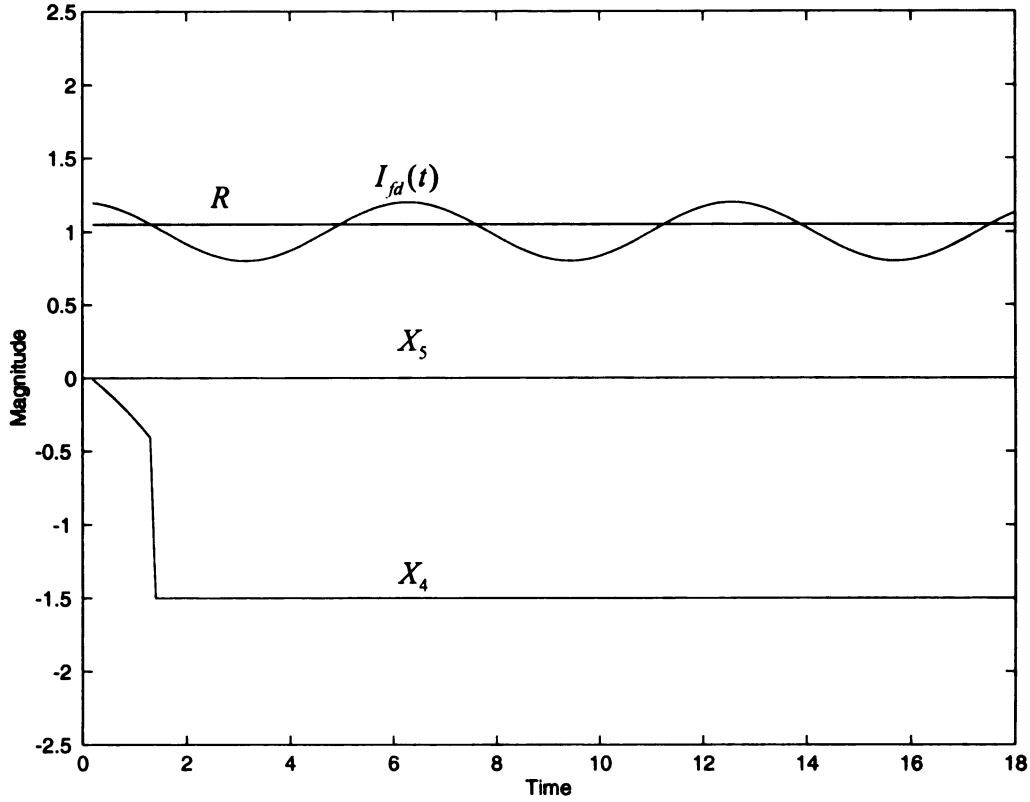


Figure 3.4 The MXL action when $I_0 < R$

Case 2: ($I_0 = R$, $\Delta = \frac{\pi}{2}$)

For this case, the simulation parameters are: $M=1.5$, $K_1=100$, $K_2=1$, $K_3=1$, $R=1.05$, $I_0=1.05$, $I_1=0.2$. Here, $I_0 = R$, $\Delta = \frac{\pi}{2}$, the MXL should not act, that is, X_5 should remain zero. Figure 3.5 shows that X_4 and X_5 go above zero a little for a short time at the very beginning because $X_4 = 0$ at $t = 0$, then X_4 decreases and reaches its lower limit $-M$, and finally oscillates around that lower limit. X_5 remains zero after a short interval where it is positive. Since the positive period for X_4 and X_5 is very short, and the magnitude is negligible, the MXL works correctly as intended.

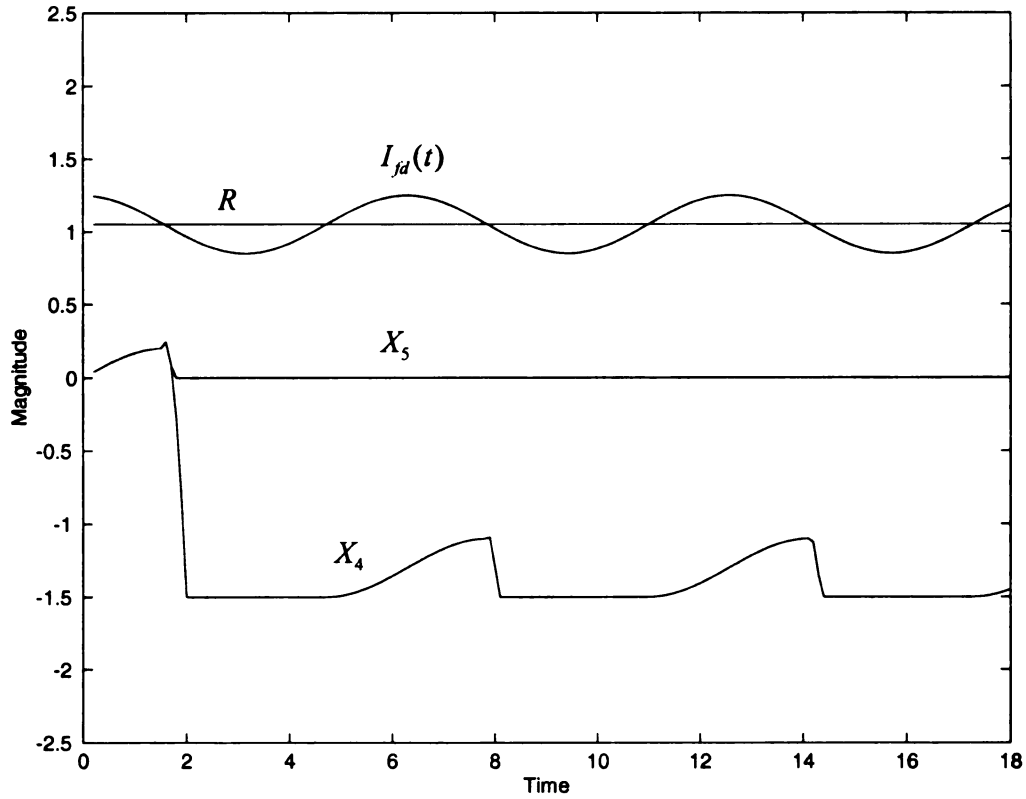


Figure 3.5 The MXL action when $I_0 = R$

Case 3: ($I_0 > R$, $\Delta > \frac{\pi}{2}$)

For this case, the simulation parameters are: $M=1.5$, $K_1=100$, $K_2=1$, $K_3=1$, $R=1.05$, $I_0=1.055$, $I_1=0.2$. Here, $I_0 > R$, $\Delta > \frac{\pi}{2}$ with $A_1 < A_2$, the MXL should act since $I_0 > R$, that is, X_4 and X_5 should be positive and go to the upper limit $+M$ after some time delay if it works correctly. Note that $I_0=1.055$ is just slightly above $R=1.05$, thus Δ is just slightly above $\frac{\pi}{2}$ and less than Δ^* . Δ is within the range where the oscillation disables the MXL. This analysis suggests that the oscillation component keeps $A_1 < A_2$, this makes it impossible for X_4 to keep positive and reach its upper limit. Therefore, X_5 remains zero most of the time and the MXL works incorrectly. Figure 3.6 displays the result that confirms this point.

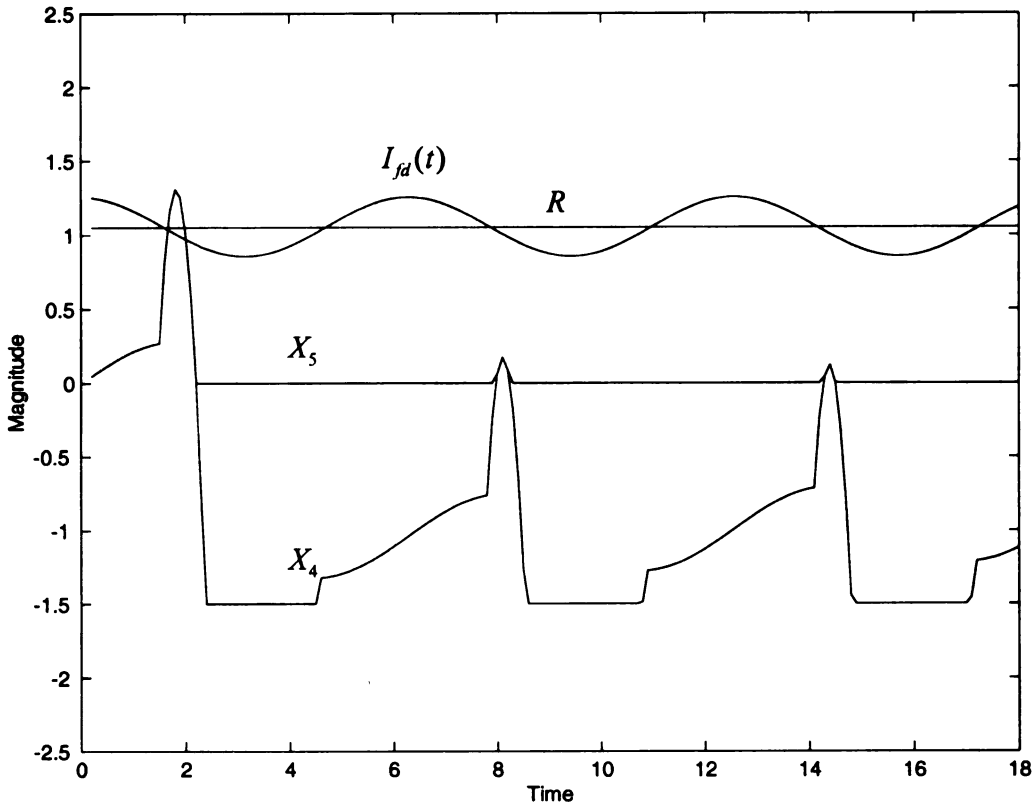


Figure 3.6 The MXL action when $I_0 > R$ but $A_1 < A_2$

Case 4: ($I_0 > R, \Delta > \Delta^*$)

For this case, the simulation parameters are: $M=1.5$, $K_1=100$, $K_2=1$, $K_3=1$, $R=1.05$, $I_0=1.07$, $I_1=0.2$, except that I_0 is increased from 1.05 to 1.07, all the other parameters are the same as those in case 3. Here, $I_0 > R$, $\Delta > \frac{\pi}{2}$ with $A_1 > A_2$, the MXL should act correctly since I_0 is sufficiently greater than R for the particular I_1 value. X_4 and X_5 should be positive and go to the upper limit after some time delay. Since the oscillation component remains small for the $I_0 - R$ value, $A_1 > A_2$, X_4 remains positive and near its upper limit. Therefore, X_5 reaches and remains at its upper limit after a short

time delay and the simulation confirms that the MXL works correctly. Figure 3.7 confirms this analysis.

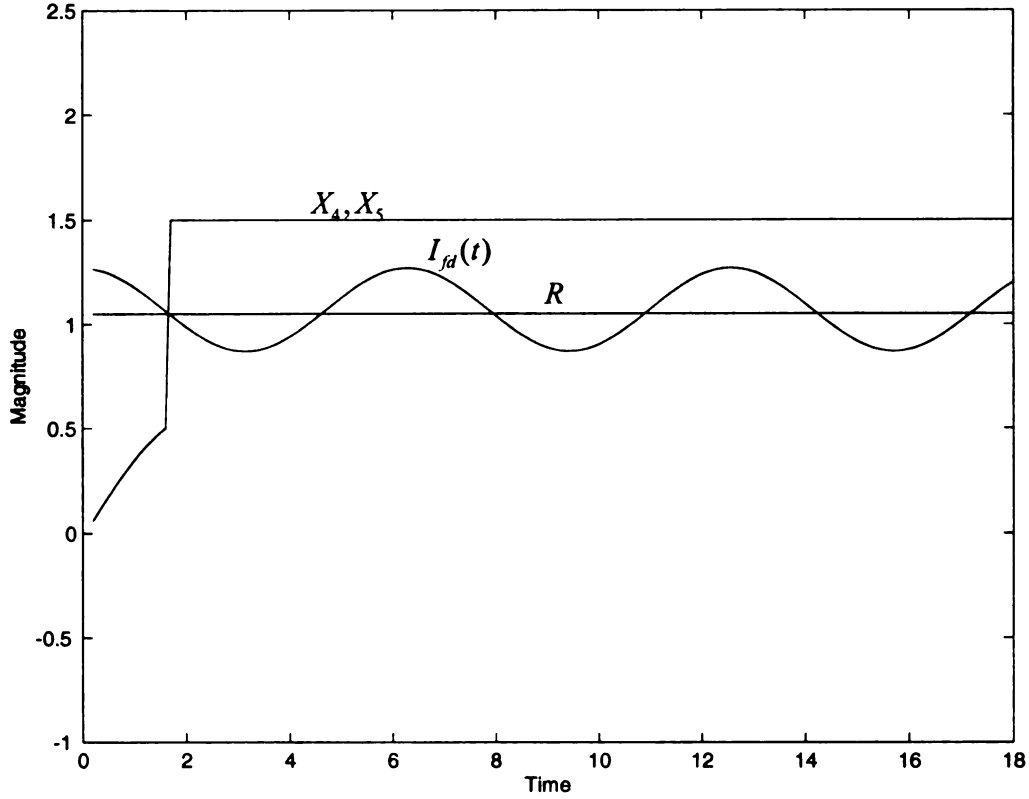


Figure 3.7 The MXL action when $I_0 > R$ but $A_1 > A_2$
(The effect of increasing I_0 for certain I_1)

Case 5: ($I_0 > R$, $\Delta < \Delta^*$ due to increase in I_1)

For this case, the simulation parameters are: $M=1.5$, $K_1=100$, $K_2=1$, $K_3=1$, $R=1.05$, $I_0=1.07$, $I_1=0.4$, except that I_1 is increased from 0.2 to 0.4, all the other parameters are the same as those in case 4. Here, $I_0 > R$, $\Delta > \frac{\pi}{2}$ with $A_1 > A_2$. This case is the same as case 3. From Figure 3.8, it is clear that the MXL does not work correctly.

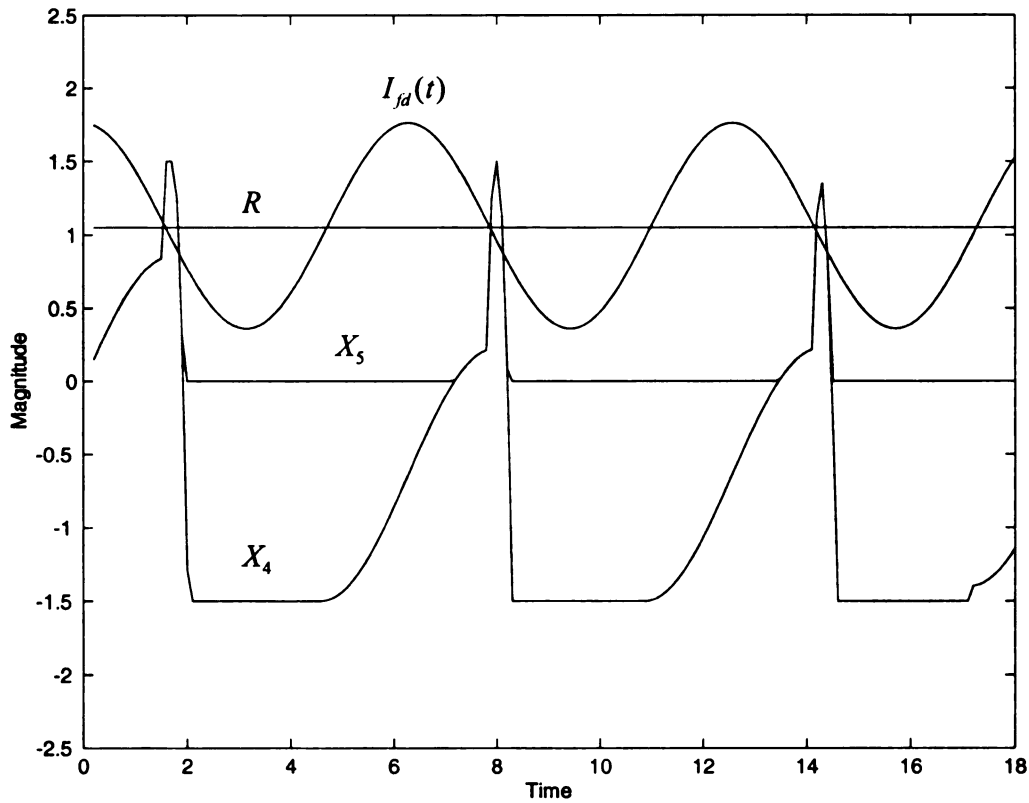


Figure 3.8 The effect of increasing I_1 for certain I_0

These results show that when I_0 is slightly above R with certain amount of oscillation component, the MXL is disabled, but the MXL will again be enabled if I_0 increases sufficiently. Another result is that for any I_0 value, if the magnitude of the oscillation component increases sufficiently, the MXL will be disabled. The large magnitude of the oscillation component (I_1) in the WSCC system for a light stress ($I_0 - R$ small) would suggest why the McNaly station unit excitation control systems to be disabled and the use of overexcitation protection relays to disable the excitation control system and its MXL.

3.2 Excitation Control System Tripping and Unit Tripping

If MXL is unable to limit the field current level due to the existence of oscillations that disable it, the OXP (Overexcitation Protection Relay) will trip the ac regulator to dc regulator or manual control and disable the excitation control system. When the excitation control system is disabled without loss of PQ controllability or PV controllability, the armature reaction on the generator is no longer masked by the excitation control system due to increased load on this generator. Generator internal voltage is reduced due to increased reactive generation output. The reduction in $E'_q(t)$ can cause a significant reduction in voltage in the transmission network, and increased network reactive losses and reduced shunt capacitive supply. This, in turn, is followed by further reduction of internal voltage $E'_q(t)$ due to armature reaction in order to override possible generator response for decrease in network shunt capacitive reactive supply and increase in network reactive losses due to the drop of network voltage. Manual control requires the operator to adjust the field voltage manually so that the generator terminal voltage $E'_q(t)$ and reactive power are about the same as what are produced out of the generator through excitation control system action. A dc regulator attempts to maintain field current at rating level but is not a feedback controller on generator terminal voltage as the excitation control system is. The use of a DC regulator or manual control does not overcome armature reaction that reduces internal voltage.

The complete disablement of the excitation control system and MXL via an overexcitation protection relay for a generator together with a slow loss of PV controllability causes immediate saddle node bifurcation in flux decay dynamics and thus loss of stability [22]. The instability drives the internal voltage to decrease slowly toward zero. As $E'_q(t)$ is reduced, loss of PQ controllability may result in $E'_q(t)$ to decrease more rapidly. Undervoltage relays or armature current relays may trip the unit off line.

If a loss of PQ controllability occurs, singularity induced or saddle node bifurcation can occur. The internal voltage response $E'_q(t)$ is stable and rapidly increasing. The MXL is not generally fast enough to overcome the increase in $E'_q(t)$ by driving the generator excitation control system setpoint to zero and $E'_q(t)$ continues to increase rapidly. As a result, the OXP relay would trip the generator. This is likely what caused the tripping of the McNary station generators during the August 1996 blackout on the WSCC system.

3.3 Uncontrollable Spreading Voltage Collapse

After the unstable generators were tripped off line, additional generators will try to pick up the reactive power from the unstable generators as well as the decreased shunt capacitive supply and increased network losses, the field current of these generators will reach their limits and these additional generators may experience the same sequence as those generators that initially get tripped. As a result, a spreading uncontrollable voltage collapse will occur.

CHAPTER 4

VOLTAGE AND LOAD CONTROLLABILITY

4.1 Introduction

Sensitivity indices have been used to help assess proximity to instability in a load flow model and in linearized mid-term power system stability models from the inception of the investigation of voltage instability at an equilibrium. The use of sensitivity matrices other than sensitivity indices was first adopted in [15] and was applied to both load flow and mid-term stability models. More recently, sensitivity matrices have been used to assess proximity to instability along a transient trajectory [12, 56, 57]. Sensitivity matrix elements have been shown to increase rapidly as the algebraic model, differential algebraic, or differential model equilibrium approaches local bifurcation[12, 56, 57, 58] or when the trajectory of the differential model approaches the boundary of the region of attraction[12, 56, 57].

This chapter utilizes the sensitivity matrices upon which PQ controllability of load buses and PV controllability of generator buses are defined and are related to the sensitivity indices that were developed at the inception of voltage instability research [33, 62]. The condition for PQ controllability of load buses and PV controllability of generator buses is based on common engineering judgement of the conditions that reflect proper control capability and response of a transmission or distribution network.

In this chapter, firstly, the results on PQ and PV controllability in [15] are extended. PV controllability of ΔQ_G is separated into voltage PV controllability and load PV controllability based on $\Delta E'_q$ and ΔQ_L changes respectively. Similarly, PQ controllability of load bus voltages ΔV is broken into voltage PQ controllability and load PQ controllability based on $\Delta E'_q$ and ΔQ_L changes respectively. Secondly, it is shown that the test matrix elements for $S_{Q_L V}^{-1}$, S_{VE} and $S_{Q_G Q_L}$ associated with a voltage control area slowly progress toward loss of load PQ controllability, (a) approach infinity, (b) discontinuously change to negative infinity, and (c) then increase toward zero. Thirdly, It is proven that if load PQ controllability is lost, then voltage PQ controllability, voltage PV controllability and load PV controllability are lost. It is also proven that loss of voltage PV controllability can occur before loss of load PQ controllability occurs. Finally, it is proven that loss of load PQ controllability can occur if shunt capacitive susceptance is added to every bus in a voltage control area, and that the margin to the point of loss of load PQ controllability increases for the addition of shunt inductive susceptance. Each of these results are related to instability in generator flux decay dynamics through simulation results where these behaviors are observed. The simulation results also validate the theoretical results. These theoretical and simulation results are derived in order to theoretically establish (in chapter 5) the time behaviors that lead to production of the sharp negative voltage spike observed in December 1994, July 1996 and August 1996 blackouts on the WSCC system.

4.2 Sensitivity Matrices

For a non-decoupled differential algebraic model

$$\begin{bmatrix} \Delta P_G \\ \Delta P_L \\ \Delta Q_G \\ \Delta Q_L \end{bmatrix} = \begin{bmatrix} A_1 & B_1 & C_1 & D_1 \\ A_2 & B_2 & C_2 & D_2 \\ A_3 & B_3 & C_3 & D_3 \\ A_4 & B_4 & C_4 & D_4 \end{bmatrix} \begin{bmatrix} \Delta \delta \\ \Delta \theta \\ \Delta E'_q/E'_q \\ \Delta V/V \end{bmatrix} \quad (4.1)$$

$\begin{bmatrix} \Delta \delta \\ \Delta \theta \end{bmatrix}$ can be determined by first setting $\begin{bmatrix} \Delta P_G \\ \Delta P_L \end{bmatrix} = 0$ in the first two equations in (4.1)

and solving to obtain:

$$\begin{bmatrix} \Delta \delta \\ \Delta \theta \end{bmatrix} = - \begin{bmatrix} A_1 & B_1 \\ A_2 & B_2 \end{bmatrix}^{-1} \begin{bmatrix} C_1 & D_1 \\ C_2 & D_2 \end{bmatrix} \begin{bmatrix} \Delta E'_q \\ \Delta V \end{bmatrix} \quad (4.2)$$

Substituting $\begin{bmatrix} \Delta \delta \\ \Delta \theta \end{bmatrix}$ in the last two equations in (4.1) produces a reduced model

$$\begin{bmatrix} \Delta Q_G \\ \Delta Q_L \end{bmatrix} = J \begin{bmatrix} \Delta E'_q \\ \Delta V \end{bmatrix} \quad (4.3)$$

where

$$\begin{aligned} J &= \begin{bmatrix} J_{11} & J_{12} \\ J_{21} & J_{22} \end{bmatrix} \\ &= \begin{bmatrix} C_3 & D_3 \\ C_4 & D_4 \end{bmatrix} - \begin{bmatrix} A_3 & B_3 \\ A_4 & B_4 \end{bmatrix} \begin{bmatrix} A_1 & B_1 \\ A_2 & B_2 \end{bmatrix}^{-1} \begin{bmatrix} C_1 & D_1 \\ C_2 & D_2 \end{bmatrix} \end{aligned} \quad (4.4)$$

Here, the sensitivity model can now be derived from (4.4) and has the form

$$\Delta V/V = S_{Q_L V}^{-1} \Delta Q_L + S_{VE} (\Delta E'_q/E'_q) \quad (4.5)$$

$$\Delta Q_G = S_{Q_G E} (\Delta E'_q/E'_q) - S_{Q_G Q_L} \Delta Q_L \quad (4.6)$$

The sensitivity matrices are defined as

$$\begin{aligned}
S_{Q_L V} &= J_{22} \\
S_{VE} &= -S_{Q_L V}^{-1} J_{21} \\
S_{Q_G Q_L} &= -J_{12} S_{Q_L V}^{-1} \\
S_{Q_G E} &= J_{11} - J_{12} S_{Q_L V}^{-1} J_{21}
\end{aligned} \tag{4.7}$$

The Jacobian can be based on a constant power model as in the Newton load flow or as in a decoupled load flow where C_1 , C_2 , D_1 , D_2 , A_3 , A_4 , B_3 and B_4 are null. In a decoupled load flow, one could assume that angle differences are small and voltage differences are small so that the remaining Jacobian elements are proportional to the admittances connecting buses in the network. A further step is to assume that the matrices include shunt admittance or constant current load [54]. A combination of constant current, constant impedance, and constant power model is often used.

In this thesis, the non-decoupled constant power load model is used when saddle node bifurcation is studied. Saddle node bifurcation occurs when an eigenvalue of the equivalent differential model approaches zero which implies that the response is infinitely slow at the bifurcation, all tap changers and switchable shunt capacitors in the distribution system have time to complete their action to cause voltage and load recovery. Thus, a constant power load model is appropriate for study of saddle node bifurcation.

Singularity induced bifurcation occurs in the network equations. This bifurcation can develop as tap changers, switchable shunt capacitors, and generator electrical and inertial dynamics respond to result in an equilibrium in an infinitesimal time interval. A constant power load model reflects the effects of distribution level under load tap changers and switchable shunt capacitors over an infinite time interval, but does not reflect the transition from saddle node bifurcation to singularity induced bifurcation if the excitation control system is disabled by an overexcitation protection relay and loss of voltage PV

controllability has occurred on the generator. The conventional combination of constant current, constant impedance, and constant power load model is not adequate to represent the aggregated distribution network and load over this transition from an infinitely slow instability to an infinitely fast instability. This is because the nature of the load model must change dynamically over time due to tap changer and switchable shunt capacitor controls aggregated in the load that change constant impedance and constant current loads to behave as constant power loads. The induction motor load dynamics and thermostatic load dynamics are also ignored if the conventional combination of constant power, constant impedance and constant current load models are used.

Recent changes of power engineering load modeling [49] practice has witnessed use of a short time transient and a long term steady state load model to handle induction motor load and thermostatic load dynamics, as well as the action of tap changer controls and switchable shunt capacitor controls in the distribution system. This short term and long term load modeling allows a transition from one to the other over time as discussed in Chapter 2. The long term model is very heavily constant power reflecting the effects of thermostatic load recovery over time and the load recovery due to underload tap changers and capacitors actions on voltage. The short term load model is often constant current and constant impedance combinations. The long term model is used in computing a stable equilibrium and the eigenvalues near saddle node bifurcation. The short term model is used in computing the eigenvalues and eigenvectors of the differential equation model near singularity induced bifurcation.

The difficulty in studying a bifurcation sequence is that the equilibrium is unstable after the first bifurcation. The use of a constant power model to compute the eigenvalue and the long term changes in the equilibrium response before and shortly after bifurcation for a saddle node bifurcation with an infinite steady state response time at bifurcation is

appropriate. Once saddle node bifurcation occurs and is transitioning to singularity induced bifurcation, one is no longer in equilibrium, a short term load model is appropriate in attempting to analyze the response. This is especially true if the unstable response after saddle node bifurcation is becoming ever faster producing the negative voltage spike.

4.3 Voltage and Load PV Controllability

4.3.1 Voltage PV Controllability

Voltage PV Controllability relates control of reactive generation(Q_G) to generator internal voltage(E'_q) at generator(PV) buses. For a system to be voltage PV controllable, the reactive power injection at the PV buses should increase when the load at PQ buses is fixed and the voltage at some PV buses is increased

Definition 4.1

A system is voltage PV controllable at any time t along the transient trajectory or at an equilibrium point if: when $\Delta Q_L = 0$, any nonzero nonnegative control ΔE causes the PV state ΔQ_G to become such that $\sum_{i=1}^M \Delta Q_{G_i} > 0$ and if $\Delta E_i > 0$ with $\Delta E_j = 0$ for all $j \neq i$ then $\Delta Q_{G_i} > 0$ and $\Delta Q_{G_j} \leq 0$ for all $j \neq i$.

Theorem 4.1

A system is voltage PV controllable if and only if the matrix $S_{Q_G E}$ is such that

$$\sum_{i=1}^M [S_{Q_G E}]_{ij} > 0, \quad j = 1, \dots, M$$

$$\left\{ S_{Q_G E} \right\}_{ij} \begin{cases} > 0, & i = j \\ \leq 0, & i \neq j \end{cases}$$

This proof is omitted but can be obtained from results in [15].

4.3.2 Load PV Controllability

Load PV Controllability relates control of reactive generation(Q_G) at generator(PV) buses to load(Q_L) at load(PQ) buses. For a system to be load PV controllable, the reactive power injection at the PV buses should increase when the voltage at PV buses is fixed and the load at PQ buses is increased.

Definition 4.2

A system is load PV controllable at any time t along the transient trajectory or at an equilibrium point if: when $\Delta E = 0$, any nonzero nonpositive disturbance ΔQ_L cause the PV state ΔQ_G to become nonzero nonnegative.

Theorem 4.2

A system is load PV controllable if and only if the matrix $S_{Q_G Q_L}$ satisfying $Q_G = -S_{Q_G Q_L} \Delta Q_L$ is nonnegative and no zero columns.

This proof is omitted but can be obtained from results in [15].

4.4 Voltage and Load PQ Controllability

4.4.1 Voltage PQ Controllability

Voltage PQ Controllability relates control of voltage(V) at load(PQ) buses to generator internal voltage(E_q') at PV buses. For a system to be voltage PQ controllable, the voltage at PQ buses should increase when the load is fixed and the voltage at some PV buses is increased.

Definition 4.3

A system is voltage PQ controllable at any time t along the transient trajectory or at an equilibrium point if:

(a) When $\Delta Q_L = 0$, any nonzero nonnegative control ΔE causes the PQ state ΔV to become nonnegative and

(b) When $\Delta Q_L = 0$, for each j there is a nonzero nonnegative control ΔE that causes ΔV_j to become positive.

Theorem 4.3

A sufficient condition for voltage PQ controllability is that S_{VE} satisfying $\Delta V = S_{VE} \Delta E$ is nonnegative with no zero rows.

This proof is omitted but can be obtained from results in [15].

4.4.2 Load PQ Controllability

Voltage PQ Controllability relates control of voltage(V) to load(Q_L) at load(PQ) buses. For a system to be load PQ controllable, the voltage at PQ buses should increase when the voltage at PV buses is fixed and the load at some PQ buses is increased

Definition 4.4

A system is load PQ controllable at any time t along the transient trajectory or at an equilibrium point if:

(a) when $\Delta E = 0$, any nonzero nonnegative disturbance ΔQ_L causes the PQ state ΔV to become nonnegative and

(b) when $\Delta E = 0$, for each j there is a nonzero nonnegative disturbance ΔQ_L that causes ΔV_j to become positive.

Theorem 4.4

A sufficient condition for load PQ controllability is that $S_{Q_L V}$ is a M-matrix.

This proof is omitted but can be obtained from results in [15].

4.5 Effects of Loss of Load PQ Controllability

Theorem 4.5

As load PQ controllability is lost and $S_{Q_L V}$ loses its M matrix property by a single eigenvalue $\lambda_{\min}(\mu)$ of $S_{Q_L V}$ approaching zero and becoming negative, matrix $S_{Q_L V}^{-1}$ elements in the voltage control area associated with $\lambda_{\min}(\mu)$ approach infinity, become negative infinity, and then increase toward zero if the constituent matrix is continuous, does not change its magnitude as rapidly as $\frac{1}{\lambda_{\min}}$, and does not change sign in the interval $[\mu_0 - \varepsilon, \mu_0 + \varepsilon]$ when ε is sufficiently small and $\mu \rightarrow \mu_0$.

Proof:

The M matrix $S_{Q_L V}$ has eigenvalues λ_i , $i = 1, 2, \dots, N$, and the matrix $S_{Q_L V}^{-1}$ has all nonnegative elements by the proven properties of an M matrix. $S_{Q_L V}$ can be written as

$$S_{Q_L V} = \sum_{i=1}^N \lambda_i Z_i \quad (4.8)$$

where λ_i is the eigenvalue of $S_{Q_L V}$ and Z_i is the constituent matrix of $S_{Q_L V}$. Matrix $S_{Q_L V}^{-1}$ can be expressed as

$$S_{Q_L V}^{-1} = \sum_{i=1}^N \frac{1}{\lambda_i} Z_i \quad (4.9)$$

Since the constituent matrices satisfy

$$\begin{aligned} Z_i Z_i &= Z_i \\ Z_i Z_j &= 0, \quad i \neq j \end{aligned} \quad (4.10)$$

As one eigenvalue λ_k approaches zero,

$$S_{Q_L V}^{-1} \approx \frac{1}{\lambda_k} Z_k \quad (4.11)$$

in the voltage control area [12] associated with that eigenvalue λ_k .

The constituent matrix Z_k must be nonnegative matrix since $S_{Q_L V}^{-1}$ is nonnegative as long as load PQ controllability holds and $S_{Q_L V}$ is an M matrix. When λ_k approaches zero, elements of $S_{Q_L V}^{-1}$ must approach infinity if $\frac{1}{\lambda_k}$ grows faster than the elements of matrix Z_k could ever approach zero. If Z_k does not have all zero elements when $\lambda_k = 0$ (because they must be nonnegative since $S_{Q_L V}$ is an M matrix until $\lambda_k = 0$), there are some elements of $S_{Q_L V}^{-1}$ in the voltage control area associated with the bifurcating eigenvalue λ_k that may approach infinity [45, 12]. If there is a small operating change that causes λ_k to move from zero continuously to negative infinitesimal value where Z_k

elements have no perceptive change (because they are also continuous), then elements of $S_{Q_L V}^{-1}$ can be near negative infinity in the voltage control area associated with eigenvalue λ_k . The elements of $S_{Q_L V}^{-1}$ may increase and approach zero as λ_k becomes more negative.

Theorem 4.6

Loss of voltage PV controllability, load PV controllability and voltage PQ controllability occur in the voltage control area associated with λ_{\min} if (i) the nonpositive continuous elements in J_{12} , J_{21} and $Z_{\lambda_{\min}}$ changes imperceptibly in $[\mu_0 - \varepsilon, \mu_0 + \varepsilon]$ when ε is sufficiently small and (ii) the elements of $S_{Q_L V}^{-1}$ approach infinity, become negative infinity and increase in $[\mu_0 - \varepsilon, \mu_0 + \varepsilon]$ when ε is sufficiently small. Loss of voltage PV controllability may occur long before loss of load PQ controllability occurs, but loss of load PV controllability and loss of voltage PQ controllability generally occur simultaneously.

proof:

The sensitivity matrices are defined as

$$S_{Q_L V} = J_{22}$$

$$S_{VE} = -S_{Q_L V}^{-1} J_{21}$$

$$S_{Q_G Q_L} = -J_{12} S_{Q_L V}^{-1}$$

$$S_{Q_G E} = J_{11} - J_{12} S_{Q_L V}^{-1} J_{21}$$

where $S_{Q_L V}^{-1}$ is the test matrix for load PQ controllability, S_{VE} is the test matrix for voltage PQ controllability, $S_{Q_G Q_L}$ is the test matrix for load PV controllability, and $S_{Q_G E}$ is the test matrix for voltage PV controllability.

When $S_{Q_L V}$ is singular, $S_{Q_L V}^{-1}$ is not technically defined, its elements may be very large positive numbers before the singularity point and very large negative numbers in a particular voltage control area after the singularity point as shown in Theorem 4.5. Since it is assumed that J_{12} and J_{21} elements are nonpositive and change continuously and imperceptibly in $[\mu_0 - \varepsilon, \mu_0 + \varepsilon]$ and elements of $S_{Q_L V}^{-1}$ in the voltage control area associated with λ_{\min} approach infinity, go to negative infinity and then approach zero as $\mu \rightarrow \mu_0$ in $[\mu_0 - \varepsilon, \mu_0 + \varepsilon]$, elements of S_{VE} and $S_{Q_G Q_L}$ in that voltage control area associated with λ_{\min} behave the same as elements of $S_{Q_L V}^{-1}$ in that voltage control area. Loss of load PV controllability and voltage PQ controllability occur in $[\mu_0 - \varepsilon, \mu_0 + \varepsilon]$ in the voltage control area associated with λ_{\min} as $\mu \rightarrow \mu_0$.

The conditions for voltage PV controllability are

$$\sum_{i=1}^M [S_{Q_G E}]_{ij} > 0, \quad j = 1, \dots, M \quad (4.12)$$

$$\{S_{Q_G E}\}_{ij} \begin{cases} > 0, & i = j \\ \leq 0, & i \neq j \end{cases} \quad (4.13)$$

where

$$S_{Q_G E} = J_{11} - J_{12} S_{Q_L V}^{-1} J_{21}$$

The diagonal elements of $S_{Q_G E}$ will approach zero and become negative because the second term should dominate at PV buses in the voltage control area associated with λ_{\min} approaches zero since

(i) $Z_{\lambda_{\min}}$ must have all nonnegative elements by assumption that change imperceptibly in $[\mu_0 - \varepsilon, \mu_0 + \varepsilon]$ if load PQ controllability holds. This is true because $S_{Q_L V}^{-1}$ must have all nonnegative elements and $Z_{\lambda_{\min}}$ is continuous;

(ii) J_{12} , and J_{21} have all nonpositive elements because they are off diagonal submatrices of matrix J and change imperceptibly in $[\mu_0 - \varepsilon, \mu_0 + \varepsilon]$ by assumption and continuity;

(iii) The il th elements of $-J_{12}S_{Q_L V}^{-1}J_{21}$ in the voltage control area associated with eigenvalue λ_{\min} are negative and grow toward infinite value as λ_{\min} approaches zero since every element of matrix

$$\sum_k \sum_j -\{J_{12}\}_{ij} \frac{1}{\lambda_{\min}} \{Z_{\lambda_{\min}}\}_{jk} \{J_{21}\}_{kl}$$

is negative because the elements in the sum associated with the voltage control area that is nonzero is negative and approaches negative infinity as λ_{\min} approaches zero due to assumed properties (i) and (ii);

(iv) S_{QGE} is approximated by J_{11} when λ_{\min} is large and by $-J_{12} \frac{1}{\lambda_{\min}} Z_{\lambda_{\min}} J_{21}$ at all buses in the voltage control area as λ_{\min} is reduced. The diagonal elements in J_{11} are positive but the elements in $-J_{12} \frac{1}{\lambda_{\min}} Z_{\lambda_{\min}} J_{21}$ in the voltage control area become more negative as λ_{\min} decreases toward zero;

(v) Since all of the elements in $-J_{12} \frac{1}{\lambda_{\min}} Z_{\lambda_{\min}} J_{21}$ are negative and the fact that condition (4.12) is violated before condition (4.13) is violated indicates that loss of voltage PV controllability occurs substantially before loss of voltage PQ controllability for buses in the voltage control area associated with λ_{\min} ;

(vi) The elements of S_{QGE} in the voltage control area associated with λ_{\min} should approach negative infinity, become positive infinity and then decrease as $\mu \rightarrow \mu_0$ in

$[\mu_0 - \varepsilon, \mu_0 + \varepsilon]$ if J_{12} , J_{21} and $Z_{\lambda_{\min}}$ elements in the voltage control area associated λ_{\min} are continuous and thus do not change perceptibly as assumed.

In summary, when load PQ controllability is lost, voltage PV controllability, load PV controllability and voltage PQ controllability can be lost. But loss of voltage PV controllability can occur before load PQ controllability is lost.

4.6 Effects of Load Characteristics

Theorem 4.7

Assume that load PQ controllability and voltage PV controllability hold at some operating point close to loss of load PQ controllability when the excitation control system is disabled

(i) If inductive load susceptances increase at all buses, then elements of $S_{Q_L V}^{-1}$ will become smaller .

(ii) If shunt capacitive susceptances increase at all buses, then $S_{Q_L V}^{-1}$ will become larger.

If the $S_{Q_L V}$ off-diagonal elements and all elements of $Z_{\lambda_{\min}}$ change imperceptibly in $[\mu_0 - \varepsilon, \mu_0 + \varepsilon]$

Proof:

From [15], for a decoupled load flow model

$$\begin{bmatrix} \Delta Q_G \\ \Delta Q_L \end{bmatrix} = J \begin{bmatrix} \Delta E'_q \\ \Delta V \end{bmatrix} = \begin{bmatrix} J_{11} & J_{12} \\ J_{21} & J_{22} \end{bmatrix} \begin{bmatrix} \Delta E'_q \\ \Delta V \end{bmatrix}$$

where J has positive diagonal elements, nonpositive off-diagonal elements. And when E'_q is specified, $\Delta E'_q = 0$, and

$$\Delta Q_L = J_{22} \Delta V = S_{Q_L V} \Delta V \quad (4.14)$$

When $V_i \approx 1$ and $\delta_{ij} \approx 0$, the Jacobians [54] can be expressed as

$$\Delta Q_L = B'' \Delta V \quad (4.15)$$

where

$$B'' = B' - 2diag\{B_{s_{m+1,m+1}}, B_{s_{m+2,m+2}}, \dots, B_{s_{n,n}}\} \quad (4.16)$$

where B' has positive diagonal elements and nonpositive off-diagonal elements. The fact that off-diagonal elements of $S_{Q_L V}$ are assumed to change imperceptibly justifies use of the decoupled model. The diagonal elements of B' are the negative of the sum of its off diagonal elements in a row plus the negative sum of the elements connecting that bus to PV buses. Element $B_{s_{ii}}$'s are negative when the susceptance is inductive, $B_{s_{ii}}$'s are positive when the susceptance is capacitive.

From (4.14) and (4.15), we obtain

$$S_{Q_L V} = B'' = B' - 2diag\{B_{s_{m+1,m+1}}, B_{s_{m+2,m+2}}, \dots, B_{s_{n,n}}\} \quad (4.17)$$

(i) If inductive load susceptances increase at all buses, all the B_s 's are negative and becomes more negative. This will make the minimum row sum of $S_{Q_L V}$ increase since the diagonal elements increase from (4.17), so that the lower bound on the minimum eigenvalue λ_{\min} of $S_{Q_L V}$, which is the minimum row sum of $S_{Q_L V}$, will increase. Since it was assumed that the operating point is close to loss of load PQ controllability, the minimum eigenvalue term in the modal expansion dominates in the voltage control area

associated with that minimum eigenvalue. Therefore, $S_{Q_L V}^{-1} \approx \frac{1}{\lambda_{\min}} Z_{\lambda_{\min}}$ will become smaller in the voltage control area associated with eigenvalue λ_{\min} for increase in shunt inductive susceptance at all buses as long as changes in the discontinuous function of $\mu \frac{1}{\lambda_{\min}}$ are greater than changes in $Z_{\lambda_{\min}}$ which are a continuous at μ_0 and $\lambda_{\min} = 0$.

(ii) If shunt capacitive susceptances increase at all buses, all the B_i 's are positive and increase. This will make the minimum row sum of $S_{Q_L V}$ decrease since diagonal elements of $S_{Q_L V}$ are decreasing from (4.17). The minimum eigenvalue of $S_{Q_L V}$ should also decrease since it is assumed that the operating point is close to loss of load PQ controllability and λ_{\min} is small, the minimum eigenvalue term in the modal expansion of $S_{Q_L V}^{-1}$ dominates in the voltage control area associated with that minimum eigenvalue. This suggests that the elements of $S_{Q_L V}^{-1}$ in the voltage control area associated with λ_{\min} are increasing toward infinite value as shunt capacitive susceptances are increasing.

Based on Theorem 4.6 and Theorem 4.7, the conclusion is that a network that has sufficiently large line charging and shunt capacitive susceptance will experience loss of voltage PV controllability long before it has experienced loss of load PV controllability, loss of voltage PQ controllability and loss of load PQ controllability.

It should be noted that the i th diagonal element of $S_{Q_L V}^{-1}$ should describe the slope of the Q-V curve which is positive and decreases toward zero as $Q_{Li} = \mu \rightarrow \mu_0$. Since a Q-V curve is really a reactive load stress test and the system should be stable as $Q_{Li} = \mu \rightarrow \mu_0$, the elements of vector $\Delta Q_G = -S_{Q_G Q_L} \Delta Q_{Li} e_i$ should be positive since $\Delta Q_{Li} < 0$ for increase in load at bus i , e_i is a unit vector with 1 in the i th element and zeros elsewhere, the i th column of $S_{Q_G Q_L}$ has all non-negative elements when load PV controllability holds. This last condition on $S_{Q_G Q_L}$ is important since the increase in reactive load should cause reactive generation increase and exhaustion of reactive

reserves on certain generators in the reactive reserve basin at generator i . When the system is stable, if a Q-V curve is run at generator i , the i th diagonal element of $S_{Q_G E}$ must be positive and decrease toward zero as $\mu \rightarrow \mu_0$ since it is the slope of the Q-V curve.

To establish that the Q-V curve stress test is administered under stable operating conditions and that reactive load would produce the same result as reducing voltage ΔE_i to reduce ΔQ_{Gi} to more negative values, all elements of $S_{Q_G Q_L}$ should be positive indicating reactive load increase at any bus j would cause increased generation at every generator.

4.7 Validation of Theory

The objective of this section is to (a) validate that $S_{Q_L V}^{-1}$ approaches positive infinity, jumps to negative infinity, and goes back to zero when a power system experiences a negative voltage as observed in the WSCC system blackouts (b) validate that infinity phenomena can occur both when all the exciters present and when one exciter is disabled by an over-excitation protection relay (c) validate that $S_{V E}$, $S_{Q_G E}$ and $S_{Q_G Q_L}$ all show that same infinity phenomena, and (d) establish the effects of load characteristics on $S_{Q_L V}^{-1}$ when an exciter is disabled by the over-excitation protection relay.

The example system studied here is taken from Fouad [55]. It is a 3-machine 9-bus system, and the network is shown in Figure 4.1. The bus data, line data, generation data and exciter data are summarized in Tables 4.1-4.4 respectively.

Two different cases are investigated here. The first one is the network shown in Figure 4.1 where all the excitation control systems are active on all three generators. The second case is the same network but with the excitation control system on generator 3 disabled by an over-excitation protection relay.

For the first case, a disturbance, which is a sudden reactive load increase (1.56 pu) on generator bus 3, is applied at $t = 1.1(s)$. Then the internal bus voltage E'_q at generator 3 exhibits the behavior as shown in Figure 4.2(a). The sensitivity matrices corresponding to each point of E'_q are computed, and the results are shown respectively in Figure 4.2(b), (c), (d) and (e).

In the second case where the excitation control system on generator 3 is disabled by an over-excitation protection relay, a similar disturbance as in the first case (i.e. a sudden reactive load increase of 1.56 pu) is applied at $t = 1.1(s)$ on generator bus 3. Now the internal bus voltage E'_q at generator 3 exhibits the behavior as shown in Figure 4.3(a). The sensitivity matrices corresponding to each point of E'_q are computed, and the results are shown respectively in Figure 4.3(b), (c), (d) and (e). The fact that the infinity discontinuity occurs respectively in Figure 4.1 and Figure 4.2 indicates that the trajectory is on a singular surface or continues to cross the singular surface.

In order to perform the validation clearly, different points on Figure 4.2 and Figure 4.3 are zoomed. Figure 4.4 and Figure 4.5 show the behavior of $S_{Q_L V}^{-1}$ around point B, respectively for case 1 and case 2. It goes to positive infinity, jump to negative infinity and then goes back to zero. Theorem 4.5 that states such behaviors in $S_{Q_L V}^{-1}$ is confirmed.

Figure 4.6 and Figure 4.7 show the occurrence pattern of loss of different controllabilities for case 1 and case 2 respectively. At point A, the diagonal elements of

S_{Q_GE} on generator 3 changes sign from positive to negative. Voltage PV controllability is lost first, which apparently triggers the instability in E'_q at generator 3. This instability then causes the sharp rise in $S_{Q_LV}^{-1}$, S_{Q_GE} and $S_{Q_GQ_L}$ as shown in Figure 4.6. Figure 4.7 shows the similar phenomena for case 2. At point B, $S_{Q_LV}^{-1}$ approaches positive infinity, becomes negative infinity and increase toward zero, load PQ controllability is lost. At the same time, S_{VE} and $S_{Q_GQ_L}$ go through the same infinity transition process and become negative afterwards, voltage PQ controllability and load PV controllability are lost simultaneously. Theorem 4.6 which states all of the above behaviors in S_{Q_GE} , S_{VE} and $S_{Q_GQ_L}$ is confirmed.

In Figure 4.8, there are three curves, the curve with circles is $S_{Q_LV}^{-1}$ with the same original settings as in case 2, the curve with dots is $S_{Q_LV}^{-1}$ with 0.05 pu B increase on every bus. The curve with stars is $S_{Q_LV}^{-1}$ with 0.05 pu G shunt increase on every bus, and all the other parameters are the same as in case 1. From Fig.4.8, it is shown clearly that $S_{Q_LV}^{-1}$ becomes smaller when G shunt is increased, and $S_{Q_LV}^{-1}$ becomes larger when B shunt is increased. Theorem 4.7 is thus confirmed.

bus No.	voltage(pu)	angle (deg)	p_gen (pu)	q_gen (pu)	p_load (pu)	q_load (pu)	G shunt	B shunt	bus type
1	1.04	0.00	0.716	0.27	0.00	0.03	0.00	0.00	1
2	1.025	9.30	1.63	0.07	0.00	-0.02	0.00	0.00	2
3	1.025	4.70	0.85	-0.11	0.00	-1.56	0.00	0.00	2
4	1.026	-2.20	0.00	0.00	0.00	0.00	0.00	0.00	3
5	0.996	-4.00	0.00	0.00	1.25	0.50	0.00	0.00	3
6	1.013	-3.70	0.00	0.00	0.90	0.30	0.00	0.00	3
7	1.026	3.70	0.00	0.00	0.00	0.00	0.00	0.00	3
8	1.016	0.70	0.00	0.00	1.00	0.35	0.00	0.00	3
9	1.032	2.00	0.00	0.00	0.00	1.60	0.00	0.00	3

Table 4.1 Bus data

From bus	To bus	resistance (pu)	reactance (pu)	line charging	tap ratio
1	4	0.0000	0.0576	0.0000	1.0
4	5	0.0100	0.0850	0.0880	1.0
5	7	0.0320	0.1610	0.1530	1.0
7	2	0.0000	0.0625	0.0000	1.0
7	8	0.0085	0.0072	0.0745	1.0
8	9	0.0119	0.1008	0.1045	1.0
9	3	0.0000	0.1586	0.0000	1.0
9	6	0.0390	0.1700	0.1790	1.0
9	4	0.0170	0.0920	0.0800	1.0

Table 4.2 Line data

Gen No.	Base mva	x _l	r _a	x _d	x' _d	T' _d _o	x _q	x' _q	d _o	d _l
1	247.5	0.0336	0.01	0.145	0.061	8.96	0.097	0.097	13.54	9.6
2	191.9	0.0521	0.01	0.896	0.119	6.00	0.865	0.197	5.40	2.5
3	127.9	0.0742	0.01	1.313	0.865	5.89	1.258	0.250	3.01	1.0

Table 4.3 Generator data

Gen No.	exc. type	T _R	K _A	T _A	V _R max	V _R min	K _E	E ₁	S _E 1	E ₂	S _E 2
1	1	0.06	25.0	0.06	5.0	-5.9	-0.02	0.75	0.12	1.0	0.30
2	0	0.06	25.0	0.00	5.0	-1.0	-0.05	0.75	0.07	1.0	0.30
3	2	0.06	1.00	0.01	5.0	-5.0	-0.06	0.75	0.09	1.0	0.36

Table 4.4 Exciter data

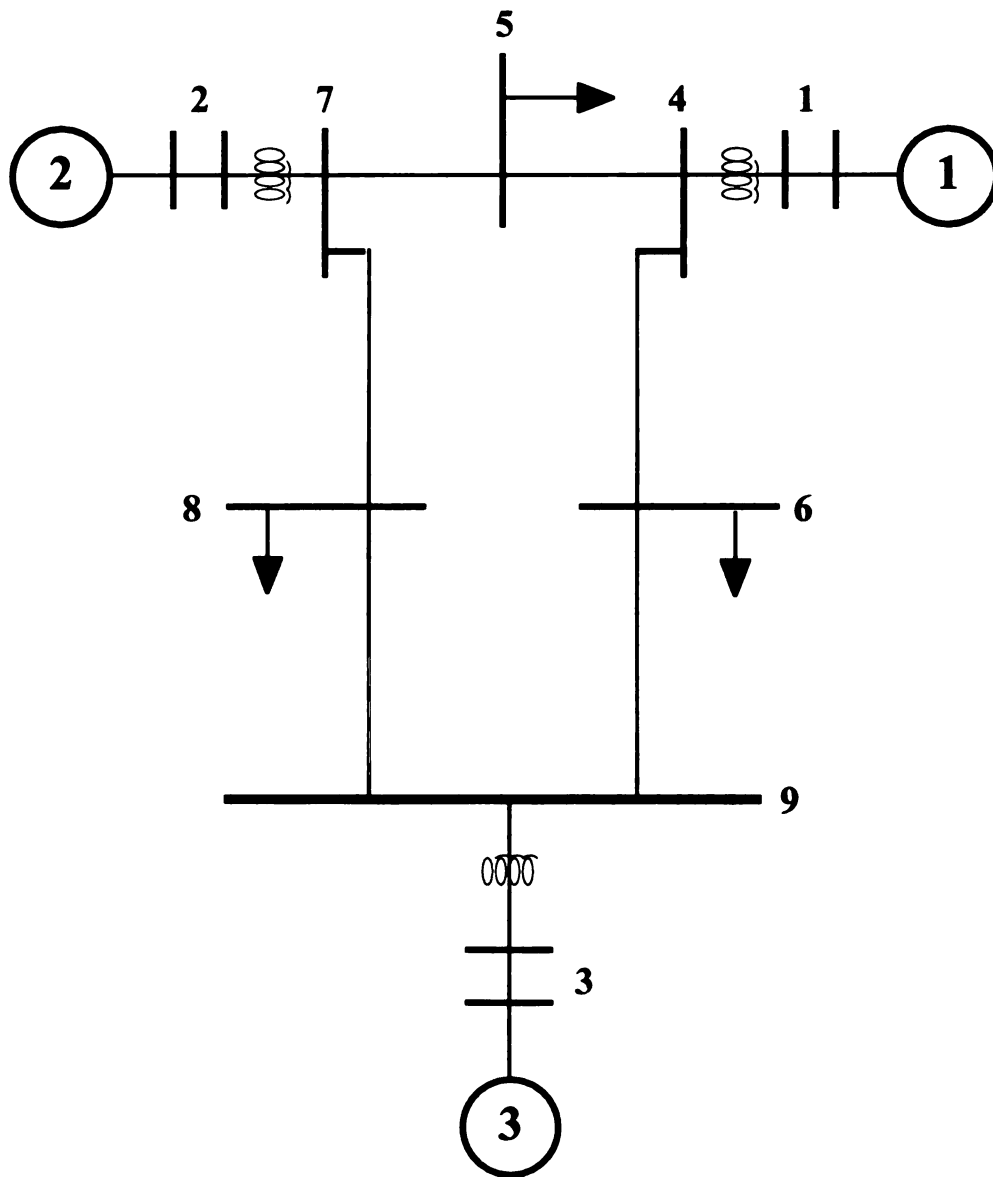


Figure 4.1 A three-machine 9-bus test system

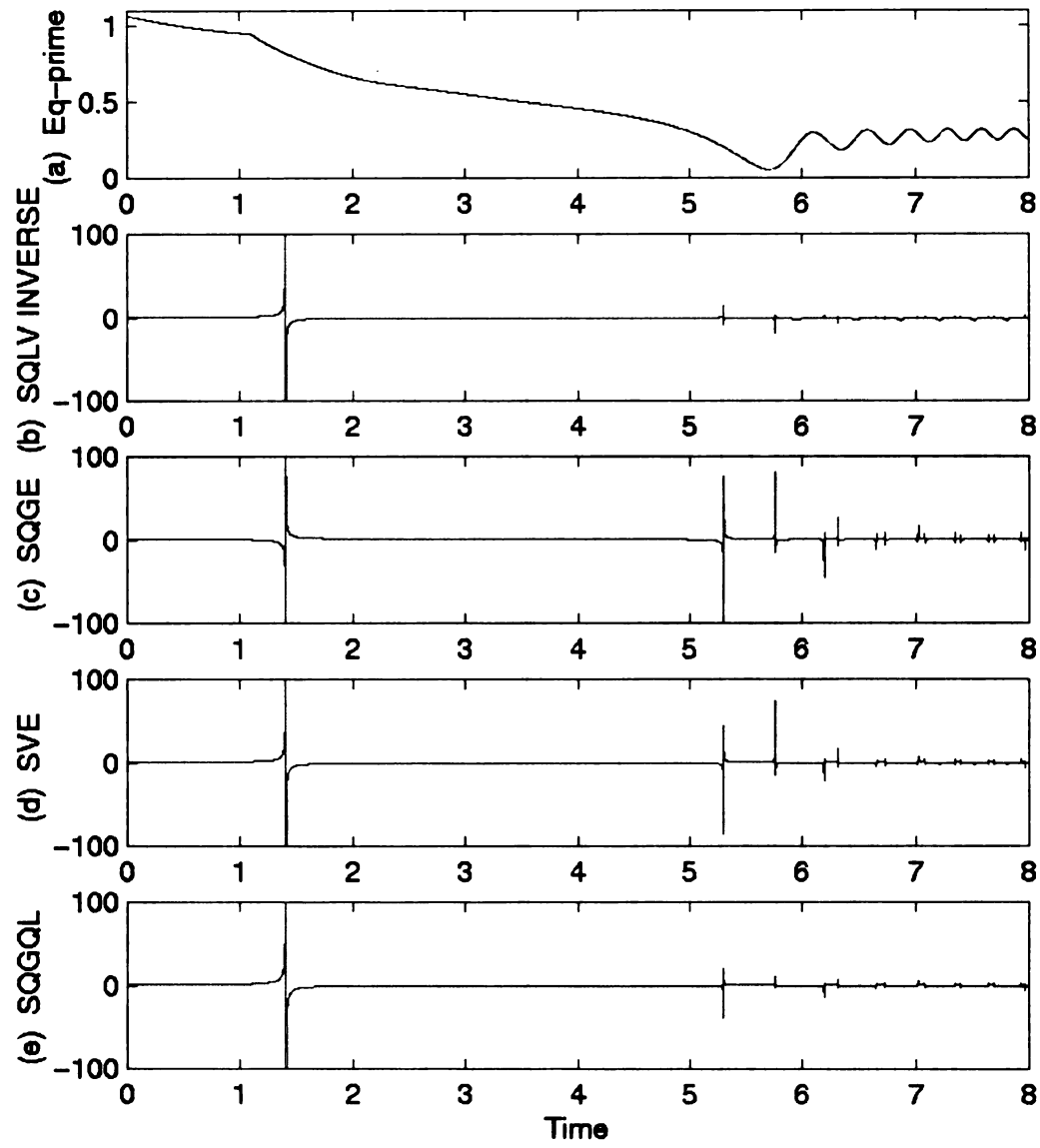


Fig. 4.2 E'_q , $S_{Q_L V}^{-1}$, $S_{Q_G E}$, $S_{V E}$ and $S_{Q_G Q_L}$ for case 1

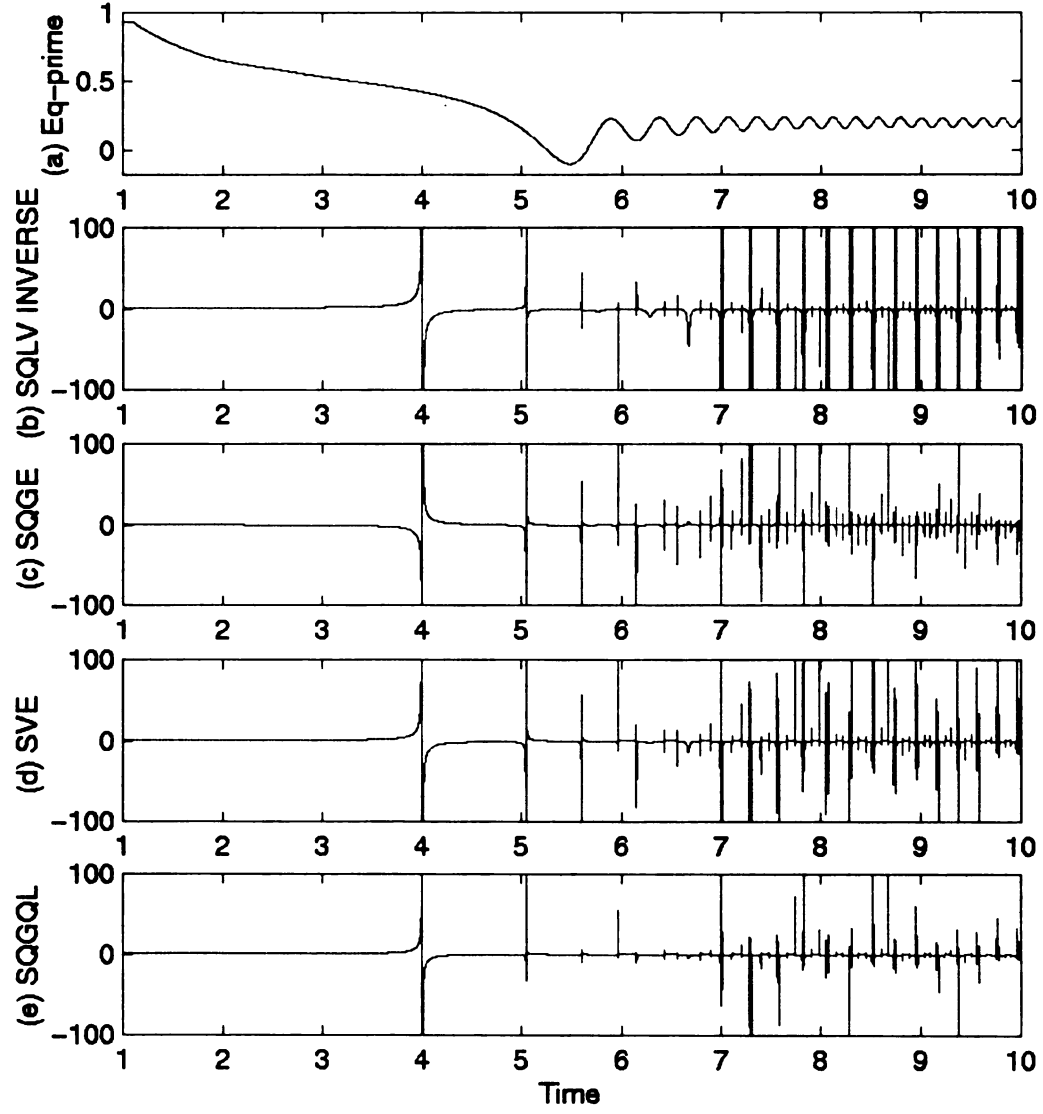


Fig. 4.3 E'_q , S_{QLV}^{-1} , S_{QGE} , S_{VE} and S_{QQL} for case 2

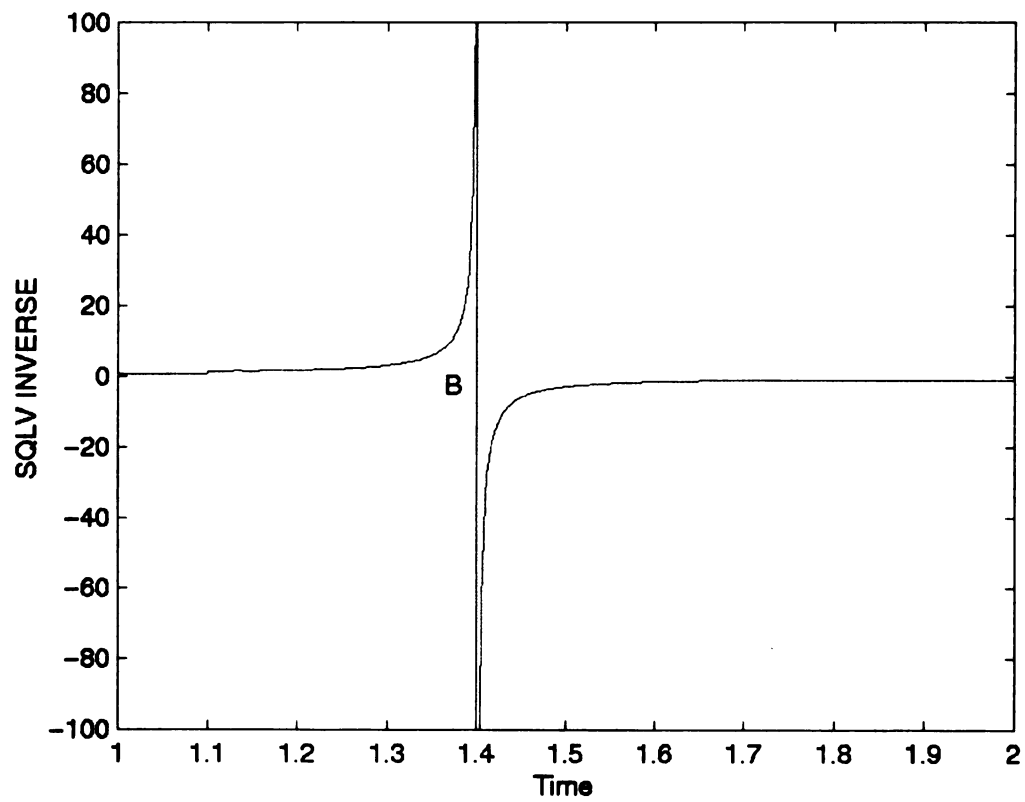


Fig. 4.4 $S_{Q_L V}^{-1}$ for case 1

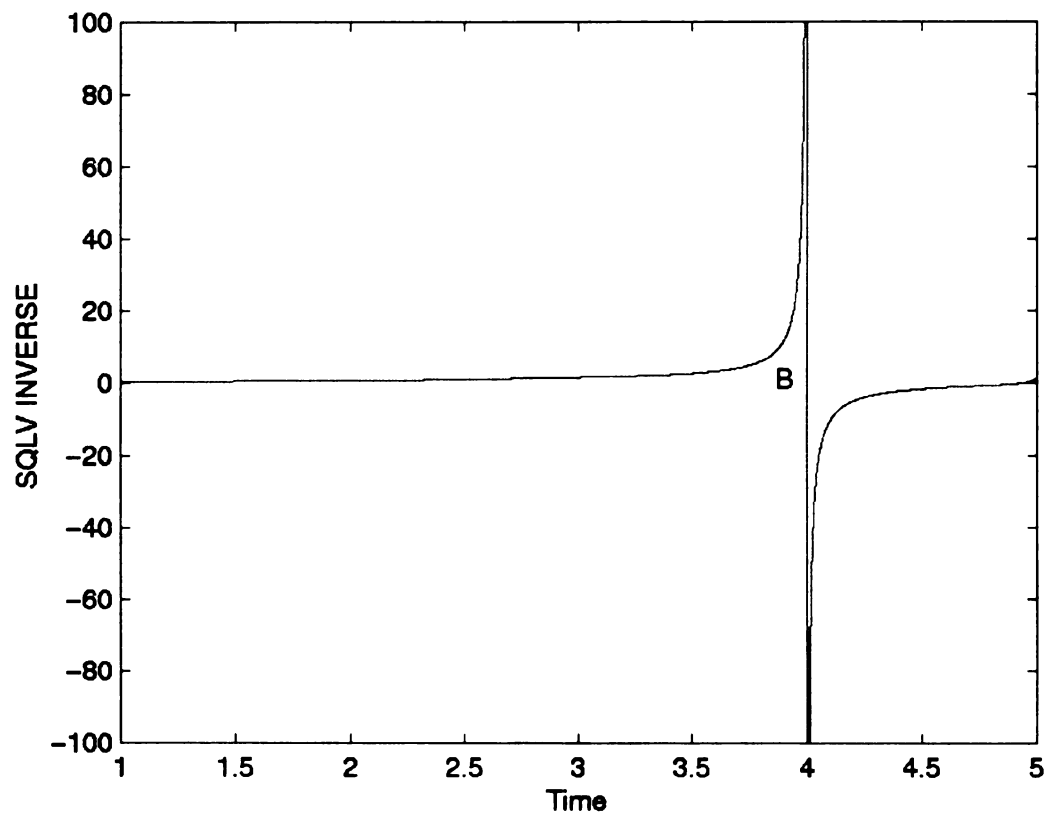


Fig. 4.5 $S_{Q_L V}^{-1}$ for case 2

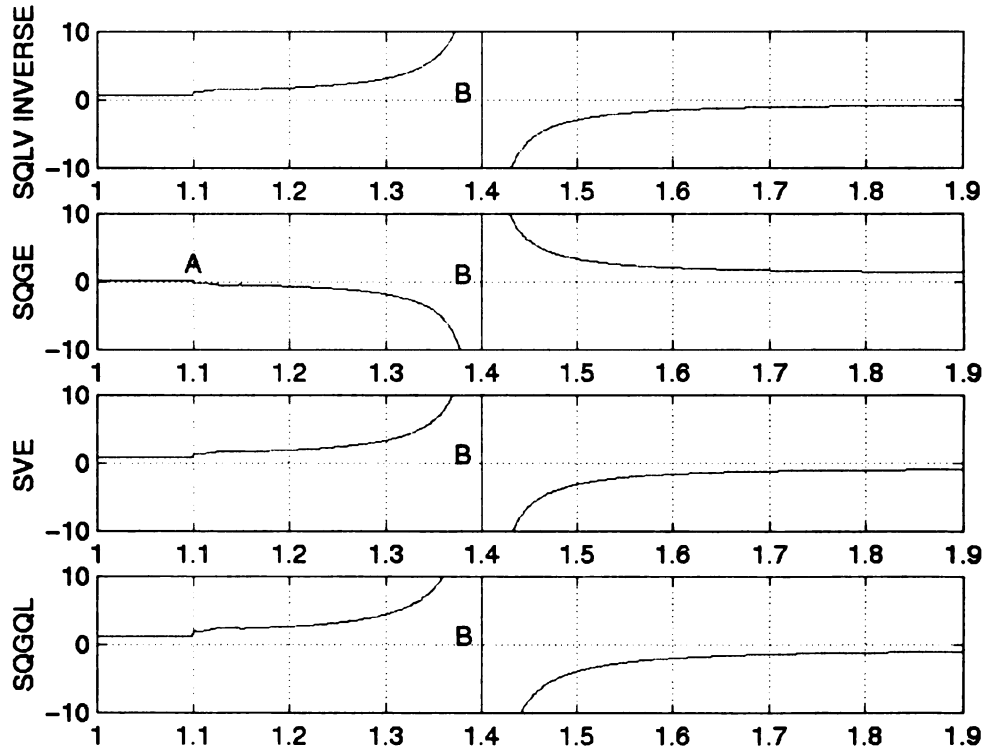


Fig. 4.6 $S_{Q_L V}^{-1}$, $S_{Q_G E}$, $S_{V E}$ and $S_{Q_G Q_L}$ for case 1

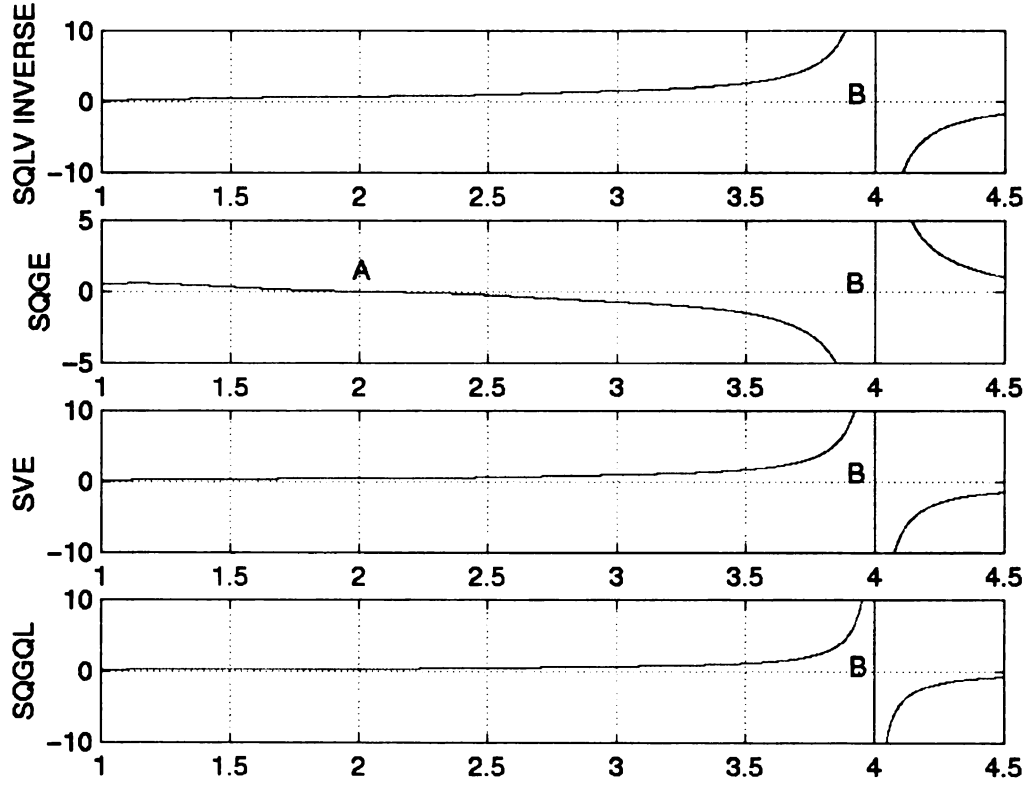


Fig. 4.7 $S_{Q_L V}^{-1}$, $S_{Q_G E}$, $S_{V E}$ and $S_{Q_G Q_L}$ for case 2

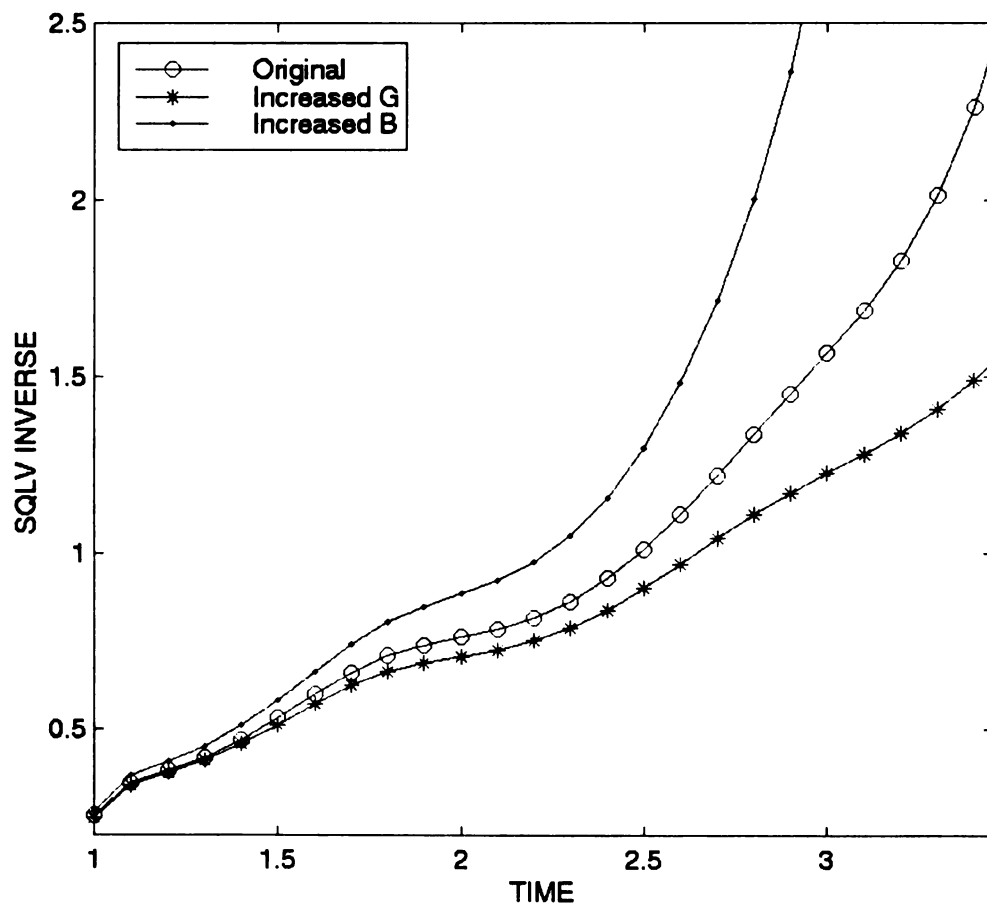


Fig.4.8 Effects of load characteristics

CHAPTER 5

THEORETICAL AND SIMULATION JUSTIFICATION FOR THE DYNAMIC RESPONSES TO BIFURCATION SEQUENCES ASSOCIATED WITH VOLTAGE COLLAPSE

This chapter establishes that a saddle node bifurcation followed by an inevitable singularity induced bifurcation produces the characteristic negative voltage spike observed on the December 14, 1994, July 2, 1996 and August 10, 1996 WSCC system voltage collapse problems. The theory uses previously defined matrices T and N [8] to show that:

(a) Disablement of the excitation control system is not enough to cause instability, but disablement of the excitation control system and slow loss of voltage PV controllability cause saddle node bifurcation and thus loss of stability. This loss of stability causes $\Delta E'_{q_i}(t)$ to decline. This can be observed in Figure 1.2(a) starting from 15:47:50 ignoring the oscillations observed in that figure. The loss of stability can be observed in an eigenvalue of T going to zero and slowly assuming positive value;

(b) The decline in voltage $\Delta E'_{q_i}(t)$ should cause a generation decrease given that $\{S_{Q_G E}\}_{ii} < 0$. A dynamic Q-V curve is then produced as long as $S_{Q_G Q_L}$ has all nonnegative elements and load PV controllability holds as $\Delta E'_{q_i}(t)$ is decreasing;

(c) The dynamic Q-V curve at a generator bus in a voltage control area should cause elements of $S_{Q_L V}^{-1}$ associated with that voltage control area to approach infinity and $\{S_{Q_G E}\}_{ii}$ to continually decrease and thus further violate voltage PV controllability conditions;

(d) A more and more rapid decline in $\Delta E'_{q_i}(t)$ should occur as the positive unstable eigenvalue of T associated with the loss of voltage PV controllability and loss of the excitation control system on generator i becomes more positive because the magnitude of the positive eigenvalue depends on the degree of violation of PV controllability at bus i . The acceleration of $S_{Q_L V}^{-1}$ elements to infinity causes acceleration in the magnitude of violation in voltage PV controllability and increase in positive value for the unstable eigenvalue of T . This acceleration of $S_{Q_L V}^{-1}$ elements to infinity causes the rate of $\Delta E'_{q_i}(t)$ decline to increase resulting in a spike and the eigenvalue approaching infinity. The evolution of the slow decline in $\Delta E'_{q_i}(t)$ at saddle node bifurcation to the more and more rapid decline associated with singularity induced bifurcation can be observed in Figure 1.2(a);

(e) The change in $S_{Q_L V}^{-1}$ values from $+\infty$ to $-\infty$ in the voltage control area causes $S_{Q_G E}$ to change from $-\infty$ to $+\infty$, and T from $+\infty$ to $-\infty$ [15, 48, 40]. This change in T causes a stable but infinitely fast rise in $\Delta E'_{q_i}(t)$. This can be observed in Figure 1.2(a).

5.1 Introduction

Sensitivity methods were very thoroughly investigated as a means of assessing proximity to voltage instability in a loadflow model [15, 33, 62] and for assessment of the stability of an equilibrium in a differential algebraic model [15, 33, 62]. More recently trajectory sensitivity methods have been applied [12, 56, 62] to assess proximity to the

boundary of the region of attraction and to assess how discontinuities due to contingencies, field current limiters, switchable shunt capacitors, and tap changers affect proximity to instability of a trajectory. In all cases, the sensitivity measures become large as proximity to instability become small. Network sensitivity matrices were first defined in chapter 4. PQ controllability of voltage (V) at load buses and PV controllability of reactive generation (Q_G) at generator or voltage control buses was defined based on the understanding of the proper response and control of these variables that not only reflected stable operation but acceptable operation. The concept of PQ controllability and PV controllability was extended in chapter 4 to differentiate the response of the variables (V , Q_G) to reactive load Q_L and generator internal voltage (E). The properties of test matrices $S_{Q_L V}^{-1}$ and S_{VE} for load and voltage PQ controllability respectively and test matrices $S_{Q_G Q_L}$ and $S_{Q_G E}$ for load and PV controllability were defined in chapter 4, are the foundation for the theory presented in this chapter on how and why large negative voltage spikes can occur as a system experiences a blackout. These large negative voltage spikes are believed to have contributed to or possibly caused the three recent blackouts on the WSCC system because (1) they represent a series of cascading bifurcations that make the dynamics unstable and ultimately destroy the network's ability to transfer power and (2) the large negative voltage spike triggers equipment protection limiters and relays that outage equipment that ultimately cascades the blackout throughout the system.

A sharp negative voltage spike has been observed on the WSCC system prior to the December 14, 1994, July 2, 1996 and August 10, 1996 blackouts. The voltage spike is proven to occur due to Maximum Excitation Limiter (MXL) action that causes an unstable trajectory crossing a singular surface due to loss of load and voltage PQ controllability. This is quite possibly the voltage spikes that occurred on the first two WSCC blackouts. A voltage spike is also proven to occur when a MXL is disabled by large interarea oscillations and an Over Excitation Protection Relay (OXP) trips the AC regulator over to the DC

regulator of the automatic voltage regulator. The voltage spike that is observed during the August 10, 1996 blackout quite possibly occurred due to a sequence of saddle node bifurcation that is inevitably followed by the unstable trajectory crossing a singular surface. The saddle node bifurcation occurs due to (a): disablement of the Maximum Excitation Limiter due to large interarea oscillations as proven in [57,60], (b) OXP relay tripping of the AC regulator of the AVR [57, 60] and loss of voltage PV controllability [60, 63]. Loss of voltage PV controllability is proven to occur on networks where the network provides the reactive supply via line charging and/or heavy shunt capacitive compensation. The instability following saddle node bifurcation is proven to administer a dynamic Q-V stress test that results in singular surface via loss of load and voltage PV controllability [57, 62]. The voltage decline portion of the negative voltage spike is proven to occur due to the saddle node bifurcation and the voltage increase is proven to occur due to the unstable trajectory crossing the singular surface. This bifurcation sequence is quite possibly what produced the voltage spike that was observed on the August 10, 1996 blackout when the large interarea oscillations apparently disabled Maximum Excitation Limiters on the McNary station generators that ultimately caused tripping of these generators.

5.2 Test Matrices for Static Bifurcation in Flux Decay Dynamics

A test matrix T for static bifurcation in flux decay dynamics is defined in [8]:

$$T = - \left[C_3 - \begin{bmatrix} A_3 & B_3 & D_3 & E_3 \end{bmatrix} \begin{bmatrix} A_1 & B_1 & D_1 & E_1 \\ A_2 & B_2 & D_2 & E_2 \\ A_4 & B_4 & D_4 & E_4 \\ A_5 & B_5 & D_5 & E_5 \end{bmatrix}^{-1} \begin{bmatrix} C_1 \\ C_2 \\ C_4 \\ C_5 \end{bmatrix} \right] \quad (5.1)$$

A second expression for T is

$$T = \text{diag}\left\{\frac{1}{T_{d_{0i}}}\right\}\left[\text{diag}\left\{-E'_{q_{0i}} + \frac{Q_{G_{0i}}(X_{d_i} - X'_{d_i})}{E'_{q_{0i}}}\right\} + \text{diag}\left\{\frac{-K_{A_i}K_{R_i}V_{0_i}}{K_{E_i} + S_{E_i} + \dot{S}_{E_i}E_{fd_{0i}}}\right\}WS_{VE} - \text{diag}\left\{\frac{X_{d_i} - X'_{d_i}}{E'_{q_{0i}}}\right\}S_{Q_GE}\right] \quad (5.2)$$

where K_{A_i} is the excitation control system gain, K_{A_i} is the voltage sensor gain, K_{E_i} and S_{E_i} are the excitation control system parameters, and N is defined as:

$$N = \text{diag}\left\{\frac{1}{T_{d_{0i}}}\right\}\left[\text{diag}\left\{\frac{-K_{A_i}K_{R_i}V_{0_i}}{K_{E_i} + S_{E_i} + \dot{S}_{E_i}E_{fd_{0i}}}\right\}WS^{-1}_{Q_LV} + \text{diag}\left\{\frac{X_{d_i} - X'_{d_i}}{E'_{q_{0i}}}\right\}S_{Q_LQ_L}\right] \quad (5.3)$$

The derivation in [8] shows that the reduced differential equation model for a system experiencing static bifurcation in flux decay dynamics is

$$\Delta\dot{E}'_q = T\frac{\Delta E'_q}{E'_{q_0}} + N\Delta Q_L \quad (5.4)$$

The following Lemma taken from [8] qualifies derivation of the linearized model (5.4) when T can be written as either (5.1) or (5.2) and N is defined by (5.3).

Lemma 5.1

Given that J_c is nonsingular so that A is defined and J_l is nonsingular so that T is defined, then matrix T is singular if and only if both A and J are singular.

The matrix J_c is a test matrix for causality[27] and causality is assured if

$$J_c = \begin{bmatrix} B_2 & D_2 \\ B_4 & D_4 \end{bmatrix} \quad (5.5)$$

is nonsingular. A is defined only when the system is causal, it acts as the text matrix for static bifurcation, a static bifurcation occurs when both J and

$$A = \left(\begin{bmatrix} A_1 & C_1 & E_1 \\ A_3 & C_3 & E_3 \\ A_5 & C_5 & E_5 \end{bmatrix} - \begin{bmatrix} B_1 & D_1 \\ B_3 & D_3 \\ B_5 & D_5 \end{bmatrix} \begin{bmatrix} B_2 & D_2 \\ B_4 & D_4 \end{bmatrix}^{-1} \begin{bmatrix} A_2 & C_2 & E_2 \\ A_4 & C_4 & E_4 \end{bmatrix} \right) \quad (5.6)$$

are singular. J_1 is the system jacobian matrix when generators are modeled by a classic machine model with constant voltage behind transient reactance and the network is not aggregated back to generator internal buses. Matrix

$$J_1 = \begin{bmatrix} A_1 & B_1 & D_1 \\ A_2 & B_2 & D_2 \\ A_4 & B_4 & D_4 \end{bmatrix} \quad (5.7)$$

is a test matrix for static bifurcation in generator inertial dynamics.

This Lemma shows that when T is defined, if loss of causality (J_c nonsingular) and angle instability (J_1 nonsingular) can not occur and if both J and A are singular(nonsingular), then T is singular(nonsingular). The analysis in [30] shows that when the exciter is disabled and the generator flux decay mode experiences saddle node bifurcation, and the equivalent model (5.4) should capture this bifurcation. The computational result in [32] on bifurcation subsystem theory suggests that on at least one example, the bifurcation subsystem for a saddle node bifurcation when the excitation

control system is disabled is just the generator flux decay dynamics $\Delta E'_q(t)$. All these results suggest that model (5.4) contains the subsystem experiencing bifurcation and T actually tests for this bifurcation that occurs in the subsystem model.

5.3 Effects of Loss of Voltage PQ Controllability on Stability of Generators with Exciters

Lemma 5.2, Theorem 5.1 and Theorem 5.2 are taken from [11] where the proofs of each result are given. Simulation results are also provided that help substantiate the theory.

Lemma 5.2:

If matrix W that specifies the voltage controlled buses is selected so that WS_{VE} is positive definite when voltage PQ controllability holds, then T is negative definite when the excitation control system gain K_{A_i} is assumed large.

Theorem 5.1

Loss of voltage PQ controllability for one or more generator control buses causes WS_{VE} and T to be singular or have an eigenvalue change sign when K_{A_i} is assumed large. This implies that loss of voltage PQ controllability causes instability in the flux decay dynamics.

The results of Lemma 5.2 and Theorem 5.1 indicate that when the excitation control system are active, preservation of voltage PQ controllability is sufficient to preserve stability in generator flux decay dynamics, but loss of voltage PQ controllability is sufficient to cause loss of stability in the generator flux decay dynamics. Simulation results in [11] suggest that the loss of voltage PQ controllability bring on Hopf bifurcation followed by node focus, and finally singularity induced bifurcation when loss of voltage

PQ controllability occurs. Such a sequence of bifurcation is shown in Figure 1.5, A saddle node bifurcation in generator flux decay dynamics follows singularity induced bifurcation since the unstable real eigenvalue crosses the $j\omega$ axis, it is solely associated with the flux decay dynamics. Theorem 5.1 theoretically confirms these experimental results. The result also indicates slow loss of voltage PQ controllability can produce saddle node bifurcation followed by the singularity induced bifurcation.

The remainder of this chapter will describe and justify the negative voltage spike that characterizes voltage collapse incidents on the WSCC system.

5.4 Effects of Loss of Voltage PV Controllability and Disablement of the Excitation Control System on Stability of Generator Dynamics

Theorem 5.2:

Given that $-T$ is irreducible, diagonally dominant, and positive definite when voltage PV and voltage PQ controllability hold, T becomes singular or indefinite when (i) voltage PV controllability is lost such that $S_{QGE_{ii}} - Q_{G_i} + \frac{E_{q_i}'^2}{X_{d_i} - X_{d_i}'} < 0$ (ii) field current limits are reached on the same generator and (iii) the excitation control system on that generator is completely disabled by an over excitation relay and placed under manual control.

Theorem 5.2, taken from the result in [11], establishes that disablement of a generator excitation system and loss of voltage PV controllability on that same generator produces loss of stability in generator flux decay dynamics. If the loss of voltage PV controllability occurs very slowly due to addition of switchable shunt capacitors that causes loss of

voltage PV controllability (Theorem 4.7), then a saddle node bifurcation appears to develop.

Theorem 5.3:

Matrix T is negative definite if an excitation control system is disabled but voltage PV controllability and voltage PQ controllability hold.

Theorem 5.3 establishes that disablement of the excitation control system alone is not a sufficient condition for loss of stability in generator flux decay dynamics. The proof of Theorem 5.3 is given in Appendix A.

5.5 Justification of the Bifurcation Sequence That Occurs due to Loss of Voltage PV Controllability and Disablement of the Excitation Control System on a Specific Generator

Theorem 5.4

Given that loss of voltage PV controllability occurs ($\sum_{j=1}^m S_{Q_G E_{ij}} < 0$, $S_{Q_G E_{ii}} - Q_{G_i} + \frac{E_{q_i}'^2}{X_{d_i} - X_{d_i}'} < 0$) on a generator control bus where the excitation control system is disabled by an overexcitation limiter relay, load PV controllability, load PQ controllability and voltage PQ controllability hold at all buses. then $\Delta E_{q_i}'(t)$ is unstable and decreasing toward zero for $\Delta E_j = 0$, $j \neq i$ and a load increase $\Delta Q_{L_i} < 0$.

The proof of Theorem 5.4 is given in Appendix A. Theorem 5.4 states that the loss of stability caused by loss of voltage PV controllability and disablement of the excitation control system on the same generator causes $\Delta E_{q_i}'(t)$ to be unstable and approach zero.

Theorem 5.5 that follows proves that the loss of stability in $\Delta E'_{q_i}(t)$ does not cause instantaneous voltage collapse, but inevitably leads to a cascading voltage collapse by causing a singularity induced bifurcation that occurs in the algebraic submodel but affects dynamics in the differential model. The slow decline in $\Delta E'_{q_i}(t)$ has exactly the same effect as computing a Q-V curve at the internal bus i .

Theorem 5.5

Given that $\{S_{Q_G E}\}_{ii} > 0$ and load PV controllability holds until load PQ controllability occurs. When voltage PV controllability is lost ($\sum_{j=1}^m S_{Q_G E_{ij}} < 0$, $S_{Q_G E_{ii}} - Q_{G_i} + \frac{E_{q_i}'^2}{X_{d_i} - X_{d_i}'} < 0$) on generators where the excitation control system is disabled and $\Delta E_j = 0$ for $j \neq i$, then a dynamic Q-V curve stress test occurs on the generator internal bus that inevitably produce loss of load PQ controllability and singularity induced bifurcation.

The proof of Theorem 5.5 is given in Appendix A.

Theorem 5.6

The dynamic Q-V curve, that is observed via elements in $S_{Q_L V}^{-1}$ associated with the voltage control area approaching $+\infty$, causes continually increasing violation of voltage PV controllability, causes an eigenvalue of T associated with the unstable generator in that voltage control area where the excitation control system is disabled to approach $+\infty$, causes the more and more rapid decline in $\Delta E'_{q_i}(t)$ to producing the negative side of the voltage spike.

The proof of Theorem 5.6 is given in Appendix A.

5.6 Justification of the Large Negative Voltage Spike That Develops due to Loss of Voltage PQ Controllability on Generator Response with or without Excitation Control

Theorem 5.7

Given that (i) loss of voltage PV controllability ($\sum_{j=1}^m S_{Q_G E_{ij}} < 0$, $S_{Q_G E_{ii}} - Q_{G_i} + \frac{E_{q_i}'^2}{X_{d_i} - X_{d_i}'} < 0$) and load PV controllability occur on a generator control bus i in a voltage control area where the excitation control system is disabled by an overexcitation limiter relay, and (ii) load and voltage PQ controllability hold at all other buses, then the system is unstable and the change in E_{q_i}' is positive when $\Delta Q_{L_i} < 0$ and $\Delta E_{q_j} = 0$, $j \neq i$, $\Delta E_{q_i} > 0$.

Theorem 5.8

Given that

- (i). loss of load PQ controllability has occurred at the generator control bus i ;
- (ii). $\{WS_{Q_L V}^{-1}\}_{ij}$ approaches positive infinity, jumps to negative infinity but increases toward zero after load PQ controllability is lost at bus j where $\{W\}_{ij} = 1.0$
- (iii). $\{WS_{VE}\}_{ii}$ for generator i approaches positive infinity, jumps to negative infinity, increase to zero and positive value after voltage PQ controllability is lost at bus i ;
- (iv) the exciters on all machines are active where $\Delta E_{q_j}' = 0$, $j \neq i$.
- (v) the system is stable;

then the steady state change $\Delta E_{q_i}'$ for increased load ($\Delta Q_L < 0$) is positive.

Theorem 5.7 and Theorem 5.8, which are proven in Appendix A, deal with the effects after the singularity induced bifurcation.

If a generator excitation control system is disabled via an overexcitation limiter relay and loss of voltage PV controllability slowly develops at that same generator, then singularity induced bifurcation inevitably follows which implies that load PV controllability may ultimately be lost, as noted from results of Theorem 5.4. Theorem 5.7 states that if voltage PV controllability and load PV controllability are lost on the generator where the excitation control system is disabled, then $\Delta E'_{q_i}$ increases. This is initially surprising because the voltage decline that occurred before singularity induced bifurcation is reversed to produce a voltage rise.

Observation of $S_{Q_G Q_L}$ as singularity induced bifurcation (singularity of $S_{Q_L V}$) develops may indicate that $S_{Q_G Q_L}$ elements in the voltage control area (elements of both Q_G and Q_L) will increase toward infinity, become negative infinity, and then increase to zero. $S_{Q_G E}$ elements approach negative infinity, become positive infinity, and then decrease. From the proof of Theorem 5.7, large positive $S_{Q_G Q_L}$ elements can have a dominant effect on $\Delta \dot{E}'_q < 0$, thus $\Delta E'_q$ will decrease more and more rapidly as loss of load PV controllability develops due to elements of $S_{Q_G Q_L}$ approaching infinity, $\Delta E'_q$ then will increase extremely rapidly after loss of load PV controllability occurs because elements of $S_{Q_G Q_L}$ are negative infinite. This could produce the large sharp negative voltage spike that has been characteristic of the WSCC system blackout observed in December 14, 1994, July 2, 1996 and August 10, 1996.

The singularity induced bifurcation effectively causes the real eigenvalue of T associated with the voltage control area to become positive, approach positive infinity, become negative infinity and then decrease when this eigenvalue depends on the elements of $S_{Q_G E}$ that approach zero and proceed to negative infinite, become positive infinite and

then decrease toward zero. This suggests a bifurcation sequence of saddle node bifurcation, that occurs if shunt susceptance is slowly added at bus i where the excitation system is disabled, and singularity induced bifurcation that inevitably follows.

Theorem 5.8 indicates that if loss of load PQ controllability occurs for generators with active excitation control, and the singularity induced bifurcation causes eigenvalues to transverse through the right half plane toward infinity, enter the left half plane at infinity, the stable response will cause $\Delta E'_q$ to increase for reactive load changes. Thus the voltages on both generators with active excitation control may enhance the voltage spike observed on generators where excitation has been disabled.

Theorem 5.9

As μ increases in the interval $[\mu_0 - \varepsilon, \mu_0 + \varepsilon]$ and loss of load PQ controllability occurs at μ_0 ,

(i) The elements of $S_{Q_L V}^{-1}$ associated with the voltage control area having the dynamic Q-V curve go to $+\infty$, discontinuously change to $-\infty$, and then increase toward zero.

(ii) The elements of $S_{Q_G E}$ associated with the voltage control area having the dynamic Q-V curve approach $-\infty$, discontinuously change to $+\infty$, and then decrease toward zero as long as J_{11} , J_{12} and J_{21} are continuous in $[\mu_0 - \varepsilon, \mu_0 + \varepsilon]$.

(iii) The eigenvalue of T associated with one unstable generator where the excitation control system is disabled, approaches $+\infty$ causes rapid decrease in $\Delta E'_{q_i}$ producing the positive part of the spike and making the eigenvalue move through $+\infty$ to the left half plane. The switching of $S_{Q_G E}$ elements from $+\infty$ to $-\infty$ causes the eigenvalue of T to switch discontinuously from $+\infty$ to $-\infty$ and causes a rapid rise in $\Delta E'_{q_i}$.

The proof of (i) and (ii) is from Theorem 4.6. The proof of (iii) is based on the proof of Theorem 5.6 and the results in Theorem 5.7 and Theorem 5.8.

5.7 Simulation Study

Based on the simulation study performed on the 3-machine 9-bus power system in chapter 4, test matrix T for static bifurcation in flux decay dynamics is computed here.

For case 1, where all the exciters are active, the simulation results for S_{VE} , $S_{Q_LV}^{-1}$, T and E'_q are shown in Figure 5.1. The diagonal element of T plotted is for generator 3, the diagonal element of $S_{Q_LV}^{-1}$ is for load bus 9, the element of S_{VE} represents the coupling of internal generator bus 3 and load bus 9. At point X, the element of S_{VE} approaches infinity, jumps to negative infinity and remains negative until the next spike point at $t = 5.4s$ as shown in Figure 5.1(a). Loss of voltage PQ controllability thus occurs at point X. At the same point of time, the element of T goes to zero and become positive as shown in Figure 5.1(c). Instability in flux decay dynamics associated with generator 3 is brought about at point X that is observed in E'_q . This confirms Theorem 5.1. In the same figure, it is also shown in (d) that E'_q reaches the lowest point and increases after point Y. Theorem 5.8 is confirmed since all the conditions (i–v) are met just prior to the increase in E'_q on generator 3.

For case 2, where the excitation control system on generator 3 is disabled, the simulation results for the appropriate elements of S_{Q_GE} , S_{VE} and T are shown in Figure 5.2 at the same buses as in case 1. At point A, the diagonal element of S_{Q_GE} associated with generator 3 changes from positive to negative as shown in Figure 5.2(a), so that voltage PV controllability is lost. Around the same time, the diagonal element of T changes from negative to positive. This confirms Theorem 5.2. From Figure 5.2, it is also shown

that before point A, S_{QGE} and S_{VE} are positive, voltage PV controllability and voltage PQ controllability hold, and the element of T is negative. This confirms the theory in Theorem 5.3.

In order to confirm the theories in Theorem 5.4, Theorem 5.5, Theorem 5.6, Theorem 5.7 and Theorem 5.9 clearly, the sensitivity matrices, the test matrix and the internal voltage of generator 3 are plotted in Figure 5.3. On this graph, it is shown that between point A and point B, the element of S_{QGE} associated with generator 3 is negative, but the appropriate elements of S_{QGE} , S_{VE} and S_{QLV}^{-1} are positive, E'_q at generator 3 is unstable and decrease toward zero. This confirms Theorem 5.4. At point B, S_{QLV}^{-1} approaches positive infinity, jumps to negative infinity and then go back toward zero, load PQ controllability is lost, and singularity induced bifurcation occurs. This confirms Theorem 5.5. Between point B and point C, the element of S_{QLV}^{-1} and T go through the infinity process, E'_q at generator 3 declines more and more rapidly and produces the negative spike. Theorem 5.6 is thus confirmed. A dynamic Q-V curve is generated that produces singularity induced bifurcation and the negative spike.

At point B, load PQ controllability at bus 9 occurs since the element of S_{QLV}^{-1} goes to positive infinity, discontinuously changes to negative infinity, and then increase toward zero. At the same time, S_{QGE} at generator 3 goes to negative infinity, discontinuously changes to positive infinity, and then decrease toward zero. And the diagonal element of matrix T associated with generator 3 switches from positive infinity to negative infinity and causes a rise in E'_q as is shown at point C. This confirms Theorem 5.9.

At point C, the diagonal element of S_{QGE} associated with generator 3 goes to negative infinity, and then positive infinity, the appropriate element of S_{QGQL} that relates generator bus 3 to load bus 9 goes to positive infinity to assure loss of voltage and load PV controllability as required by Theorem 5.7. It is not shown that load and voltage PV

controllabilities are maintained because all elements of S_{VE} and $S_{Q_G Q_L}$ are not shown but they are because there are no spikes on any of the other sensitivity matrix elements. It is then clear that the change in E'_q is positive at point C when these confirming conditions and results of Theorem 5.7.

The results show that a sharp negative voltage spike is a result of singularity induced bifurcation brought by a dynamic Q-V curve. This occurs when the exciter is disabled on a generator.

A sharp negative voltage spike also occurs when the exciter is active and a maximum excitation limiter is present as noted in the discussion of case 1 results.

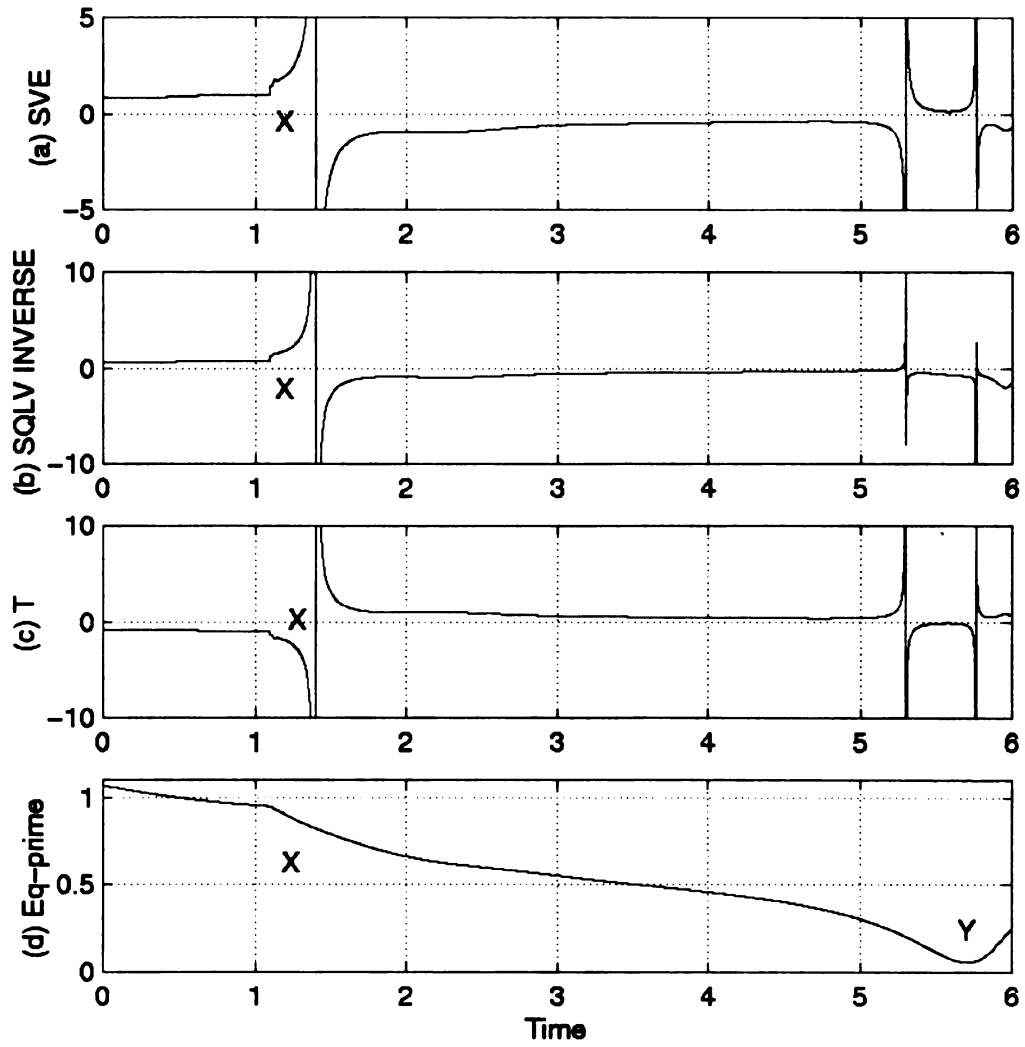


Fig. 5.1 Simulation result for theorems 5.1 and 5.8.

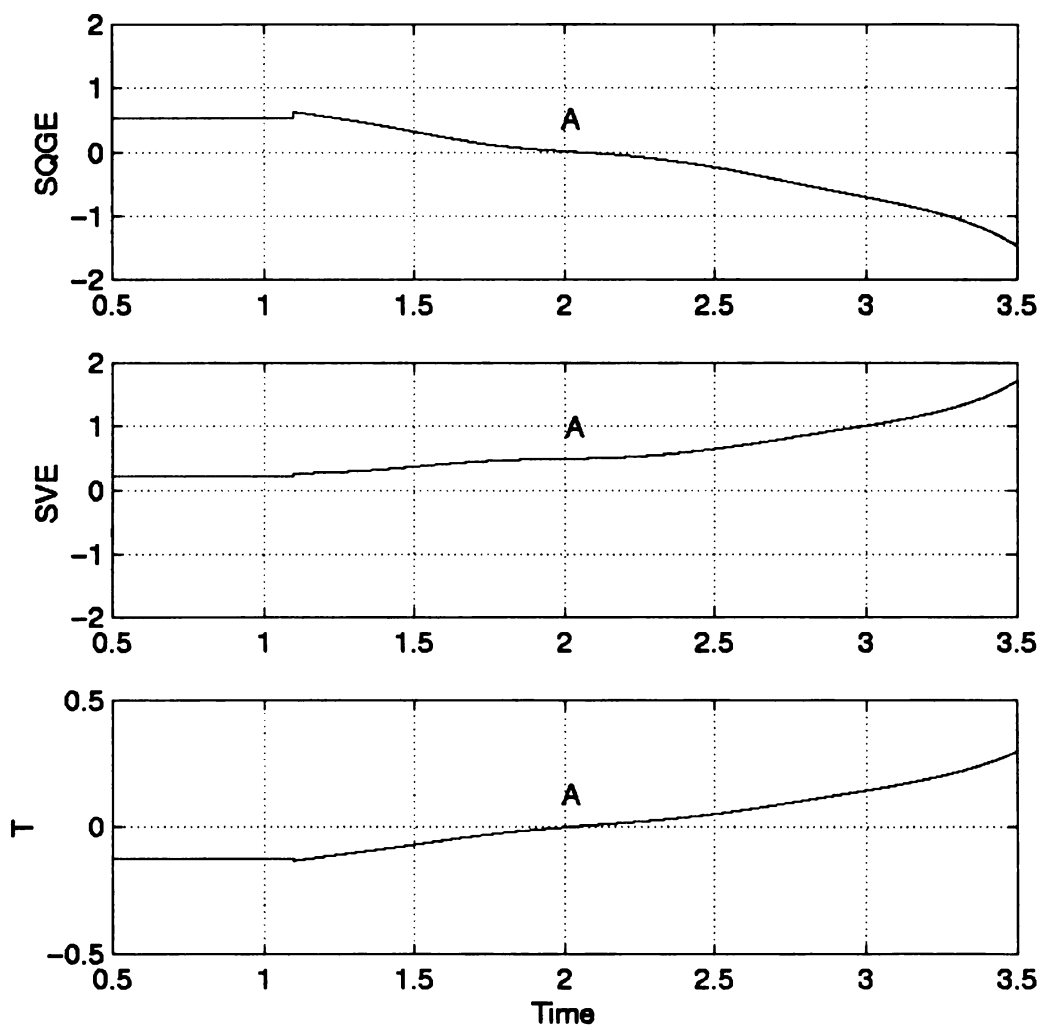


Fig. 5.2 Simulation result for theorems 5.2 and 5.3.

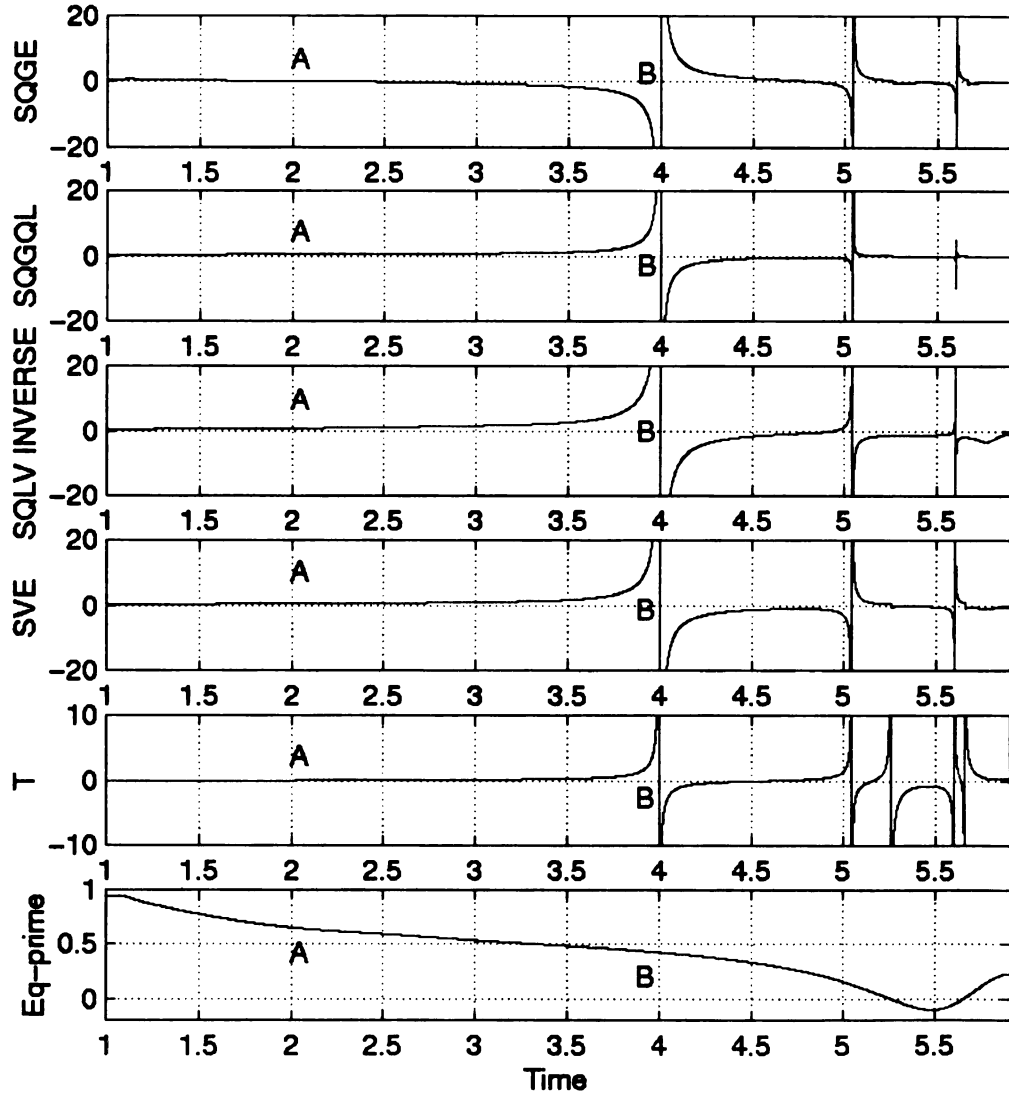


Fig.5.3 Simulation result for theorems 5.4, 5.5, 5.6, 5.7 and 5.9.

CHAPTER 6

CONCLUSIONS AND FUTURE WORK

The recent WCSS power system blackouts have some unique characteristics compared with the classical voltage instability problems, which include:

- Interarea oscillations existed before the blackout
- Loss of control voltage stability and clogging voltage instability do not occur because the dynamic submodel experiences instability before the loss of control in algebraic submodel occurs
- The stability controls were effective and responded to the contingency and became unstable
- A sharp voltage spike was observed

This dissertation has addressed three major aspects of the cause of the recent WCSS power system blackouts.

1. It explained why maximum excitation limiters fail to reduce field current limit violations when large inter-area oscillations are present and why this can lead to switching from an AC regulator to a DC regulator excitation control and finally to tripping of the generator off the system through theoretical analysis and simulation studies. It proved that if the generator field current limit is exceeded and if the field

current magnitude of the interarea oscillations slightly exceed the magnitude of the generator field current limit violation, then the maximum excitation limiter will not recognize the field current limit violation and would allow thermal damage to the generator. The failure of the maximum excitation limiter will cause the over excitation protection relay to trip out the AC regulator in an attempt to avoid the thermal damage to the generator rotor. The tripping of the AC regulator with PSS and stabilization compensator to a DC regulator, which has neither PSS nor stabilization compensator, could lead to unstable generator dynamics that inevitably cause a blackout to occur.

2. It defined voltage PV controllability, load PV controllability, voltage PQ controllability and load PQ controllability, and derived the conditions on sensitivity matrices $S_{Q_L V}^{-1}$, S_{VE} , $S_{Q_G E}$ and $S_{Q_G Q_L}$ that indicates when each type of the controllability is retained and when it is lost. It has been proven that element of $S_{Q_L V}^{-1}$ approaches positive infinity, jump to negative infinity, then increase toward zero when load PQ controllability is lost. It is further proved that loss of voltage PV controllability may occur long before loss of load PQ controllability occurs, but loss of load PV controllability and loss of voltage PQ controllability generally occur simultaneously. It is also proved that loss of load PQ controllability is affected by the load characteristics of the network. Elements of $S_{Q_L V}^{-1}$ becomes larger when shunt capacitive load increases. All the theories are proved both theoretically and through simulation.
3. It has been established that a saddle node bifurcation followed by an inevitable singularity induced bifurcation produces the characteristic negative voltage spike observed on the WSCC power system blackouts. The thorough theoretical justification and simulation studies present a clear understanding of the dynamic

responses to bifurcation sequences associated with voltage collapse. It has also been proven that disablement of the excitation control system by over excitation protection relay is not enough to cause instability, but disablement of the excitation control system and slow loss of voltage PV controllability cause saddle node bifurcation that results in slow unstable decline in E'_q . This unstable decline in E'_q causes a reactive generation decrease, a dynamic produced Q-V curve occurs as E'_q is decreasing. The dynamic Q-V curve at a generator bus in a voltage control area causes elements of S_{QGE} associated with that voltage control area to further violate voltage PV controllability conditions as E'_q decreases and voltage PV controllability is finally lost. This dynamic Q-V curve also causes the elements of S_{QLV}^{-1} approach infinity, become negative infinity and then increase toward zero. A more and more rapid decline in E'_q occurs as load PQ controllability is lost. The accelerated rate of E'_q decline causes a sharp negative voltage spike in E'_q . The change in S_{QLV}^{-1} values from $+\infty$ to $-\infty$ in the voltage control area experiencing instability causes S_{QGE} to change from $+\infty$ to $-\infty$, and the unstable eigenvalue of T to change from $+\infty$ to $-\infty$. Such a change in T causes a stable but fast rise in E'_q .

The purpose of the sensitivity analysis is to identify the subsystem which initially experience instability, to identify why this instability occurs and how this instability could cascade to other subsystems, including the algebraic model, and to identify what can be done to cure the instability problem and when and where the cure should be applied. This trajectory sensitivity approach is quite different because it focuses on the network sensitivity and controllability behaviors and how loss of one or more controllability properties produce the instability in dynamical subsystems.

Based on the achievements of this dissertation, future research is defined as follows:

- To apply the sensitivity approach to the generator inertial dynamics, or the inertial dynamics and flux decay dynamics of generators together because some bifurcation actually produce instability in these subsystems of a power system model.
- To apply the sensitivity approach to the inertial dynamics, or the inertial dynamics and flux decay dynamics of inductions motors together.
- To apply the sensitivity approach to underload tap changer and switchable shunt capacitor control dynamics.
- To link the trajectory sensitivity method to bifurcation subsystems that experience the instability produced by bifurcation.

APPENDIX A

THEOREM PROOFS

Proof of Theorem 5.3

When voltage PV controllability holds, S_{QGE} is α diagonally dominant, and

$$diag\left\{\frac{E_{q_i}'^2}{X_{d_i} - X_{d_i}'} - Q_{G_{0_i}}\right\} \quad (A1)$$

is a diagonal matrix with positive elements since

$$Q_{G_{0_i}} < \frac{E_{q_i}'^2}{X_{d_i}} < \frac{E_{q_i}'^2}{X_{d_i} - X_{d_i}'} \quad (A2)$$

Therefore, the matrix

$$diag\left\{\frac{E_{q_i}'^2}{X_{d_i} - X_{d_i}'} - Q_{G_{0_i}}\right\} + S_{QGE} \quad (A3)$$

should also be diagonally dominant. Since

$$diag\left\{\frac{1}{T_{d_{0_i}}'}\right\} \quad \text{and} \quad diag\left\{\frac{X_{d_i} - X_{d_i}'}{E_{q_i}}\right\} \quad (A4)$$

have all positive elements, matrix

$$\text{diag}\left\{\frac{1}{T'_{d_{0i}}}\right\}\text{diag}\left\{\frac{X_{d_i} - X'_{d_i}}{E'_{q_i}}\right\}\left[\text{diag}\left\{\frac{E'^2_{q_i}}{X_{d_i} - X'_{d_i}} - Q_{G_{0i}}\right\} + S_{Q_{GE}}\right] \quad (\text{A5})$$

is diagonally dominant and has positive eigenvalues, and

$$-\text{diag}\left\{\frac{1}{T'_{d_{0i}}}\right\}\text{diag}\left\{\frac{X_{d_i} - X'_{d_i}}{E'_{q_i}}\right\}\left[\text{diag}\left\{\frac{E'^2_{q_i}}{X_{d_i} - X'_{d_i}} - Q_{G_{0i}}\right\} + S_{Q_{GE}}\right] \quad (\text{A6})$$

has all negative eigenvalues. From [8,11], matrix (A6) is matrix T when $K_{A_i} = 0$, for all i , matrix (A5) is matrix $-T$ when $K_{A_i} = 0$ for all i .

If field current limits are reached on a generator and the excitation control system is disabled, the row of $-T$ associated with that generator is replaced by a row of (A5), and this row has the smallest row sum since the elements of this row are the elements of $-T$ with $K_{A_i} = 0$. This row sum is positive since (A5) is diagonally dominant. Thus the minimum row sum is a lower bound on all eigenvalues of $-T$, all eigenvalues of $-T$ are positive. If the smallest row sum of $-T$ is positive with $-T$ having all positive eigenvalues, the largest row sum of T is negative and T has all negative eigenvalues.

In summary, if an excitation system is disabled, matrix T is diagonally dominant and has all negative eigenvalues when voltage PV controllability and voltage PQ controllability hold, that is, matrix T is negative definite.

Proof of Theorem 5.4

From[11], we know that

$$\Delta \dot{E}'_q = T \frac{\Delta E'_q}{E'_{q_0}} + N \Delta Q_L \quad (\text{A7})$$

$$T = \text{diag}\left\{\frac{1}{T_{d_{0i}}}\right\} \left[\text{diag}\left\{-E'_{q_{0i}} + \frac{Q_{G_{0i}}(X_{d_i} - X'_{d_i})}{E'_{q_{0i}}}\right\} + \text{diag}\left\{\frac{-K_{A_i} K_{R_i} V_{0_i}}{K_{E_i} + S_{E_i} + \dot{S}_{E_i} E_{fd_{0i}}}\right\} WS_{VE} - \text{diag}\left\{\frac{X_{d_i} - X'_{d_i}}{E'_{q_{0i}}}\right\} S_{QGE} \right] \quad (\text{A8})$$

$$N = \text{diag}\left\{\frac{1}{T_{d_{0i}}}\right\} \left[\text{diag}\left\{\frac{-K_{A_i} K_{R_i} V_{0_i}}{K_{E_i} + S_{E_i} + \dot{S}_{E_i} E_{fd_{0i}}}\right\} WS^{-1}_{Q_L V} + \text{diag}\left\{\frac{X_{d_i} - X'_{d_i}}{E_{q_{0i}}}\right\} S_{Q_G Q_L} \right] \quad (\text{A9})$$

When the excitation system on the i th generator is disabled by over field current limiter relay, $K_{A_i} = 0$, the i th row of T is replaced by the i th row of (A6),

$$-\text{diag}\left\{\frac{1}{T'_{d_{0i}}}\right\} \text{diag}\left\{\frac{X_{d_i} - X'_{d_i}}{E'_{q_i}}\right\} \left[\text{diag}\left\{\frac{E'^2_{q_i}}{X_{d_i} - X'_{d_i}} - Q_{G_{0i}}\right\} + S_{QGE} \right] \quad (\text{A10})$$

the i th row of N is replaced by the i th row of

$$\text{diag}\left\{\frac{1}{T_{d_{0i}}}\right\} \left[\text{diag}\left\{\frac{X_{d_i} - X'_{d_i}}{E_{q_{0i}}}\right\} S_{Q_G Q_L} \right] \quad (\text{A11})$$

When loss of voltage PV controllability occurs, S_{QGE} is not diagonally dominant and $S_{QGE_{ii}} - Q_{G_i} + \frac{E'^2_{q_i}}{X_{d_i} - X'_{d_i}} < 0$, so matrix (A6) will not be diagonally dominant

and the i th row sum of $T \frac{\Delta E'_q}{E'_{q_0}} \left\{ T \frac{\Delta E'_q}{E'_{q_0}} \right\}_i$ will be negative if

$S_{QGE_{ii}} - Q_{G_i} + \frac{E'^2_{q_i}}{X_{d_i} - X'_{d_i}} < 0$ for $\Delta E'_{q_i} < 0$ and $\Delta E_j = 0$, $j \neq i$. Note that

$\Delta E_j = 0 \ j \neq i$ is an approximation of the small changes in internal generator voltage for generators with exciters compared to the unstable generator $j = i$. The increased generation causes (a) generators to reach field current limits, (b) action of field current limiters, and (c) ultimately singularity induced bifurcation.

When the system is load PV controllable, $S_{Q_G Q_L}$ is nonnegative and no zero columns, so the elements in i th row of matrix (A7) are nonnegative, the i th element of $N\Delta Q_L \{N\Delta Q_L\}_i < 0$ for $\Delta Q_L < 0$.

From Theorem 2, we know that the generator that loses its excitation control and those voltage control buses which experience loss of voltage PV controllability becomes unstable.

$$\text{Therefore, } \Delta \dot{E}'_{q_i} = \left\{ T \frac{\Delta E'_q}{E'_{q_0}} \right\}_i + \{N\Delta Q_L\}_i < 0 \text{ for } \Delta E'_{q_i} < 0, \text{ and } \Delta Q_L < 0.$$

and thus \dot{E}'_{q_i} is unstable and decreases toward zero.

Proof of Theorem 5.5:

The computing of a Q-V curve implies adding reactive load by decreasing voltage at a bifurcation generator bus. Letting $\Delta E'_{q_i}(t)$ decrease at bus i with $\Delta E_j = 0$ for $j \neq i$ and

assuming $S_{Q_G E_{ii}} - Q_{G_i} + \frac{E'^2_{q_i}}{X_{d_i} - X'_{d_i}} < 0$ with loss of voltage PV controllability but

without loss of load PV controllability implies instability in flux decay dynamics causing $\Delta E'_{q_i}(t)$ to continue to decrease producing a dynamic Q-V curve at bus i that causes increasing reactive generation at bus j $\Delta Q_{G_j} = \{S_{Q_G E}\}_{ji} \Delta E_i > 0$ when $\Delta Q_L \leq 0$ for

$j \neq i$. This analysis confirms that a Q-V curve stress test is administered through the unstable generator dynamics resulting in inevitable bifurcation in the algebraic submodel of

the differential algebraic model and singularity induced bifurcation in the differential algebraic model because the effects are so dramatic on generator flux decay dynamics. This dynamic Q-V curve causes $S_{Q_L V}^{-1}$, $S_{Q_G Q_L}$ and $S_{V E}$ to approach infinity, become negative infinity, and then increase, and $S_{Q_G E}$ to approach zero, become negative infinity, then become infinity and then decrease in the voltage control area associated with λ_{\min} as noted in Theorem (4.6).

Proof of Theorem 5.6

The slope of the Q-V curve at generator i where the dynamic Q-V curve occurs is $\{S_{Q_L V}\}_{ii}$, it approaches zero from Theorem 5.5 and the discussion of Q-V curves at the end of Chapter 4. $S_{Q_G E} = J_{11} - J_{12} S_{Q_L V}^{-1} J_{21}$ elements associated with the voltage control area containing generator i where the dynamic Q-V curve occurs become negative infinite as $S_{Q_L V}^{-1}$ elements approach $+\infty$ because J_{11} , J_{12} and J_{21} are continuous functions of the bifurcation parameter ΔQ_{Li} and change little compared to $S_{Q_L V}^{-1}$ elements approaching $+\infty$. The eigenvalue of T associated with generator i , where loss of PV controllability occurs and the excitation control system is disabled, approaches $+\infty$, since (i) the lower bound eigenvalue estimate computed via a minimum column sum of $S_{Q_G E}$ is associated with the generator bus i experiencing the dynamic Q-V curve in the voltage control area where $S_{Q_L V}^{-1}$ elements approaches infinite, and (ii) the minimum eigenvalue of $S_{Q_G E}$ is related to this large eigenvalue of T by a negative constant diagonal. The eigenvalue of T approaching $+\infty$ explains the rapid decline in $\Delta E'_{qi}$ as the dynamic Q-V curve ultimately causes loss of load PQ controllability from Theorem 5.4. Note that the minimum column sum of $S_{Q_G E}$ is also a measure of violation for voltage PV controllability condition, and the condition $\{S_{Q_G E}\}_{ii} > 0$ is never violated before condition $\sum_{j=1}^N \{S_{Q_G E}\}_{ij} > 0$ is violated.

Proof of Theorem 5.7

When the excitation system on the i th generator is disabled by over field current limiter relay, $K_{A_i} = 0$, the i th row of T is replaced by the i th row of (21),

$$-diag\left\{\frac{1}{T'_{d_{0i}}}\right\}diag\left\{\frac{X_{d_i} - X'_{d_i}}{E'_{q_i}}\right\}\left[diag\left\{\frac{E'^2_{q_i}}{X_{d_i} - X'_{d_i}} - Q_{G_{0i}}\right\} + S_{Q_G E}\right] \quad (A12)$$

the i th row of N is replaced by the i th row of (22)

$$diag\left\{\frac{1}{T_{d_{0i}}}\right\}\left[diag\left\{\frac{X_{d_i} - X'_{d_i}}{E_{q_{0i}}}\right\}S_{Q_G Q_L}\right] \quad (A13)$$

When loss of voltage PV controllability occurs in a voltage control area such that $S_{Q_G E_{ii}} - Q_{G_i} + \frac{E'^2_{q_i}}{X_{d_i} - X'_{d_i}} < 0$ for a bus in that voltage control area, matrix (A12) is

not diagonally dominant and the i th row sum of $T \frac{\Delta E'_q}{E'_{q_0}} \left\{ T \frac{\Delta E'_q}{E'_{q_0}} \right\}_i$ is positive for $\Delta E'_{q_i} > 0$ and $\Delta E'_{q_j} \approx 0, j \neq i$.

When loss of load PV controllability occurs at generator bus i , elements of $S_{Q_G Q_L}$ in row i associated with the voltage control area containing the dynamic Q-V curve are negative, elements in row i of matrix (A13) are negative, the i th element of $N\Delta Q_L \{N\Delta Q_L\}_i$ is generally then positive for $\Delta Q_L < 0$ when i belongs to that voltage control area experiencing the dynamic Q-V curve once load PV controllability is lost..

From Theorem 5.4, we know that the generator that loses its excitation control and those voltage control buses which experience loss of voltage PV controllability becomes unstable.

$$\text{Therefore, } \Delta \dot{E}'_{q_i} = \left\{ T \frac{\Delta E'_q}{E'_{q_0}} \right\}_i + \{ N \Delta Q_L \}_i > 0 \text{ for } \Delta E'_{q_i} > 0, \Delta E'_{q_j} \approx 0, j \neq i,$$

and $\Delta Q_L < 0$, the system is unstable and the change in E'_{q_i} is positive once load PV controllability is lost in the voltage control area containing bus i .

Proof of Theorem 5.8

If the system is stable after loss of load PQ and load and voltage PV controllability, at steady state,

$$T \Delta E'_q = -N \Delta Q_L \quad (\text{A14})$$

for the i th row of the equation above

$$\{T\}_i \Delta E'_q = -\{N\}_i \Delta Q_L \quad (\text{A15})$$

Since the excitation control systems on all machines are active, T and N can be represented as

$$T \approx \text{diag} \left\{ \frac{1}{T_{d_{0i}}} \right\} \text{diag} \left\{ \frac{-K_{A_i} K_{R_i} V_{0i}}{K_{E_i} + S_{E_i} + \dot{S}_{E_i} E_{fd_{0i}}} \right\} W S_{VE} \quad (\text{A16})$$

$$N \approx \text{diag} \left\{ \frac{1}{T_{d_{0i}}} \right\} \text{diag} \left\{ \frac{-K_{A_i} K_{R_i} V_{0i}}{K_{E_i} + S_{E_i} + \dot{S}_{E_i} E_{fd_{0i}}} \right\} W S^{-1}_{Q_L V} \quad (\text{A17})$$

From theorem 4.6, when loss of load PQ controllability occurs, loss of voltage PQ controllability may also occur, therefore, from given (i), (ii), (iii) and the above equations for T and N , we know that $\{T\}_{ii}$ will dominate the i th row of T as long as generator i is the only generator in the voltage control area and W measures voltage in that voltage control area that experiences loss of load PQ controllability and loss of load and voltage PV controllability, $\{N\}_{ij}$ will dominate the i th row of N as long as generator bus i and load bus j lie in the voltage control area where loss of load PQ controllability and loss of load and voltage PV controllability occur, and (a) can be represented as

$$\{T\}_{ii} \Delta E'_{q_i} \approx \sum_{k \in VCA} -\{N\}_{ik} \Delta Q_{Lk} \quad (\text{A18})$$

since $\Delta E'_{q_j} = 0$, $j \neq i$, where $\{T\}_{ii}$ and $\{N\}_{ik}$ will be negative, and $N_{ij} \approx 0$, ΔQ_{Lk} is negative. As a result, $\Delta E'_{q_i}$ is positive.

APPENDIX B

PUBLICATIONS

- [1] R. A. Schlueter and S. Liu, "Intelligent control for a power system in a deregulated environment", *Proc. of the North American Power Symposium*, MIT, November, 1996, pp. 81-88.
- [2] S. Liu and R. A. Schlueter, "Intelligent control for a power system ", *Proc. of American Control Conference*, Dearborn, Sept. 1996, pp. 456-460.
- [3] R. A. Schlueter, S. Liu, K. B. Kilani and I. P. Hu, "Static voltage instability in flux decay dynamics of a midterm stability model", Accepted for publication in the *J. of Electrical Power Systems Research*.
- [4] R. A. Schlueter, S. Liu, K. B. Kilani and I. P. Hu, "Static voltage instability in generator flux decay dynamics as cause of voltage collapse", Submitted to *IEEE Trans. on Power Systems*.
- [5] R. A. Schlueter and S. Liu, "A structure-based hierarchy for intelligent voltage stability control in operation planning, scheduling, and dispatching power systems", Submitted to *IEEE Trans. on Power Systems*.
- [6] R. A. Schlueter, K. B. Kilani, S. Liu, "Justification of the voltage stability security assessment and diagnostic procedure using bifurcation subsystem method", accepted by *the 1998 Large Engineering Conference on Power Engineering*, Nova Scotia, Canada, June 7-9, 1998.
- [7] R. A. Schlueter, and S. Liu, "A structure based intelligent voltage stability control in scheduling and distaching power systems", accepted by *the 1998 Large Engineering Conference on Power Engineering*, Nova Scotia, Canada, June 7-9, 1998.
- [8] R. A. Schlueter, S. Liu, "Justification of the voltage stability security assessment as an improved modal analysis procedure", accepted by *the 1998 Large Engineering Conference on Power Engineering*, Nova Scotia, Canada, June 7-9, 1998.
- [9] R. A. Schlueter, S. Liu, N. Alemadi, "Intelligent voltage stability assessment, diagnosis and control of power system using a modal structure", accepted by *Bulk Power System Voltage Phenomena: Dynamics and Control IV*, Santorini, Greece, Aug.1998.

REFERENCES

- [1] P. Kundur, "Power System Stability and Control", *McGraw Hill*, New York, 1994.
- [2] C. W. Taylor, "Power System Voltage Stability", *McGraw Hill*, New York, 1994.
- [3] Hassan K. Khalil, "Nonlinear Systems", *Macmillan Publishing Company*, New York, 1992.
- [4] T. V. Cutsem and C. Vournas, "Voltage Stability of Electric Power Systems", *Kluwer Academic Publishers*, Massachusetts, 1998.
- [5] R. A. Schlueter, "A voltage stability security assessment method", *IEEE 1997 Summer Power Meeting Paper*, No. PE-735-PWRS-0-10-1997 and accepted for publication by *IEEE Trans. on Power Systems*.
- [6] R. A. Schlueter, K. B. Kilani and U. Ahn, "Impact of modeling accuracy on type, kind, and class of stability problems in a power system model", *Proceedings of the ECC & NSF International Workshop on Bulk Power System Voltage Stability, Security and Control, Phenomena-III*, Aug. 1994, pp. 117-156.
- [7] I. Hu and R. A. Schlueter, "Types of voltage instability and the associated modeling in a transient stability model", *Journal on Electric Power Systems Research*, Vol.29, 1994, pp. 131-145.
- [8] I. Hu, "Voltage Collapse Bifurcation of a Power System Transient Stability Model", *Ph.D Dissertation*, Michigan State University, July 1990.

- [9] B. Lee and V. Ajjarapu, "A piecewise global small-disturbance voltage-stability analysis of structure-preserving power system models", *IEEE Trans. on Power Systems*, Vol.10, No.4, November 1995, pp. 1963-1971.
- [10] B. Lee and V. Ajjarapu, "A general approach to study static and dynamic aspects of voltage instability", *Proceedings of the 31st Conference on Decision and Control*, Tucson, Arizona, December 1992, pp. 2916-2919.
- [11] R. A. Schlueter, S. Liu, K. B. Kilani and I. P. Hu, "Static voltage instability in flux decay dynamics of a midterm stability model", Accepted for publication in the *J. of Electrical Power Research*.
- [12] R. A. Schlueter, S. Liu, K. B. Kilani and I. P. Hu, "Static voltage instability in generator flux decay dynamics as cause of voltage collapse", Submitted to *IEEE Trans. on Power Systems*.
- [13] V. Ajjarapu and B. Lee, "Bifurcation theory and its application to nonlinear dynamical phenomena in an electrical power system". *IEEE Trans. on Power Systems*, Vol.7, No.1, February 1992, pp. 424-431.
- [14] C. A. Canizares, "On bifurcations, voltage collapse and load modeling", *IEEE Trans. on Power Systems*, Vol.10, No.1, February 1995, pp. 512-518.
- [15] R. A. Schlueter, A. G. Costi, H. L. Forgey and J. E. Sekerke, "Voltage stability and security assessment", *EPRI project RP 1999-8*, No. EL-5967, Electric Power Research Institute, Palo Alto, May 1988.
- [16] T. Guo and R. A. Schlueter, "Identification of generic bifurcation and stability problems in power system differential-algebraic model", *IEEE Trans. on Power Systems*, Vol.9, No.2, May 1994, pp. 1032-1044.
- [17] R. A. Schlueter, K. B. Kilani, S. Liu, "Justification of the voltage stability security assessment and diagnostic procedure using bifurcation subsystem method", *1998 Large Engineering Conference on Power Engineering*, Nova Scotia, Canada, June 7-9, 1998.

- [18] C. W. Taylor and D. C. Erickson, "Recording and analyzing the July 2 cascading outage", *IEEE Computer Applications in Power*, January 1997, pp. 26-30.
- [19] B. Kokanos and B. Fitzgerald, "System monitors shed light on blackouts", *Transmission & Distribution World*, Vol.49, No.4, April 1997, pp. 40-47.
- [20] C. W. Taylor, J. R. Mechenbier and J. W. Burns, "December 14, 1994 breakup of the Western North American Power System: failures, successes, and lessons", Paper for *V Symposium of Specialists in Electric Operational and Expansion Planning*, Recife, Brazil, May 19-24, 1996.
- [21] D. N. Kosterev, C. W. Taylor and W. A. Mittelstatd, "Model Validation for the August 10, 1996 WSCC System Outage", *IEEE 1997 Summer Power Meeting Paper*, No. PE-226-PWRS-0-12-1997.
- [22] R. A. Schlueter, S. Liu, N. Alemadi, "Intelligent voltage stability assessment, diagnosis and control of power system using a modal structure", accepted by *Bulk Power System Voltage Phenomena: Dynamics and Control IV*, Santorini, Greece, Aug.1998.
- [23] M. M. Begovic and A. G. Phadke, "Dynamic simulation of voltage collapse", *IEEE Trans. on Power Systems*, Vol.5, No.1, February 1990, pp. 198-203.
- [24] H. O. Wang, E. H. Abed and A. Hamdan, "Bifurcations, chaos, and crises in voltage collapse of a model power systems", *IEEE Trans. on Circuits and Systems*. Vol. 41, No. 4, pp. 294-302, April 1994.
- [25] R. A. Schlueter, "Unification and classification of algebraic tests for voltage stability", *Journal on electric Machines and Power Systems*, Vol.21, No.6. 1993, pp. 557-590.
- [26] R. A. Schlueter, I. Hu and T. Y. Guo, "Dynamic/static voltage stability security criteria", *Proceedings of Bulk Power System Voltage Phenomena-Voltage Stability and Security Seminar*, Deep Creek Lake, MD, August 1991.

- [27] H. G. Kwatny, A. K. Pasrija and L. Y. Bahar, "Loss of steady-state stability and voltage collapse in electric power systems", *Proceedings of the 24th Conference on Decision and Control*, Ft. Lauderdale, FL, December 1985.
- [28] R. J. Thomas and A. Tiranuchit, "Dynamic voltage instability", *Proc. of the 26th Conference on Decision and Control*, Los Angeles, California, 1987.
- [29] I. Dobson and H. Chiang, "Towards a theory of voltage collapse in electric power systems", *System and Control Letters*, Vol.13, 1989, pp. 253-262.
- [30] Athur R. Burgen, "Power System Analysis". *Prentice Hall, Inc.*, New Jersey, 1986.
- [31] R. A. Schlueter, S. Liu, "Justification of the voltage stability security assessment as an improved modal analysis procedure", *1998 Large Engineering Conference on Power Engineering*, Nova Scotia, Canada, June 7-9, 1998.
- [32] K. B. Kilani, "Bifurcation subsystem method and its application to diagnosis of power system bifurcations produced by discontinuities", *Ph.D Dissertation*, Michigan State University, August 1997.
- [33] IEEE Systems Dynamic Performance Report, "Suggested techniques for voltage stability analysis", *IEEE Power Engineering Society Publication*., No. 93 0620-5PWR.
- [34] M. Klein, G. J. Rogers and P. Kundur, "A Fundamental study of inter-area oscillations in power systems", *IEEE Trans. on Power Systems*, Vol.6, No.3, August 1991, pp. 914-921.
- [35] C. Rajagopalan, B. Lesieutre, P.W. Sauer and M. A. Pai, "Dynamic aspects of voltage/power characteristics", *IEEE Trans. on Power Systems*, Vol.7, No.3, August 1992, pp. 990-1000.
- [36] R. A. Schlueter and S. Liu, "A structure-based hierarchy for intelligent voltage stability control in operation planning, scheduling, and dispatching power systems", Submitted to *IEEE Trans. on Power Systems*.

- [37] R. A. Schlueter, and S. Liu, "A structure based intelligent voltage stability control in scheduling and dispatching power systems", *1998 Large Engineering Conference on Power Engineering*, Nova Scotia, Canada, June 7-9, 1998.
- [38] T. Ohyama, "Voltage dependence of composite loads in power systems". *IEEE Trans. on Power Apparatus and Systems*, Vol.140, No.11, November 1985, pp. 3065-3073.
- [39] G. J. Berg, "Power system load representation", *Proc. IEE*, Vol.120, No.3, March 1973, pp. 344-348.
- [40] D. J. Hill, "Nonlinear Dynamic Load Models with Recovery for Voltage Stability Studies", *IEEE Trans. on Power Systems*, Vol.8, No.1, February 1993, pp. 166-176.
- [41] A. Borghetti, R. Caldon, A. Mari and C. A. Nucci, "On dynamic load models for voltage stability studies", *IEEE Trans. on Power Systems*, Vol.12, No.1, February 1997, pp. 293-303.
- [42] C. A. Canizares, "Conditions for saddle-node bifurcations in AC/DC power systems", *Electrical Power and Energy Systems*, Vol.17, No.1, 1995, pp. 61-68.
- [43] M. A. Pai, P.W. Sauer, B. Lesieutre and R. Adapa, "Structural Stability in Power Systems- Effects of Load Models", *Proc. of IEEE/NTUA Athens Power Tech Conference*, Athens, Greece, Sept. 5-8, 1993, pp. 228-232.
- [44] IEEE Committee Report, "Excitation System Models For Power System Stability Studies", *IEEE Trans. on Power Apparatus and Systems*, Vol.100, Feb. 1981, pp. 494-509.
- [45] V. Venkatasubramanian and J. Zaborsky, "A taxonomy of the dynamics of the large power system with emphasis on its voltage stability", *Proceedings of the NSF Workshop Bulk Power Systems Voltage Phenomena: Voltage Stability and Security*, Deep Creek Lake, MD, 1991, pp. 9-52.

- [46] H. D. Chiang, I. Dobson and R. J. Thomas, "On Voltage Collapse in Electric Power Systems", *IEEE Trans. on Power Systems*, Vol.5, No.2, 1990, pp. 601-611.
- [47] H. O. Wang, E. H. Abed and A. Hamdan, "Bifurcations, chaos, and crises in voltage collapse of a model power system", *IEEE Trans. on Circuits and Systems*, Vol.41, No.4, April 1994, pp. 294-302.
- [48] IEEE Task Force on Excitation Limiters, "Recommended models for Overexcitation limiting devices", *IEEE Trans. on Energy Conversion*, Vol.10, No.4, 1995, pp. 706-713.
- [49] R. A. Schlueter and S. Liu, "Intelligent Control for a Power System in a Deregulated Environment", *Proc. of the North American Power Symposium*, MIT, November, 1996, pp. 81-88.
- [50] S. Liu and R. A. Schlueter, "Intelligent Control for a Power System ", *Proc. of American Control Conference*, Dearborn, Sept. 1996, pp. 456-460.
- [51] IEEE System Oscillations Working Group, "Inter-area oscillations in power systems", *IEEE Power Engineering Society Publication*, October, 1995.
- [52] CIGRE Task Force on Analysis and Control of Power System Oscillations, "Analysis and control of power system oscillations", *CIGRE Technical Brochure*, December, 1996.
- [53] Electric Power Research Institute, "Small Signal Stability Analysis Program Package", Vol.1, February 1993.
- [54] A. Debs, "Modern Power Systems Control and Operation", *Kluwer Academic Publishers*, 1988.
- [55] A. A. Fouad and P. M. Anderson, "Power System Stability and Control", *Iowa State Press*, 1977.
- [56] S. Greene, "Margin and Sensitivity Methods for Security Analysis of Electric Power Systems", Ph. D. Thesis, Univ. of Wisconsin-Madison, 1998.

- [57] M. J. Laufenberg, "Dynamic Sensitivity Functions and the Stability of Power Systems with Facts Controllers", Research Reports (PAP-TR-97-2), Univ. of Illinois, 1997.
- [58] Shuzhen Liu and R. A. Schlueter, "Effects of Loss of PQ Controllability and PV Controllability on Stability of Generator Flux Decay Dynamics", 1999 Large Engineering Systems Conference on Power Engineering, June 1999.
- [59] Shuzhen Liu and R. A. Schlueter, "Bifurcation Dynamics as a Cause of the Voltage Collapse Problems on the WSCC System", 1999 Large Engineering Systems Conference on Power Engineering, June 1999.
- [60] Khadija Ben-Kilani and R. A. Schlueter, "An Approach for Determining the Bifurcation in a Power Subsystem Experiencing and Producing Bifurcation in a Power System Dynamic Model", 1999 Large Engineering Systems Conference on Power Engineering, June 1999.
- [61] Shuzhen Liu and R. A. Schlueter, "Effects of Large Interarea Oscillation on Disablement of a Generator's Excitation Control and Subsequent Tripping of the Generator", 1999 Large Engineering Systems Conference on Power Engineering, June 1999.
- [62] IEEE Special Publication 90th 0358-2-PWR, "Voltage Stability of Power Systems: Concepts, Analytical Tools, and Industry Experience", Prepared by the IEEE Working Group on Voltage Stability, 1990.